



Constructing 3D variable-density groundwater flow models for six deltas using global data sets

Master's degree thesis

Author:

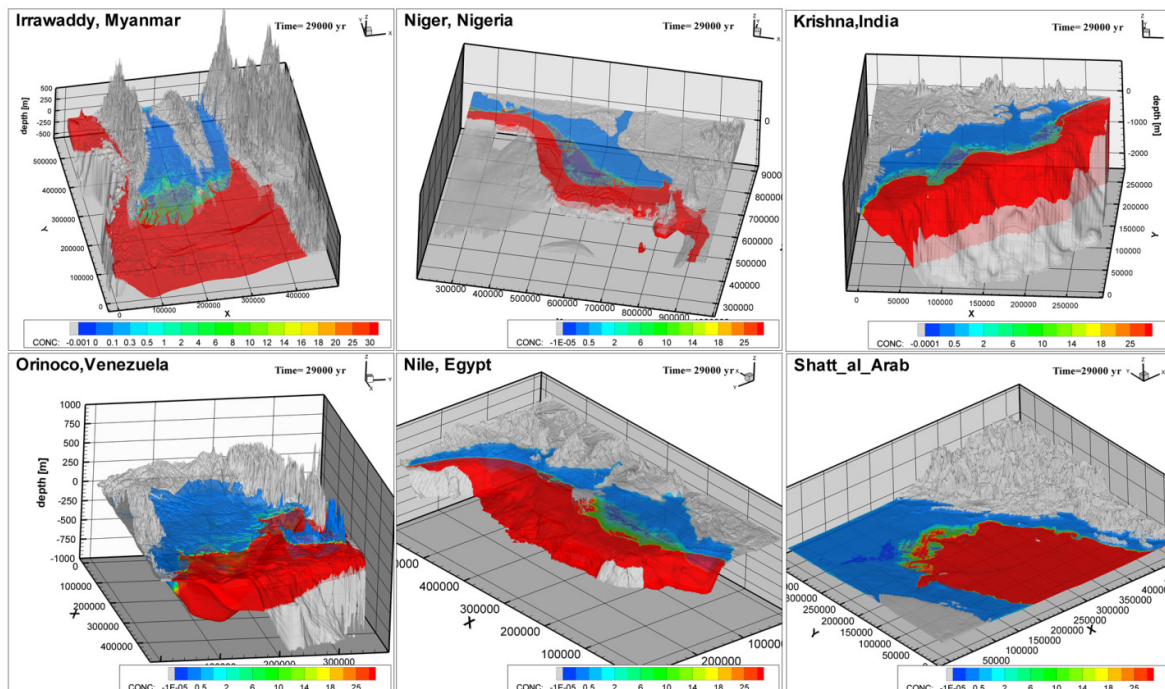
Tobias Mulder
Student ID: 3692183

supervisors:

dr. ir. Gualbert Oude Essink
prof. dr. ir. Marc Bierkens

In partial fulfilment of the requirements for the degree of
Master of Science in Earth Surface and Water

April 2018





Deltares
Groundwater Management
Daltonlaan 600, Utrecht



Universiteit Utrecht

Utrecht University
Faculty of Geosciences
Department of Physical Geography
Princetonlaan 8a, Utrecht

Master of Science Thesis by Tobias Mulder

Title: Constructing 3D variable-density groundwater flow models for six deltas using global data sets.

Subtitle: Can 3D models constructed with global data sets represent hydrogeological processes properly.

1st supervisor: dr.ir. Gualbert Oude Essink,
Associate professor at Utrecht University and senior specialist at Deltares.

2nd supervisor: prof.dr.ir. Marc Bierkens,
Professor Earth Surface Hydrology at Utrecht University and senior specialist at Deltares.

In collaboration with PhD students: Daniel Zamrsky and Joeri van Engelen from Utrecht University.

Abstract

One third of the world's population lives within 100 km from the shoreline. High population densities in deltaic areas create a very high demand for high-quality fresh water. To meet this demand, groundwater is extracted. Sea level rise, land subsidence, coastal erosion and fresh groundwater extraction enhance salt water intrusion and threaten the fresh groundwater reserves. For this study six 3D variable-density groundwater flow models were constructed from global data sets to quantify the fresh groundwater gaps in 6 deltas. A global hydrogeological dataset does not exist so 6 possible geological scenarios were tested. Second, a method was created to determine the dynamic equilibrium time τ for all six models. The dynamic equilibrium time, is the time it takes for a disturbed system to reach a point where fresh and salt groundwater volumes do not change over time. The τ helps to understand how far back in time a paleo-reconstructive model should go to make a better estimation of the initial salt and fresh groundwater distribution.

The time it took for the models to reach τ was in-between 30.000 and 90.000 years. The 6 deltas have a different τ because of the difference in geometry, precipitation and river network. Within a delta the different geological scenarios cause a difference in τ . The higher the velocities in groundwater flow the shorter the τ . Scenarios were both tested for a system that starts completely fresh and gradually becomes salt (the so-called fresh-to-salt scenario) as for a so-called salt-to-fresh scenario. The salt-to-fresh scenario showed that inland in deep parts of the delta, salt groundwater can be stagnant and therefore remain stable under the right conditions. The bodies of salt groundwater can originate from the times when the sea level was higher than the present sea level (last time this happened was 120.000 years ago). When deep inland salt paleo groundwater is not taken into account, the computed volume of the fresh groundwater reserve can be overestimated. This will affect the projections of water policy makers.

Keywords: 3D variable density-density groundwater modelling, dynamic equilibrium time τ , fresh groundwater reserves, paleo hydrogeology

Acknowledgements

I am most thankful to my first supervisor dr. ir. Gualbert Oude Essink. His vision, questions, meetings, emails, and computer tools helped me in the construction of both the models and this thesis. I am also very thankful to my second supervisor prof. dr. ir. Marc Bierkens who advised me on the general direction of this researched.

I am very much thankful to Daniel Zamrsky and Joeri van Engelen for their immense contribution to this thesis. Not only did they provide me with data and the necessary python tools, they also substantially contributed to every meeting and discussion with my first supervisor.

I would also like to thank dr. Kim Cohen who helped me to formulate a rule of thumb for the number of aquifers and aquitards in a delta according to the age of the system. His knowledge on the subject helped to outline the geological scenarios.

Special thanks go out to MSc. Huite Bootsma from Deltares who was always interested in my thesis. Discussions with him made me rethink steps in the modelling phase and his construction of the python tool to replace the times in my output files drastically decreased the time it took to process all the data.

Last but not least I would like to thank all my colleagues at Deltares whom I worked with during the six months of my master's thesis and also for the six months during my internship prior to this thesis.

Table of Contents

1. Introduction	- 1 -
1.1 Background	- 1 -
1.2 Problem definition	- 1 -
1.3 Objectives	- 2 -
1.4 Research questions	- 2 -
1.4.1 Main research question:	- 2 -
1.4.2 Sub-research questions:	- 3 -
1.5 Organisation of report	- 3 -
2. Background groundwater modelling, salt water intrusion and study areas	- 4 -
2.1 Theoretical background in groundwater processes and modelling	- 4 -
2.1.1. Introduction	- 4 -
2.1.2. Groundwater flow equation	- 4 -
2.1.3. The variable density groundwater flow equation	- 5 -
2.1.4. Dynamic equilibrium and equilibrium time Tau (τ)	- 6 -
2.2 Salt water intrusion	- 7 -
2.2.1. Fresh saline groundwater distribution	- 7 -
2.2.2. Badon Ghijben Herzberg principle	- 8 -
2.2.3. Eustatic and relative sea level change.	- 9 -
2.3 Information model area	- 10 -
3. Research methodology	- 13 -
3.1. Collection, clipping and adjusting of global data.	- 13 -
3.1.1. General Bathymetric Chart of the Oceans (GEBCO):	- 13 -
3.1.2. The estimated thickness of the deltas.	- 14 -
3.1.3. GAIA river network	- 14 -
3.1.4. The Global Lithological Map (GLiM)	- 16 -
3.1.5. PALEO precipitation (WorldClim1.4)	- 16 -
3.2. Initial model setup and setup for testing different geologies	- 17 -
3.2.1. Initial model and parameters	- 17 -
3.2.2. Modelling different geologies	- 21 -
4. Results	- 23 -
4.1 Initial model results	- 23 -
4.2 Dynamic equilibrium time Tau	- 25 -
4.2.1. Initial Tau results	- 25 -
4.2.2. Tau results per delta for all 12 scenarios	- 25 -
4.2.3 Comparing different scenarios in detail	- 30 -

4.3 Computational time different models, scenarios and solvers	- 35 -
4.3.1 Average computational time over the 12 scenarios per model.....	- 35 -
4.3.2. Average computational time over the 6 models per scenario.....	- 36 -
4.3.3. Comparing different solvers	- 37 -
4.4. Comparing different conductivities for the top system	- 38 -
5. Discussion	- 40 -
5.1 Parameters in initial model results	- 40 -
5.2 hypotheses how dynamic equilibrium forms under different scenarios	- 40 -
5.2.1. Explanation to observations in results section 4.2.2.....	- 40 -
5.3 Computational time under different scenarios and solvers	- 42 -
5.4 Influence of top system on deep paleo groundwater	- 42 -
6. Conclusions	- 43 -
7. Recommendations	- 45 -
8. References:	- 46 -
9. Appendices	- 50 -

List of Figures

Figure 1: Left: the 6 directions in the 3D groundwater model to where water can flow. Right: the flow has to be calculated from the centre of one cell to the centre of another cell (from $i, j-1/2, k$ to $i, j+1/2, k$) (McDonald and Harbaugh, 1988)	5 -
Figure 2: A theoretical representation how dynamic equilibrium time τ can evolve. At $t=0$ the system is disturbed (delta is completely filled with either only fresh or salt groundwater). At $t=1$ the dynamic equilibrium time starting saline is reached. At $t=2$ the dynamic equilibrium time starting fresh is reached (Oude Essink & Waterman, 2018).	7 -
Figure 3: The general composition of sea water. Chloride, Sodium, Sulphate, Magnesium, Calcium and Potassium are the most important total dissolved solids (TDS) in sea water. The table on the left shows that for sea water, in general, the concentration of the TDS makes up 35g/L.	7 -
Figure 4: The different sources which contribute to the salinization of groundwater. sea water intrusion is the most important process, but inland different sources can also contribute to salinization of groundwater (Kloppmann et al., 2010).	8 -
Figure 5: A cross section showing how the Badon Ghijben Herzberg principle works. The salt/fresh groundwater interface in this homogeneous aquifer is formed by the relative difference in density of fresh and salt groundwater (Oude Essink, 2014).	8 -
Figure 6: (a) The estimated eustatic sea level for the last 35 Million years, estimated with $\delta^{18}\text{O}$ values by Zachos et al. (2008).	9 -
Figure 7: model area of the Krishna-Godavari delta in red.	10 -
Figure 8: model area of the Shatt al Arab delta in red.	11 -
Figure 9: model area of the Irrawaddy delta in red.	11 -
Figure 10: model area of the Niger delta in red.	12 -
Figure 11: model area of the Nile delta in red.	12 -
Figure 12: model area of the Orinoco delta in red.	12 -
Figure 13: Visualization of GEBCO 2014, a global bathymetry and digital elevation map.	13 -
Figure 14: Clipped width for the rivers in the Irrawaddy. The width varies from 7 m to 2000m and is used to make an estimation on river conductance. The width estimation of the rivers comes from the GAIA data set.	15 -
Figure 15: Clipped depth of the rivers in the Irrawaddy delta. The estimated depth of the rivers varies from 30 cm to 20 m. The depth estimation of the rivers comes from the GAIA data set.	16 -
Figure 16: Cross section of the Nile delta showing the discretization of the model in 10 model layers.	18 -
Figure 17: Boundary conditions (red = fixed, dark blue= inactive and green = active) clock ward from top left: Irrawaddy, Krishna, Nile, Niger, Orinoco and Shatt al Arab.	18 -
Figure 18: Schematic representation of the 6 different geological scenarios.	22 -
Figure 19: Initial model results for the Irrawaddy, Krishna and Niger delta. Hydraulic head (left) and concentration (right)	23 -
Figure 20: Initial model results for the Orinoco, Nile and Shatt al Arab delta. Hydraulic head (left) and concentration (right)	24 -
Figure 21: Computed concentration for scenario A1B1C1 after 29.000 years for all 6 deltas.	25 -
Figure 22: Theoretical evolution of Tau scenarios. For the Irrawaddy delta the lines are extrapolated (in black). If a scenario is stable before $t=61000$ years the simulation was stopped.	25 -
Figure 23a: Evolution of the 12 Tau scenarios for the Irrawaddy delta.	26 -
Figure 23b: Evolution of the 12 Tau scenarios for the Krishna delta.	27 -
Figure 23c: Evolution of the 12 Tau scenarios for the Nile delta.	27 -
Figure 23d: Evolution of the 12 Tau scenarios for the Niger delta.	28 -
Figure 23e: Evolution of the 12 Tau scenarios for the Orinoco delta.	28 -
Figure 23f: Evolution of the 12 Tau scenarios for the Shatt al Arab delta.	29 -
Figure 24: left: cross sections trough the Irrawaddy delta for scenario A1B2C3. Large pockets of fresh water surrounded by salt water are clearly visible. Right: close-up of a top-view of the Irrawaddy delta for scenario A1B2C3. The 'gaps' are visible as light red square patches indicating a higher concentration.	29 -
Figure 25: Evolution of the fresh water volume in the Irrawaddy delta for scenario A1B1C1 and A1B2C2. The lines for the fresh water volumes are parallel in the end and do not seem to meet.	30 -

Figure 26: Translucent top view of the Irrawaddy delta for scenario A1B1C1 (Closed_Salt-to-Fresh_Clay-on-Top). In the first 12.000 years (top 3) the fresh water volume changes significantly. From 20.000 to 60.000 years (bottom 3) the volume only changes slightly.	31 -
Figure 27: Translucent top view of the Irrawaddy delta for scenario A1B2C2 (Closed_Fresh-to-Salt_Claylayers). The timeframes are different from Figure 26. The reason why they are different is because a dynamic equilibrium is reached much faster. Within 7000 years (top 3 + bottom left) the volumes of salt and fresh groundwater seem at equilibrium.	31 -
Figure 28: Cross section through the Irrawaddy delta for scenario A1B1C. At 60.000 years (bottom right) there is still a large brackish and salt groundwater volume inland.	32 -
Figure 29: Cross section through the Irrawaddy delta for scenario A1B2C2. At 60.000 years (bottom right) all offshore cells are salt (TDS >5 g/L). When comparing the results to figure 28 it becomes clear that deep salt groundwater is stagnant in Figure 28.	32 -
Figure 30: Evolution of fresh water volumes in the Irrawaddy delta for scenarios A1B1C3 and A2B2C1. The lines almost meet which means that almost the same fresh water volume is present at the dynamic equilibrium. -	33 -
Figure 31: Translucent top view of the Irrawaddy delta for scenario A1B1C3 . In the first 12.000 years (top 3) the fresh water volume changes significantly. From 20.000 - 60.000 years (bottom) the fresh water volume still changes slowly.	34 -
Figure 32: Translucent top view of the Irrawaddy delta for scenario A2B2C1 (add:). 6 frames from 0 - 7000 years are shown. In 7000 years all offshore cells get a concentration of 35 g/L TDS.	34 -
Figure 33: Top view and cross sections in X and Y-direction at t=60.000 years for Scenario A1B1C3. A small amount of salt groundwater is present in the deep inland parts of the Irrawaddy delta.	35 -
Figure 34: Top view and cross sections in X and Y direction at t= 60.000 years for A2B2C1. All offshore cells are salt and a brackish fresh/salt interface has formed inland. The cross sections look similar to figure 33.	35 -
Figure 35: The average computational time it takes to model 1 scenario to compute the head and concentration for the 6 deltas	36 -
Figure 36: The average computational time it takes to model 1 delta to compute the head and concentration for 11/12 scenarios.	36 -
Figure 37: Comparison of the computed fresh water volume over time for the MOC, FD and TVD solver.	37 -
Figure 38: Top view of concentration difference for scenario A1B1C1. From top to bottom = TVD minus FD, MOC minus FD and TVD minus MOC.	38 -
Figure 39: Comparing different conductivities of the top layer for scenario A1B1C1 and A2B2C1. The Krishna model was used to construct the sensitivity analysis for hydraulic conductivity of the confining top system. -	39 -
Figure 40: Cross sections through the Krishna delta for scenario A1B1C1. Different conductivities of the top layer have a strong effect on the dynamic equilibrium of fresh and salt groundwater. The higher the conductivity of the top system the more salt groundwater remains stable inland.	39 -

List of Tables

Table 1: Global data sets	- 13 -
Table 2: Settings and coordinates per delta to smoothen the rasters with the Focal statistics tool after using the IDW kriging tool in ArcMap 10.5	- 14 -
Table 3: Set variables in the DSP package.	- 20 -
Table 4: Parameters for the slope of the equation of state.	- 21 -
Table 5: Abbreviations for all 12 modelled scenarios.	- 22 -
Table 6: The range in computed fresh groundwater volume.	- 30 -
Table 7: Difference in computational time per solver.	- 37 -

Abbreviation

LGM	Last Glacial Maximum
TDS	Total Dissolved Solids
RSL	Relative Sea Level
DEM	Digital Elevation Model
ATE	Aquifer Thickness Estimation
IDW	Inverse Distance Weighting
SRTM	Nasa Shuttle Radar Topographic Mission
GEBCO	General Bathymetric Chart of the Oceans
MODFLOW	Modular Three-Dimensional Finite-Difference Ground-Water Flow-Model
Bm ³	Billion kubic meters
Kyrs	Thousand years
SEAWAT	Generic MODFLOW/MT3DMS-based computer program designed to simulate three-dimensional variable-density groundwater flow coupled with multi-species solute and heat transport
MT3DMS	Modular Transport Three Dimensional Model Simulator
WGS	World Geodetic System
UTM	Universal Transverse Mercator
A1B1C1	Closed _ Salt-To-Fresh _ Clay-On-Top
A1B1C2	Closed _ Salt-To-Fresh _ Clay-Layers
A1B1C3	Closed _ Salt-To-Fresh _ Gaps-Clay_Layers
A1B2C1	Closed _ Fresh-To-Salt _ Clay-On-Top
A1B2C2	Closed _ Fresh-To-Salt _ Clay-Layers
A1B2C3	Closed _ Fresh-To-Salt _ Gaps-Clay_Layers
A2B1C1	Open _ Salt-To-Fresh _ Clay-On-Top
A2B1C2	Open _ Salt-To-Fresh _ Clay-Layers
A2B1C3	Open _ Salt-To-Fresh _ Gaps-Clay_Layers
A2B2C1	Open _ Fresh-To-Salt _ Clay-On-Top
A2B2C2	Open _ Fresh-To-Salt _ Clay-Layers
A2B2C3	Open _ Fresh-To-Salt _ Gaps-Clay_Layers

1. Introduction

1.1 Background

Coastal regions have always been and still are associated with a large and growing concentration of human population, socioeconomic activities and therefore include many of the world's largest cities (Small and Nicholls, 2003). One third of the world's population lives within 100 km from the shoreline (Oude Essink, 2001; De Louw, 2013). This includes 12 of the 16 world's cities with populations greater than 10 million (Nicholls et al., 2007). High population densities in deltaic areas create a very high demand for high-quality fresh water. To meet this demand, groundwater is extracted. In general, groundwater is of high quality compared to surface water, and available in large quantities (Oude Essink, 2001). This being said, freshwater resources are not inexhaustible and extraction can lead to a series of problems.

Fresh groundwater extraction, together with a rising sea level, pollution, land subsidence and coastal erosion threaten these densely populated areas. A strong trend in urbanization of coastal areas (Nicholls and Lowe, 2004), will likely further increase the problems deltaic areas are facing. One of the consequences of sea level rise, land subsidence, coastal erosion and fresh groundwater extraction is saltwater intrusion, being (Custodio & Bruggeman, 1987; Stuyfzand & Stuurman, 1994; Oude Essink 2001; Post & Abarca, 2010; Oude Essink et al., 2010; Werner et al., 2013, de Louw, 2013) the encroachment of saline water into fresh groundwater (Werner & Simmons, 2009). In low lying areas, salt groundwater can reach the subsurface by upward groundwater flow. This process is called 'saline seepage' (de Louw, 2013). Salt water intrusion forms a threat to low lying areas all around the world. Salinization of groundwater used for drinking water threatens the livelihoods of the people in the delta and the vicinity of the delta. Also, saline seepage can result in poor crop yield when salt groundwater enters the root zone, affecting crop growth (Oude Essink et al., 2010; de Louw, 2013). Salinization of the freshwater resources will affect the population, agriculture and industries using fresh groundwater and surface water as a natural resource.

To predict whether saltwater intrusion threatens the available fresh groundwater in the present situation or in the future, groundwater flow models with variable density can be constructed. Together with measurements these groundwater models can be validated and used to make water management plans to ensure a sustainable freshwater future. But what if a regional data is not available, the area is too remote to acquire the data or the area is not accessible due to present conflict? Some innovative rapid data collections such as airborne geophysical surveys seem promising (Delsman et al., 2018; Siemon et al., 2017), but is still labour intensive and rather expensive.

To reduce saltwater intrusion and the problems associated with it, countermeasures need to be taken. These measures can be either technical or administrative. Technical measures such as desalinization or land reclamation can be very costly and developing countries often do not have the resources to implement these expensive technical measures. Monitoring and measuring the amount of fresh and salt water in the subsurface is a good way to know the current state of the system. Measurements can also help to evaluate hydrogeological models. In the last few decades, modelling of variable density groundwater flow has made big steps forward. The models have become larger, more detailed and faster. The improvement opens the door to model major delta systems in a short amount of time. Hydrogeological models can help to get insight into future scenarios such as business as usual extraction rates or the effect of the implementation of a certain measure to increase sustainable use of resources.

1.2 Problem definition

Making a 3D variable-density groundwater model is difficult for various reasons. The lack of subsurface data makes modelling of certain areas almost impossible. With the improvements in computational facilities and datasets, deltaic areas could possibly be modelled. Making these models can be a time-consuming process and therefore alternatives have to be found to speed up the modelling process while

limiting the deterioration of the quality of the models. When good quality 3D variable-density groundwater flow models can be constructed for a lot of deltas, decision makers for water management in all parts of the world can be assisted tools to predict the fresh groundwater reserves in the future. With a growing world population and a rising sea level, this is of vital importance for most deltaic areas in the world.

Fast construction of 3D groundwater models from global data is still in its infancy. Simplifications and assumptions about geology complexity have to be made because there is no hydrogeological dataset which covers all deltaic areas. 12 different hydrogeological scenarios were created to test how hydrogeology can affect the distribution of fresh and salt groundwater.

When making a 3D numerical groundwater model with variable density flow using global data as input datasets, the initial distribution of fresh and salt groundwater is unknown. A paleo reconstruction of the salt distribution is one of the procedures/methods to predict where salt water is most likely present in the subsurface (Delsman et al., 2014). To make a paleo reconstruction of the salt distribution one moment be taken as a starting point for the modelling where the distribution of salt is presumably known. One of the possibilities is the low stand during the last glacial maximum (LGM) 21.000 years ago. The sea level stood 120-130 meters lower than today (Lambeck, Yokoyama, Purcell, 2002). This period can be taken to estimate the initial saltwater distribution of a model area. The Holocene sea level transgression can be modelled and the current salt/fresh distribution constructed (Delsman et al., 2014). Post et al. (2003) showed extensive freshening of the Pleistocene aquifers in the Weichselien glacial period (Last glacial maximum LGM) prior to the Holocene interglacial. This assumption does however not take into account that saltwater might have been trapped when the sea level was higher in aquifers older than the Pleistocene aquifers. This very old saline groundwater will be called “paleo saltwater”. If not all paleo saltwater was flushed out before the end of the LGM the initial estimation of the fresh salt distribution can be false.

1.3 Objectives

The research objective is to construct plausible 3D density variable groundwater flow models in a relatively short amount of time using global data sets. To make a better estimation of the initial salt distribution at the start of the paleo reconstruction, better understanding of the time it takes for a completely distorted fresh/salt distribution to reach its equilibrium must be known. This equilibrium time will be called Tau (τ). The models need to be able to predict the fresh groundwater volume, and equilibrium time under 12 different scenarios. The models will cover the following areas:

- Irrawaddy delta in Myanmar
- Krishna/Godavari delta in India
- Shatt al Arab delta, Gulf of Persia
- Nile delta in Egypt
- Niger delta in Nigeria
- Orinoco delta in Venezuela

1.4 Research questions

1.4.1 Main research question:

To what extent are 3D models of variable density-groundwater flow and coupled salt transport constructed with global hydro(geo)logical data sets able to properly represent hydrogeological processes?

To address the main research question, different sub-research questions need to be answered.

1.4.2 Sub-research questions:

- a) *What are the most relevant hydrogeological processes that have to be taken into account to end up with a plausible model? (River network, geometry of the system, geology, precipitation, boundary conditions)*
- b) *What is the equilibrium time (time to the dynamic equilibrium of the fresh-saline distribution) of the different delta models? How far back in time do you need to go to determine the initial fresh-saline distribution with paleo-reconstruction?*
- c) *What factor (theme/process/parameter/solver) causes the biggest increase in computational time?*
- d) *Can salt water older than the Holocene be present in deep parts of a delta?*

1.5 Organisation of report

To meet the research objectives and to answer the main and sub research questions a thorough understanding of the involved hydrogeological processes must be acquired. Chapter 2 will give the background in hydrological modelling, information about salt water intrusion and information about the model areas. In chapter 3 the research methodology will be discussed, explaining which global data was acquired and how it is used. Also, the model setup and different theoretical geological scenarios for the models will be given in this chapter. Chapter 4 shows the results for the initial results, the results for the 12 dynamic equilibrium time scenarios and will show the differences in computational time per scenario, delta and solver. In Chapter 5 the different hypotheses will be discussed. Chapter 6 will give the conclusion to the main research question and the sub research questions. In Chapter 7 recommendations for further use of the models will be given. An overview will be given how 3D groundwater models with variable-density flow made with global data sets can be further improved to increase their value as a tool for policymakers and water management plans. The thesis ends with references (chapter 8) and appendices (chapter 9).

2. Background groundwater modelling, salt water intrusion and study areas

2.1 Theoretical background in groundwater processes and modelling

2.1.1. Introduction

Different hydrogeological processes need to be solved in order to make a 3D numerical groundwater model with hydrogeological transport phenomena and variable density flow. The groundwater flow equation needs to be solved with a variable density term, and the coupled transport flow equation needs to be solved. The higher the salinity of water, the higher the density (when temperature and pressure are constant). When modelling the fresh/salt groundwater distribution, this density-driven flow is a key factor in the displacement and mixing of fresh and salt groundwater. The models were made using iMOD-SEAWAT software (Langevin et al., 2003). The different characteristics of groundwater flow in coastal aquifers will be discussed in this chapter.

2.1.2. Groundwater flow equation

iMOD-SEAWAT uses parts of the MODFLOW (McDonald and Harbaugh, 1988) code that solves the groundwater flow equation. The movement of groundwater is described with Darcy's law (1) in the x-direction.

$$q_x = -K_x \frac{\partial h}{\partial L_x} \quad (1)$$

- q_x = flow rate in the x direction ($\frac{L}{T}$)
- K_x = hydraulic conductivity in the x direction ($\frac{L}{T}$)
- ∂h = head difference (L)
- ∂L_x = difference in length (L)

The United States Geological Survey (USGS) developed MODFLOW in the early 1980's. MODFLOW has since then developed (McDonald and Harbaugh, 2003). The core, however, remains the same. "The 3-dimensional movement of groundwater with a constant density is described by the partial differential equation" (2) (McDonald and Harbaugh, 1988).

$$\frac{\partial}{\partial x} * \left(K_{xx} \frac{\partial h}{\partial x} \right) + \frac{\partial}{\partial y} * \left(K_{yy} \frac{\partial h}{\partial y} \right) + \frac{\partial}{\partial z} * \left(K_{zz} \frac{\partial h}{\partial z} \right) - W = S_s \frac{\partial h}{\partial t} \quad (2)$$

- K_{xx}, K_{yy}, K_{zz} are hydraulic conductivities along the x, y and z-direction (units length /time (LT^{-1}))
- h = hydraulic head (units length (L))
- $\partial x, \partial y, \partial z$ = difference in length in the x, y and z- direction (units length (L))
- W = volumetric flux which represents the source and sinks of water (units T^{-1})
- S_s = specific storage (L^{-1})
- t = time (T)

"The equation assumes that the axes of the hydraulic conductivities are aligned with the direction of the coordinates x, y and z" (McDonald and Harbaugh, 1988). Finite difference method describes the flow towards and from a cell in 6 directions in 3D (figure 1).

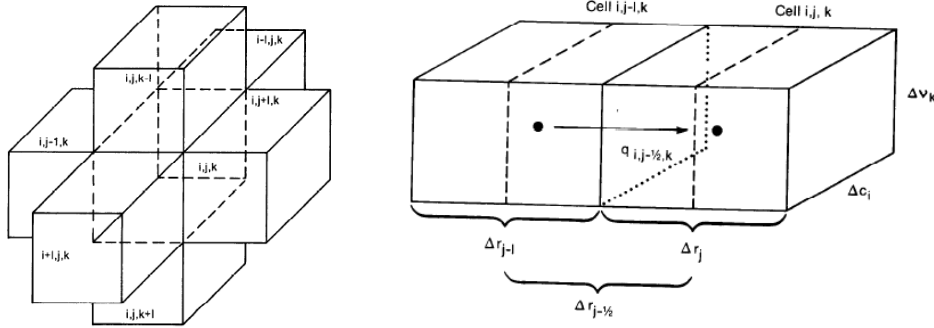


Figure 1: Left: the 6 directions in the 3D groundwater model to where water can flow. Right: the flow has to be calculated from the centre of one cell to the centre of another cell (from $i, j-1/2, k$ to $i, j+1/2, k$) (McDonald and Harbaugh, 1988)

By determining the equation of flow for 6 directions and accounting for external sources or stresses, the specific storage can be given as shown in equation 3 (McDonald and Harbaugh, 1988).

$$q_1 + q_2 + q_3 + q_4 + q_5 + q_6 + P + Q = SS * dh/dt \quad (3)$$

- $q_1, 2, 3, 4, 5, 6$ = flow from a centre of a cell to the centre of a neighbouring cell in 6 directions.
- P = external negative flow
- Q = external positive flow
- SS = specific storage
- dh/dt = difference in head over difference in time.

The linearization in 6 directions is necessary for the finite difference method to numerically solve this partial differential equation. The full derivation can be found at McDonald and Harbough (1988) (p 2.7 to 2.19).

2.1.3. The variable density groundwater flow equation

To model groundwater flow with variable density, the partial differential equation (2) from McDonald and Harbaugh (1988) needs to be adjusted. MODFLOW itself cannot calculate variable-density flow or groundwater flow with coupled transport. A computer program that does account for variable density in groundwater flow and transport phenomena is SEAWAT (Langevin et al., 2003). SEAWAT and MODFLOW are coupled in the iMOD-SEAWAT software (Verkaik and Janssen, 2015). The software solves the groundwater flow equation with variable density (4) and can solve for the solute transport equation (4) using the implicit finite-difference method (Langevin et al., 2003).

Saturated variable-density groundwater flow equation (Langevin et al., 2003)

$$\nabla * \left[\rho K_f \left(\nabla h_f + \frac{\rho - \rho_f}{\rho_f} \nabla z \right) \right] = \rho S_{sf} \frac{\partial h_f}{\partial t} + n \frac{\partial \rho}{\partial c} \frac{\partial c}{\partial t} - \rho_s q'_s \quad (4)$$

- ∇ = differential operator = $(\frac{\partial}{\partial x}, \frac{\partial}{\partial y}, \frac{\partial}{\partial z})$
- $h_f = \frac{p}{\rho_f g} + z$ Fresh water head (L) (Luszczynski, 1961)
- $\frac{p}{\rho_f g}$ = pressure head (M/L/T²)
- z = elevation head (L)
- p = fluid pressure Pa (N/L²)
- ρ = density of the solute (M/L³)
- ρ_f = density of the fluid (M/L³)

- g = gravitational acceleration (L^2/T)
- $K_f = k\rho_f g/\mu_f$ = Freshwater hydraulic conductivity tensor
- μ_f = dynamic viscosity of the fluid ($M/L/T$)
- k is the permeability tensor (L^2)
- S_{sf} = fresh water specific storage (L^{-1})
- n = porosity (-)
- C = concentration of solute (M/L^3)
- q'_s = source or sink with density (ρ_s)

General solute transport equation (Zheng and Wang, 1999):

$$\frac{\partial(nC)}{\partial t} = \nabla * (nD * \nabla C) - \nabla * (qC) - q'_s C_s \quad (5)$$

- D = hydrodynamic dispersion coefficient (L^2/T)
Hydrodynamic dispersion consists of two processes: mechanical dispersion caused by velocity variations in the pores, and molecular diffusion which is caused by the random movement of molecules in a fluid (Oude Essink, 2001)
- C_s = sink or source concentration M/L^3

Concentrations resulting from the solute transport equation are used by an equation of state to calculate the fluid density (Langevin & Guo, 2006).

$$\rho_{i,j,k} = \rho_f + \frac{\partial \rho}{\partial C} * C_{i,j,k} \quad (6)$$

- $\rho_{i,j,k}$ = density of the fluid at i,j,k ($\frac{M}{L^3}$)
- ρ_f = density of the water (M/L^3)
- $\partial \rho$ = difference in density between water and fluid (-)
- ∂C = difference in concentration between freshwater and fluid (-)
- $C_{i,j,k}$ = concentration of the fluid ($\frac{M}{L^3}$)

For more information see Langevin & Guo (2006) and Zheng and Wang (1999)

2.1.4. Dynamic equilibrium and equilibrium time Tau (τ)

When there is no data on the distribution of fresh and salt groundwater, a paleo reconstruction can help to make an estimation of the fresh/salt distribution. Delsman et al. (2014) used this conceptual method to model the present day distribution for the coastal area of the Netherlands. Due to regression and transgression of the sea level, a delta is rarely in equilibrium. The long timescales involved in the build-up of a delta often still reflects events which occurred thousands or even million years ago (Vallejos et al., 2017; Delsman, 2014; Groen et al., 2000; Post et al., 2003; Stuyfzand, 1993). The time it takes under constant conditions for a completely distorted system to reach a dynamic equilibrium of what with constant boundary conditions is called the equilibrium time Tau (τ)(Figure 2). This thesis will describe and test the method to find Tau for six different deltas under different geological scenarios. That knowledge can help paleo-reconstructive models to estimate how far back in time they should go the make a more accurate fresh/salt distribution with little to no knowledge of the present-day situation. Figure 6 shows the sea level estimations by Waelbroeck et al. (2002). Around 130.000 years ago the estimated mean sea level was higher than it is today. Salt groundwater which intruded in the deltas from 150.000 to 130.000 years ago could be trapped in the deeper parts of the delta systems. Deep sediments in deltaic areas can be millions of years old (van Engelen et al., 2018 (Egypt); Amajor, 1991 (Niger); Berendsen, 2004 (Netherlands) so the possibility of salt water entering a system and staying there for a long period of time is very plausible.

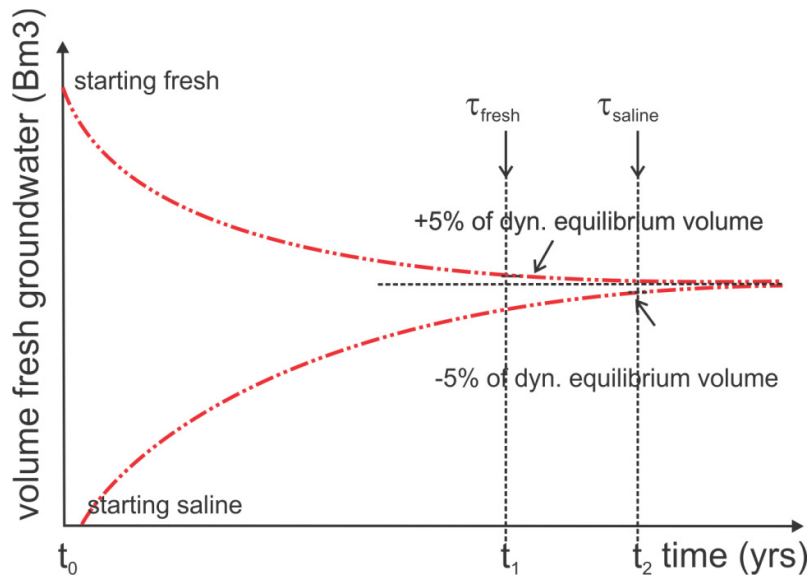


Figure 2: A theoretical representation how dynamic equilibrium time τ can evolve. At $t=0$ the system is disturbed (delta is completely filled with either only fresh or salt groundwater). At $t=1$ the dynamic equilibrium time starting saline is reached. At $t=2$ the dynamic equilibrium time starting fresh is reached (Oude Essink & Waterman, 2018).

2.2 Salt water intrusion

2.2.1. Fresh saline groundwater distribution

Under constant pressure and temperature, the density of groundwater depends only on the number of total dissolved solids (TDS) in the water. Therefore the density of water is directly related to the total dissolved solids. In coastal regions chloride, sodium, potassium, calcium, sulphate and magnesium are dissolved in the water (Nayar et al., 2016; Mostafa et al., 2010). Other dissolved solids are solved in a negligibly small amount. The general composition of the main total dissolved solids (TDS) in sea water is shown in figure 3.

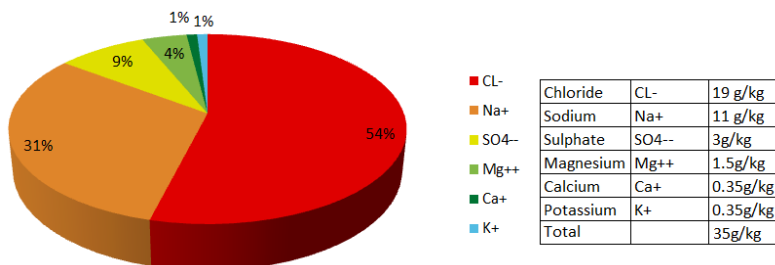


Figure 3: The general composition of sea water. Chloride, Sodium, Sulphate, Magnesium, Calcium and Potassium are the most important total dissolved solids (TDS) in sea water. The table on the left shows that for sea water, in general, the concentration of the TDS makes up 35g/L.

At atmospheric pressure and at 20 degrees Celsius, water with a concentration of 35g/L TDS, has a density of 1024.9 kg/m³. Appendix A (Nayar et al., 2016; Mostafa et al., 2010) shows the density of water under different salinity and temperature conditions. As shown in the table 35g/L is not the maximum concentration of TDS. It is only the average concentration of TDS in sea water. When water has a salinity of > 35 g/L it is called “hypersaline” (van Engelen et al., 2018) or “brine”. Seawater is not the only source for saline groundwater. Figure 4 shows the hydrological cycle for the natural origin of saline groundwater in aquifers. Knowing that sea water is not the only cause for salinization of groundwater is important because if other sources are not taken into account the amount of fresh groundwater in the system can be overestimated. The dissolution of marine evaporates can enhance salinization of groundwater at great

depth. Extraction of fresh groundwater can further enhance salinization because of the upconing of salt water into fresh groundwater aquifers (Oude Essink et al., 2010; de Louw, 2013).

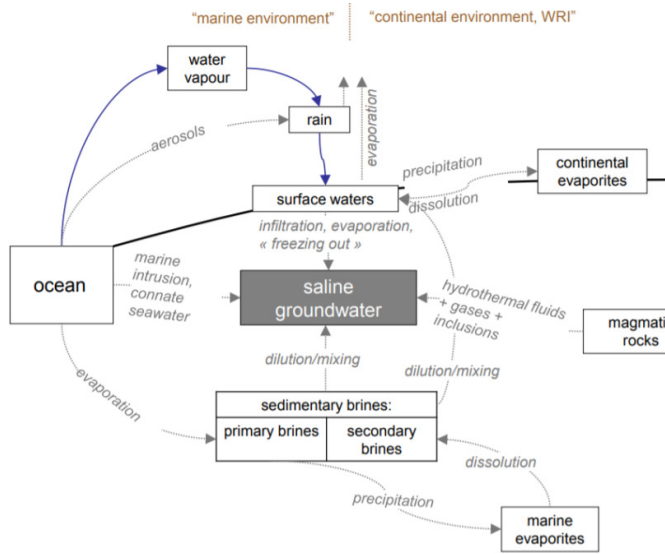


Figure 4: The different sources which contribute to the salinization of groundwater. sea water intrusion is the most important process, but inland different sources can also contribute to salinization of groundwater (Kloppmann et al., 2010).

2.2.2. Badon Ghijben Herzberg principle

The Badon-Ghijben Herzberg principle (7) describes the relationship between fresh and salt water in a unique system under the following conditions (Oude Essink, 2001):

- The fresh salt interface forms in a homogeneous aquifer
- There is no horizontal flow in the aquitard
- There is no vertical flow in the aquifer
- Hydrodynamic dispersion is negligible
- The system is in a (dynamic) equilibrium

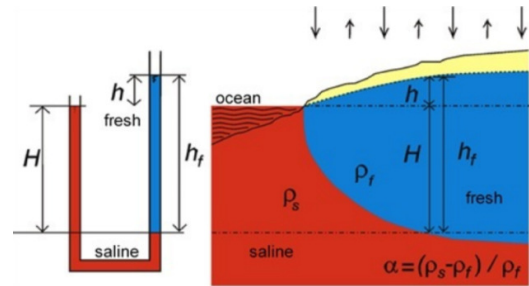


Figure 5: A cross section showing how the Badon Ghijben Herzberg principle works. The salt/fresh groundwater interface in this homogeneous aquifer is formed by the relative difference in density of fresh and salt groundwater (Oude Essink, 2014).

These unique conditions are sometimes met for unspoiled sand dunes and or (coral) islands (Figure 5) (Oude Essink, 2001). In the case of the 6 deltas, these conditions are not met and the fresh salt interface will most likely form in a different way. However, the general principle of salt and fresh groundwater in a system creating density-driven flow holds.

$$h = \frac{\rho_s - \rho_f}{\rho_f} H \leftrightarrow h = \alpha H \quad (7)$$

h = piezometric head from the top of the water table to the mean sea level (L)

H = Depth from the mean sea level to the fresh salt interface (L)

ρ_f = reference density (in this case the density of fresh water (1000 kg/m³)

ρ_s = density of sea water (1025 kg/m³)

α = relative density difference

For $\rho_f = 1000 \text{ kg/m}^3$ & $\rho_s = 1025 \text{ kg/m}^3 \rightarrow \alpha = 0.025$

2.2.3. Eustatic and relative sea level change.

Suess (1906) was the first to describe the transgression and regression of the sea level with the term “eustasy” (Rovere et al., 2016). Suess was also the first who suggested that old shorelines (preserved in sediment) observed below and above the present sea level could be linked to glacial and interglacial periods. According to the term “eustasy” of Suess, the polar ice sheet and oceans mass variation would result in a uniform global sea level rise or drop (Rovere et al., 2016). Figure 6 shows the eustatic sea level changes for the past 450 thousand years, the past 5 million years and the past 35 million years. Periods of transgression and regression form a saw tooth pattern in the sea level variations.

During the Pliocene, the sea level could be as much as 25 meters higher than present. On average the temperature during the Pliocene was only 1-2 degrees warmer than in pre-industrial times. The Panama seaway was open and the strong arctic warming contributed to this high sea level. The closure of the Panama seaway changed the thermohaline circulation of the oceans (Bartoli, 2005). This resulted in the climate crash 2.74 million years ago.

Sea level rise has geographic variability, triggered by ice and water load variations. These variations cause earth deformations and gravitational and rotational perturbations that give rise to the spatial varying sea level changes (Kopp et al., 2015; Rovere et al., 2016). Together, the solid earth surface movement and the eustatic sea level variations are called the relative sea level (RSL) change.

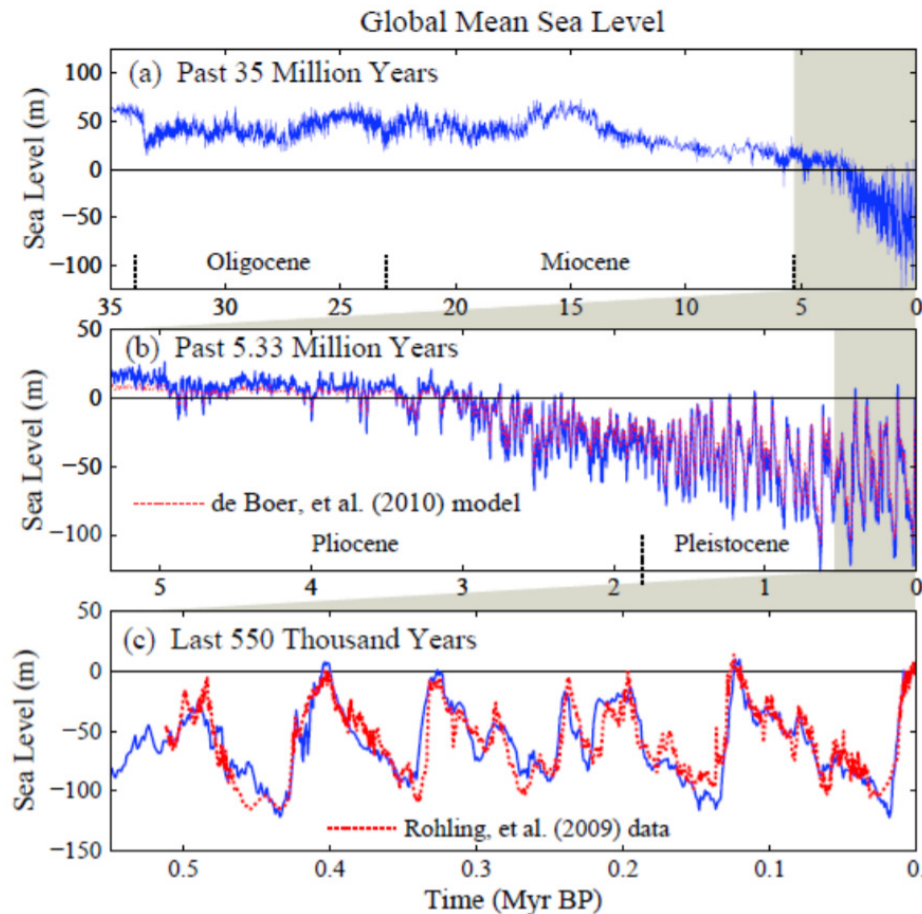


Figure 6: (a) The estimated eustatic sea level for the last 35 Million years, estimated with $\delta^{18}\text{O}$ values by Zachos et al. (2008). (b) The estimated sea level for the last 5 million years (de Boer et al., 2010). In the Pliocene the sea levels were 25 meters higher compared to the Pleistocene. The temperature was only 1-2 degrees warmer. Arctic warming and an open Panama seaway contributed to the high sea level. (c): The estimated sea level for the last 550 kyr. 120 kyr ago the sea level was higher than today. The figure consists of coral reef low stand estimates by Rohling et al. (2009). (Hansen et al., 2013)

A delta which started to build-up during the Pliocene would have been largely submerged compared to the position of the delta today. This has to do with the relative sea level decline during the Pliocene. The delta system build-up and the sea level dropped. Because this did not happen gradually, salt and fresh groundwater can get trapped in either transgression or regression periods. The time it takes for a disturbed major deltaic system to reach a state of a dynamic equilibrium when the boundary conditions do not change has not yet been studied.

2.3 Information model area

The choice of the following six deltas was based on the following criteria:

First, the estimation of the bottoms of the deltas by Zamrsky (2018) had to cover a large part of the study area. Some deltas were covered better than others so this had to be incorporated in choosing the deltas in the beginning. Second, the deltas should not all be situated in or around the same continent. Third, the models preferably cover developing countries where groundwater models are scarce. In this way, the models built can provide a base for modelling these areas in the future. The study area of the 6 models will briefly be discussed:

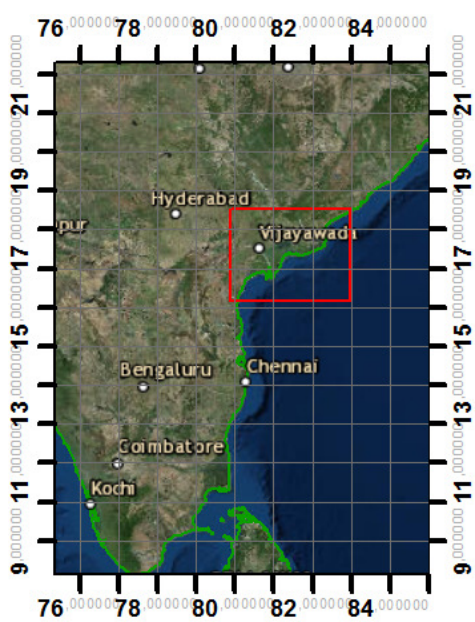
Name of the delta	Krishna-Godavari, India	
Total area of the catchment	Krishna 258.948 km ² Godavari 314.829 km ² (Kumar et al. 2005)	
Population density	729 people per km ² (WRI, Watersheds of the world, 2005)	
Delta classification according to Galloway(1975)	Wave and fluvial dominated system	
Discharge of the main rivers	The Krishna yearly discharges 69.8 km ³ of water and the Godavari 110.5 km ³ / year (Kumar et al. 2005).	
Age of the delta	Neogene origin (NDR India, 2018)	
Trivia	- The Krishna Godavari delta is a delta comprising of 2 delta systems fed by the Krishna and Godavari rivers draining into the Bay of Bengal.	

Figure 7: model area of the Krishna-Godavari delta in red.

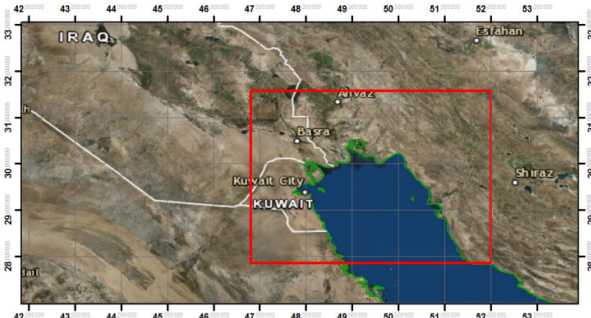
Name of the delta	Shatt al Arab, Iraq and Kuwait	
Total area of the catchment	765.742 km ² (WRI, Watersheds of the world, 2005)	
Population density	57.17 people per km ² (WRI, Watersheds of the world, 2005)	
Delta classification according to Galloway(1975)	Tide-dominated system	
Discharge of the main rivers	84.2 km ³ per year (Isaev, & Mikhailova, 2009)	
Age of the delta	10.000 years (Holocene origin)	
Trivia	The Shatt al Arab river is one of the few rivers where its tributaries are more famous than the river itself. Because the Euphrates and the Tigris flow through the catchment independently and only merge at the very end of its course into the Persian Gulf (Isaev, & Mikhailova, 2009).	

Figure 8: model area of the Shatt al Arab delta in red.

Figure 8: model area of the Shatt al Arab delta in red.

Name of the delta	Irrawaddy, Myanmar
Total area of the catchment	$0.7 \cdot 10^6 \text{ km}^2$ (Robinson et al. 2007)
Population density	583 people/ km^2
Delta classification according to Galloway(1975)	tide-dominated system (Hayes, 1979; Orton and Reading, 1993; Hedley et al. 2010)
Discharge of the main rivers	$442 \text{ km}^3/\text{year} \pm 41 \text{ km}^3$ containing 226 – 364 mega-tonnes (Mt) of sediment to the ocean (Robinson et al. 2007)
Age of the delta	50 million years (Eocene origin)(Nyi Nyi 1967; Bender 1983)
Trivia	<ul style="list-style-type: none">- Tidal influences reach as much as 300 km inland(Hedley et a. 2010), with saline water intruding up to 100 km upstream(Aung, 2003)- During glacial periods the sea level was much lower. The shape and depth of the Martaban canyon under the Gulf of Martaban indicates that it is a relict feature of a much larger paleo Irrawaddy delta system (Nyi Nyi, 1967).

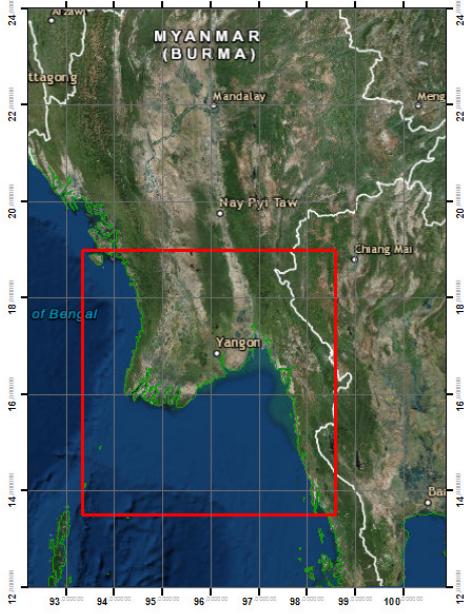
A topographic map of Myanmar (Burma) and surrounding regions. The map shows the Irrawaddy River flowing from the north towards the Bay of Bengal. A red rectangle is drawn over the lower portion of the river, indicating the model area. Key locations labeled include Mandalay, Nay Pyi Taw, Yangon, and Chiang Mai. The Bay of Bengal is visible to the west. The map includes latitude and longitude coordinates along the edges.

Figure 9: model area of the Irrawaddy delta in red.

Figure 9: model area of the Irrawaddy delta in red.

Name of the delta	Niger delta, Nigeria
Total area of the catchment	2,261,741 km ² (WRI, Watersheds of the world, 2005)
Population density	31.4 people per km ²
Delta classification according to Galloway(1975)	Modern delta: wave dominated (Durogbitan,2016; Galloway,1975)
Discharge of the main rivers	190 km ³ /year (Milliman and Farnsworth, 2013)
Age of the delta	Miocene (Amajor,1991)
Trivia	In the Miocene, the Niger delta was a fluvial dominated system.

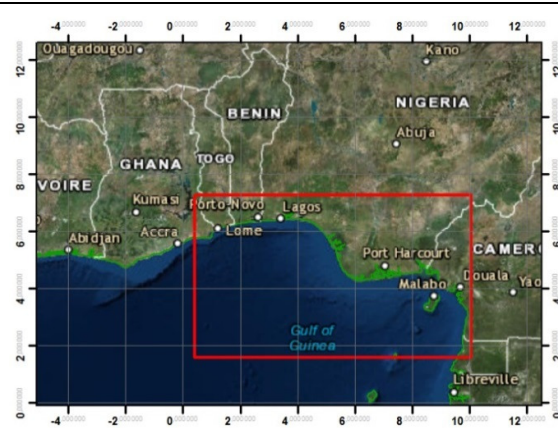


Figure 10: model area of the Niger delta in red.

Name of the delta	Nile delta, Egypt
Total area of the catchment	3,254,853 km ² (WRI, Watersheds of the world, 2005)
Population density	46.2 people per km ² (WRI, Watersheds of the world, 2005)
Delta classification according to Galloway(1975)	Wave-dominated system (Anthony,2015; Galloway,1975)
Discharge of the main rivers	89.24 km ³ per year
Age of the delta	Middle Miocene (Rizzini et al., 1978)
trivia	The Nile river is the longest river system in the world and runs through 10 countries(World Resources Institute,2015) The Aswan dam constructed in the 1960s heavily regulates water flow towards the Nile delta and acts as a sediment trap, which enhances coastal erosion.

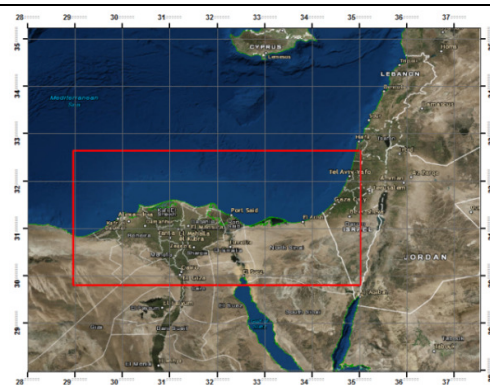


Figure 11: model area of the Nile delta in red.

Name of the delta	Orinoco delta, Venezuela
Total area of the catchment	1.1 million km ² (Seelinger & Kjerfve,2013)
Population density	16.93 people per km ² (WRI, Watersheds of the world, 2005)
Delta classification according to Galloway(1975)	Wave-dominated (Galloway,1975)
Discharge of the main rivers	1135 km ³ per year (MacKee et al, 1989)
Age of the delta	Late Miocene (Gamero,1996)
Trivia	Daily mean discharges can vary from 1,050 m ³ /s to 82,100 m ³ /s at the outflow point of the Orinoco river. On average the Orinoco has the 3 rd largest discharge of river systems in the world (Schot et al., 2001).

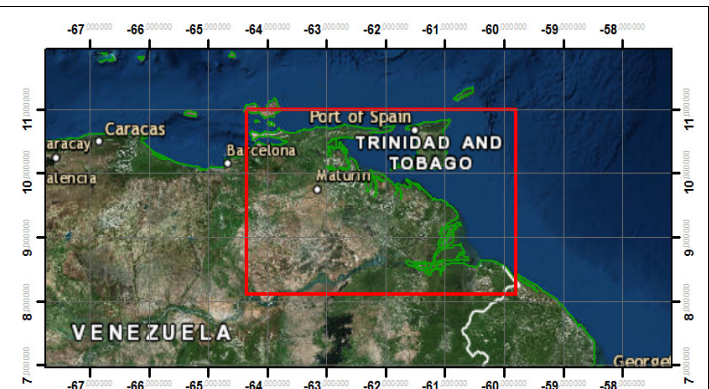


Figure 12: model area of the Orinoco delta in red.

3. Research methodology

3.1. Collection, clipping and adjusting of global data.

The objective of this thesis is to build models constructed with global datasets as input. The reason why only global data sets are used is to test the validity that everywhere on earth a 3D numerical groundwater model with coupled transport and variable density flow can be constructed. Local data is often not available so therefore global data is used in all 6 models. The different global data sets will be described in this section (for overview see table 1).

Table 1: Global data sets

Physical property	Global dataset
Digital elevation inland and offshore	GEBCO 2014 (Weatherall et al., 2015)
Bedrock	Dataset regolith thickness (Zamrsky et al., 2017)
Lithology top system	GLiM (Hartmann and Moosdorf, 2012)
River width and depth	GAIA Hartmann and Moosdorf (2012)
Paleo Precipitation	MIROC-ESM (Wanatabe et al., 2011)

3.1.1. General Bathymetric Chart of the Oceans (GEBCO):

The bathymetry is the underwater depth of a lake or the depth of the ocean floor (Weatherall et al., 2015). Over a century ago, in 1903 Prince Albert the first of Monaco initiated GEBCO with the goal of mapping the world's oceans (Hall, 2006). Nowadays GEBCO releases publically available grids of a digital bathymetric model of the world merged with land topography. These digital elevation models (DEM's) consist of a variety of data sets to cover the entire world (for example SRTM30_PLUS, NASA version 5.0 (Becker et al., 2009), (GMTED2010) dataset (Danielson and Gesch, 2011)). For the full list of data sets comprising the GEBCO_2014 version used as the top system in the models see Weatherall et al., table 1 (2015).

The GEBCO_2014 data consist of a world covering gridded data set with a grid spacing of 30 arcsec (figure 13). With ArcMap 10.5 the data was clipped by using the square shape files shown in red in the model area (Figures 7 – 12, “clip (data management)” tool Arcmap10.5) After the data was clipped the data was transformed from its geographic coordinate system to the projected coordinate system “WGS_1984_EASE-Grid_2.0_Global” using the tool “project raster” in ArcMap 10.5.

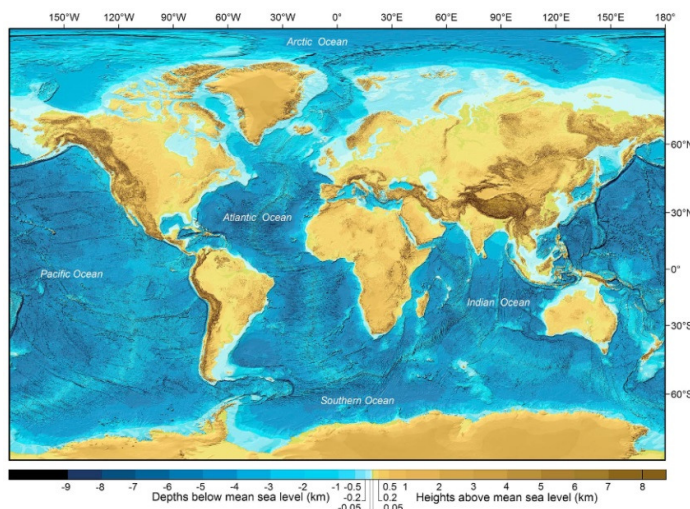


Figure 13, Visualization of GEBCO 2014, a global bathymetry and digital elevation map (Weatherall et al., 2015).

3.1.2. The estimated thickness of the deltas.

The estimation of the thickness of the delta's and therefore the base of the hydrogeological systems is generated by point estimations by Daniel Zamrsky. Zamrsky et al. (2018) constructed a coastal aquifer thickness estimation (ATE) method which uses data from:

- topography and bathymetry (Weatherall et al. 2015)
- thickness estimation of surface sediments (Pelletier et al. 2016)
- aquifer thickness estimations from the PCR_GLOBWB hydrological model (de Graaf et al. 2015)
- lithology (GLiM data set, Hartmann & Moosdorf, 2012)
- coastal position (Natural Earth, 2017)

The data consist of coastal points 5 km apart covering the entire world. Perpendicular to these coastal points, point estimations are made from the coast to 400km inland. The GLiM dataset (Hartmann & Moosdorf), which consist of a lithological map, is used to only make point estimations for places classified as unconsolidated matter (Zamrsky, 2018).

The coastal points and cross section points were merged in ArcMap using the “merge” tool. The merged shape files were clipped accordingly to the model domain of the 6 deltas. To convert the point dataset to a grid that covers the whole bottom of the model domain the inverse distance weighted interpolation (IDW tool) was used in ArcMap. This tool uses a linearly weighted combination of sample points (In our case the merged thickness estimation points). The weight is a function of inverse distance (Watson & Philip, 1985).

Due to the large number of points in some parts of the model domain the IDW gives a rather coarse representation of the estimated thickness of deltas. In order to smoothen the result, the tool “Focal Statistics” is used in ArcMap. The settings for each of the 6 models are shown in table 2. The choice of these settings has been made after visual inspection of the IDW results. The chosen settings smoothened local extreme values (very high or very low thickness estimations) that were not consistent with the surrounding area. In some cases, a single line with cross section points was removed after visual inspection if the thickness estimations were completely off (for example 3-7 km instead of 300 – 700 meters). In most cases these high estimations were cross sections that linked 2 parts of land with an ocean/ body of water in-between. The results of the bottoms are shown in appendix B

Table 2: Settings and coordinates per delta to smoothen the rasters with the Focal statistics tool after using the IDW kriging tool in ArcMap 10.5

	first			second			LL	UR coordinate
delta	geometry	Cells in rectangle	extent	geometry	Cells in rectangle	extent		
Irrawaddy	rectangle	35	minimum	rectangle	25	mean	9028304,1984197	9383304,2366197
KrishnaGodavari	rectangle	25	mean	-	-	-	7717892,1920937	7997892,2188937
Niger	rectangle	35	minimum	rectangle	25	mean	242848,271981	970848,893981
Nile	rectangle	25	mean	-	-	-	2797004,3632164	3383004,3948164
Orinoco	rectangle	25	mean	-	-	-	-6208133,1030505	-5736133,1396505
Shatt al Arab	rectangle	25	mean	-	-	-	4516186, 3415038	5021186,3836038

3.1.3. GAIA river network

The GAIA database (Andreadis, 2013) consists of river widths and depths (Figure 14 and 15.) based on hydraulic geometry equations and the HydroSHEDS hydrography data (Lehner et al., 2008). The great benefit of using GAIA instead of HydroSHEDS is the width estimation. Small and shallow rivers can be given a different conductance than larger rivers. This discretization was not possible in HydroSHEDS.

The function for river conductance (unit for interaction between river and groundwater) (McDonald and Harbough 1988)) is given as:

$$C = K * l * w / b \quad (8)$$

- C= conductance (m2/d)
- K = the hydraulic conductivity (m/d)
- l = length (m)
- w = width (m)
- b = thickness of streambed sediments (m)

GAIA only gives an estimation of the height of the water level in the river and the width of the river. The chosen dimensions of a modelcell are 1000*1000 m so the GAIA data has to be converted from estimated width to the estimated conductance of the river bed for a 1000*1000-meter modelcell. K is unknown and b is unknown and varies for different river types. However, for a rough estimation, the estimated width can still be used, and indirectly also the length. For all models, the river conductance is equal to 10 times the width of a river. The example in appendix C will show why this rough estimate makes sense. Variations in b or K, and up and downscaling for cells can, however, cause large differences in the river conductance (de Lange, 1996). A multiplication factor is, however, useful to distinguish between larger and smaller rivers.

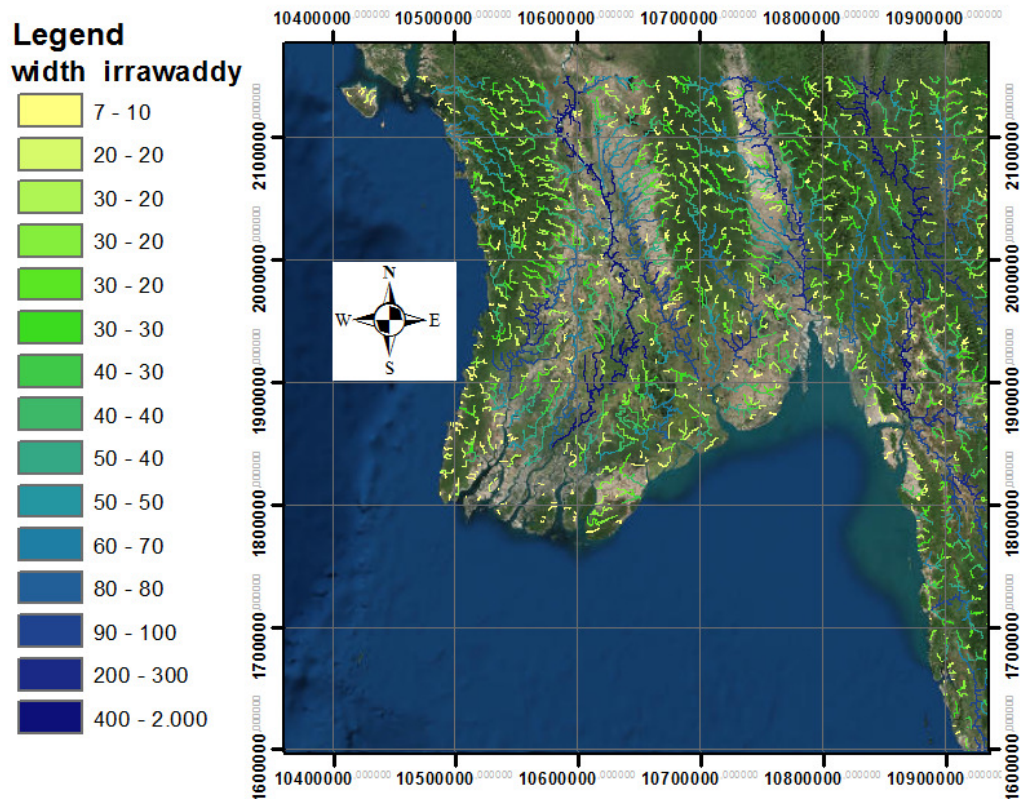


Figure 14: Clipped width for the rivers in the Irrawaddy. The width varies from 7 m to 2000m and is used to make an estimation on river conductance. The width estimation of the rivers comes from the GAIA data set.

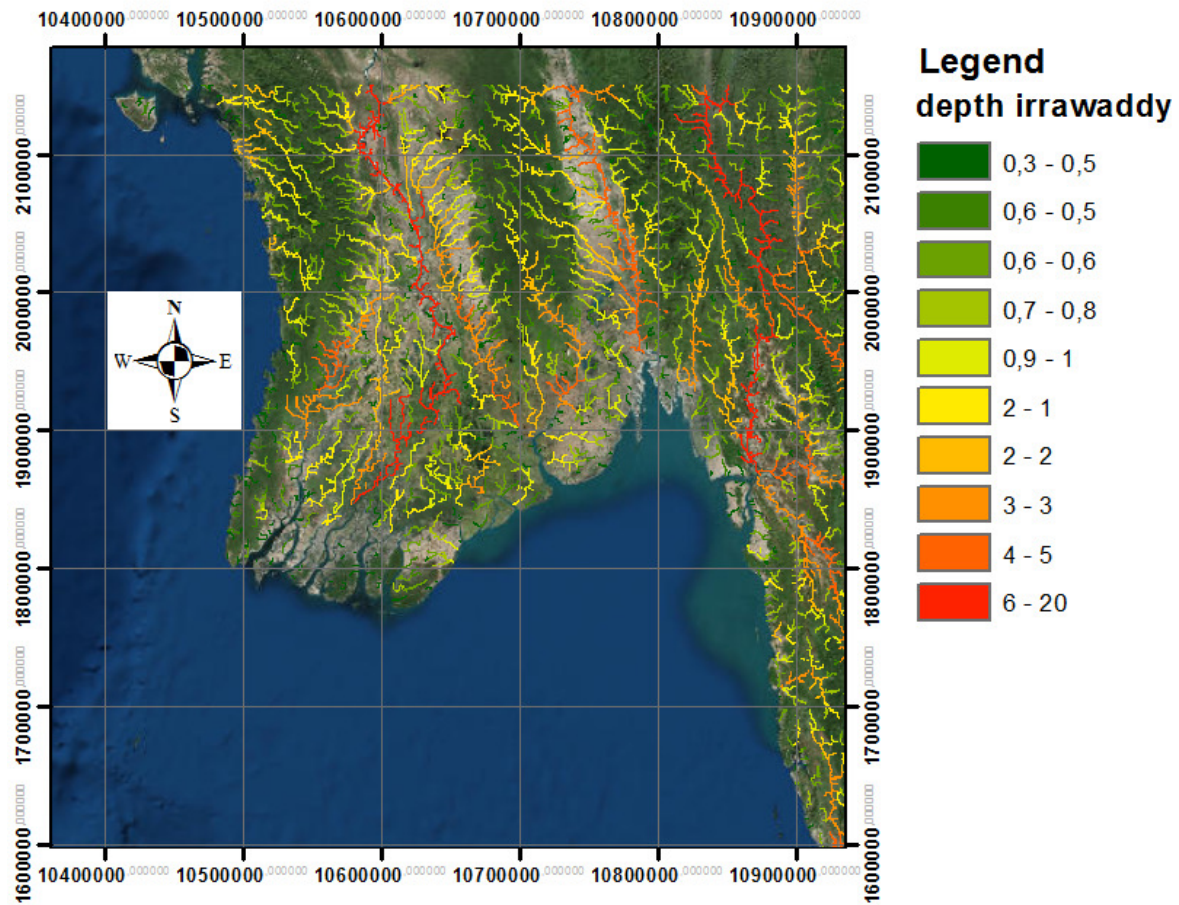


Figure 15: Clipped depth of the rivers in the Irrawaddy delta. The estimated depth of the rivers varies from 30 cm to 20 m. The depth estimation of the rivers comes from the GAIA data set.

3.1.4. The Global Lithological Map (GLiM)

GLiM is an assembly by Hartmann and Moosdorf (2012) of 92 regional lithological maps of the highest available resolution scale. It forms a world covering lithological map which in this case is used to outline the boundary of the model inland. The GLiM dataset was converted to an ASCi file in ArcMap using the tool “raster to ascii”. In iMOD, the classification of unconsolidated matter was used to form the active part of the model domain. This was relevant in order to outline the boundary conditions of the models.

3.1.5. PALEO precipitation (WorldClim1.4)

The paleo precipitation estimates come from the WorldClim1.4 (Hijmans et al., 2005) dataset collection. The specific data set used is the “precipitation over 22.000 years” from MIROC-ESM (Wanatabe et al., 2011). The paleo-precipitation is calculated with General Circulation Model (GCMs) simulations representing physical processes on the land surface, oceans and in the atmosphere. This result in temperature and precipitation estimates. The average precipitation over 22.000 years is given by the dataset in mm/month for each month. In ArcMap, these 12 monthly averages are converted to a yearly average. The difference between the MIROC-ESM paleo precipitation and the **GSMaP** data set (Okamoto et al., 2005; Kubota et al., 2007; Aonashi et al., 2009; Ushio et al., 2009) for the current precipitation estimates can be found in appendix D.

3.2. Initial model setup and setup for testing different geologies

This chapter will discuss the setup of the basic model with constant recharge and an initial salt concentration where all offshore cells are salt and inland cells are fresh. This basic model was made to test if the models were set up correctly and to correct for modelling errors. iMOD-SEAWAT uses a runfile with packages to set paths to input files and to set parameters. The input files are rasters with the extension IDF. This is the raster format used by iMOD (Vermeulen, 2006). Necessary IDF files for the model are for example the raster with the boundary conditions or the raster with the height of the river level. All these different packages with different parameters and IDF files will be discussed according to the complete runfile for the Irrawaddy model in appendix H.

3.2.1. Initial model and parameters

3.2.1.1. [GEN] General information package

The general information package holds the information on which packages are active. The lower left X and Y coordinates are stated in the GEN package. The clipped global data has an initial coordinate system with 7 digits. iMOD can only work with a 6 digit coordinate and therefore all models are set to 0,0 for the lower left X and Y. The start year of the model is also stated in the GEN package. The calendar in iMOD-SEAWAT can run up to 10.000 years when the starting year is set to 0. The calendar cannot be switched off and therefore different the maximum amount of years for 1 runfile is 10.000 years. The long runs necessary to determine the equilibrium times (Tau) were created by running the models sequentially. In this way, the results for head and concentration of runfile 1 were used as input for runfile 2 and so on.

3.2.1.2. [DIS] Discretization package

The base for the model dimensions and structure is set in the discretization package. The number of layers (10 layers for all 6 models), number of cells in the X and Y direction and the length of these cells is given in the DIS package, as well as the number of time steps and the length of each time step. The top and bottoms of the model layers are given in the DIS package. The model layers have a varying thickness and are generated by a batch file which calculates the thickness between the top and bottom. The thickness is divided by 10 and added to the corresponding layer. 10 layers are chosen to be able to represent geological features and to keep the computational time of the models low. The result for the Niger delta is shown in figure 16. The intersection of the estimated thickness with the continental crust gives the offshore boundary of the models. In the case of the Shatt al Arab, these lines do not intersect because the red sea is too shallow and does not have a steep drop in the ocean floor (therefor the offshore boundary I placed at the border of the model domain).

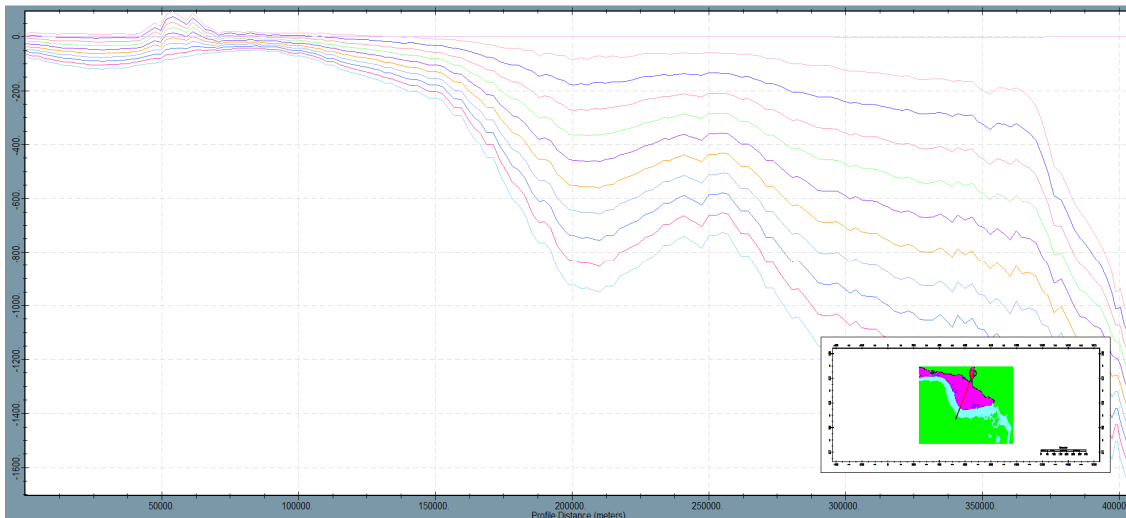


Figure 16: Cross section of the Nile delta showing the discretization of the model in 10 model layers.

3.2.1.3. [BAS6] Basic package

The basic package contains the location for the IDF's with the boundary conditions for the models as well as the initial heads of the model. The model calculates the heads accordingly. The boundary conditions for the 6 models are given in figure 17. The IDF's for the boundary conditions (MODFLOW package IBOUND) consist of -1, 1 and 0 values. A cell with value -1 is a fixed cell so the initial head given in the BAS package does not change for this cell. Cells with value 0 are inactive and cells with value 1 are the active cells where the head is computed. All offshore cells (elevation smaller than 0) are set to -1, meaning a fixed sea level. Cells with an elevation higher than 300 are set to 0, and all cells where the GLiM lithological database does not consist of unconsolidated material is set to 0 as well. In this way, the actual delta plain with unconsolidated material can be set to 1 (active).

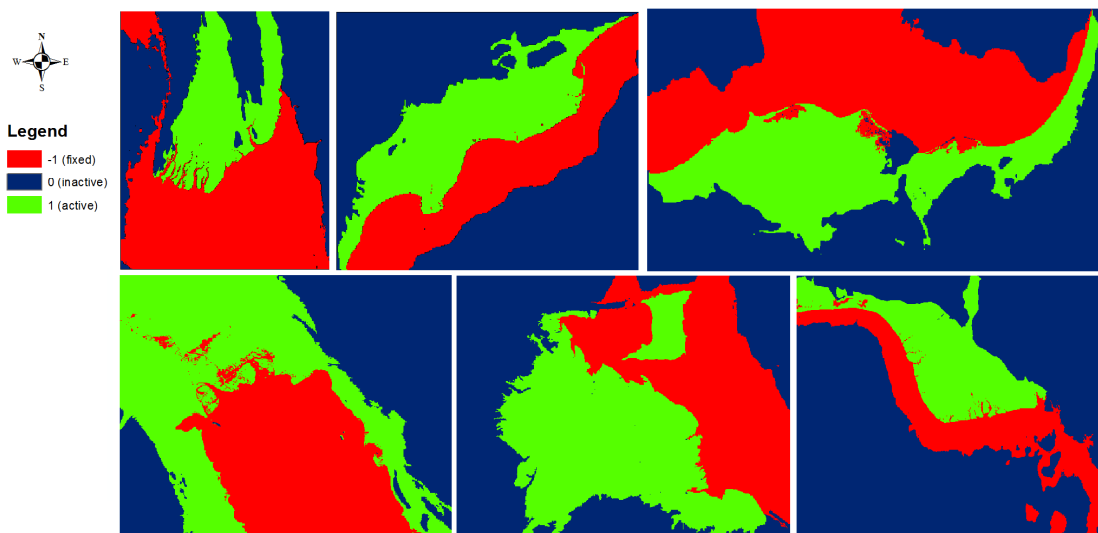


Figure 17: Boundary conditions (red = fixed, dark blue= inactive and green = active) clock ward from top left: Irrawaddy, Krishna, Nile, Niger, Orinoco and Shatt al Arab.

3.2.1.4. [OC] Output Control package

In the output control package option are given to either save the head, concentration or budget for specified layers and stress periods as IDF files or not. Also options are given to save the head, concentration and velocity in x,y and z-direction as TECPLOT files.

3.2.1.5. [LPF] Layer Property package

The LPF package contains information about the physical properties of the model layers. The hydraulic conductivity in the vertical and horizontal direction are given in the LPF package. For the initial model the first layer is set to 0.005 m/d, layers 2-10 are set to 10 m/d (Bot, 2011). The anisotropy factor is 0.4 and the storage coefficient is 0.0021 (as used in Asano,2016) In this way, a delta with a confining top layer and with one main aquifer below is constructed; this is the reference case. Later more geological geometries are considered. To change the number of aquifers/aquitards or the change the physical properties of the layers changes will be made in the LPF package. These different geological scenarios and how to implement them in the LPF package will be discussed in section 3.2.2.

3.2.1.6. [DRN] Drainage package

The drainage package holds information on the location, elevation and conductivity of a drain. When water is present above the drainage level the drain is active, otherwise the drain becomes inactive. There is no global data-set on the location of drains. Because drainage in deltaic areas is usually extensive, the assumption has been made to mimic the drainage system with a ‘mask’ drainage system. This ‘mask’ gives all active cells a drain with an elevation of – 0.5 meter below the surface. The conductivity of the drains is set to 1000 m²/d. The conductance of a drain should in reality be calculated as in 3.1.3. However, because none of the parameters in equation 8 are known for the drains, an estimation of 1000 m²/d was made. This was done by trial and error and checking the water balance to see to what extent the drains were active or not.

3.2.1.7. [GHB] General Head Boundary package

In the general head boundary package a path to an IDF can be given with active GHB cells. The variables for the GHB cells are the head, conductance and density. The general head boundary cells are still active but by varying the conductance the initial elevation heads can either be kept almost constant or variable. On the boundary between active and inactive cells the general head boundary is placed to maintain the elevation heads of the active cells setting the inland boundary. The GHB package together with the BAS package outlines the boundary of the model for active, inactive and fixed cells.

3.2.1.9. [RIV] River package

The input for the river package comes from the GAIA dataset (section 3.1.3). The main variables for the river package are the amount of river systems and the water level, conductance and bottoms of each river system. The water level for the models is given as the surface elevation of that cell. The bottoms come from the GAIA data-set and the conductance is determined according to section 3.1.3.

3.2.1.10. [PCG] Preconditioned Conjugate Gradient package

In the PCG package the settings of the PCG solver can be set. The PCG solver solves the general groundwater flow equation. Settings such as the maximum amount of inner and outer iterations can be set, as well as the convergence criteria. The head change criterion (HCLOSE) and the residual criterion (RCLOSE) determine the convergence criteria. The stricter the HCLOSE and RCLOSE the more accurate the model outcome. However, setting the convergence criteria too strict can result in larger computational times. The convergence criteria used for all 6 models equals HCLOSE = 0.05 m and RCLOSE 200 m³/d.

3.2.1.11. [GCG] Generalized Conjugate Gradient solver package

The generalized conjugate gradient solver solves the advection/dispersion, sink/source and reaction terms (Zheng and Wang, 1999). The maximum number of outer and inner iterations is given in the GCG solver together with the solver type.

3.2.1.12. [BTN] Basic transport package

The BTN package is used to set the starting concentration and the boundary condition for each cell. For the initial model all offshore cell are given an initial concentration of 35 g/L TDS and the inland cells 0.0 g/L TDS. The cells can be active, inactive or fixed just as in the BAS package. A fixed cell in the BAS package can however be set to active in the BTN package. This is useful when the head of a cell should be fixed but the concentration should be calculated by iMOD-SEAWAT. The porosity is given in the BTN package (0.3 for all models) and the transport time step can be adjusted as well. For the Finite Difference solver a transport time step of 1000 days is used. When using a different solver (MOC/TVD) the transport time step can be set to 0 in order to let the solver determine which time step should be used. These solvers use this explicit time stepping to determine that the maximum stable courant number (1) will not be exceeded.

3.2.1.13. [SSM] Sink source mixing package

‘The SSM package solves the concentration change due to sink and source mixing explicitly or formulates the coefficient matrix of all sink and source terms for the matrix solver’ (Zheng and Wang, 1999). The concentration of the rivers is given 0.2 g/L TDS and the recharge is given a concentration of 0.001 g/L TDS in the SSM package.

3.2.1.14. [ADV] Advection package

The advection package consists of variables to find the advection solution. Advection is an important hydrological process in the distribution of salt. The advection term can be solved by the following methods:

- Finite Difference method
- MOC method where particle distribution control needs to be set in the ADV package
- MMOC
- HMOC
- TVD

The solver which is used for this thesis research is the finite difference (FD) method. The FD method is not the most accurate but is much faster than the others making it a useful solver for the long runs to calculate the equilibrium time Tau. A comparison between the FD, MOC and TVD solver will be given in the results section 4.3.3.

3.2.1.15. [DSP] Dispersion package

The dispersion package holds different variables which are given in table 3. Dispersion can become a significant process when modelling thousands of years even though advection is the most important transport process.

Table 3: Set variables in the DSP package.

Longitudinal dispersivity (m)	10.
Ratio of horizontal transverse dispersivity to longitudinal dispersivity	0.1
Ratio of vertical transverse dispersivity to longitudinal dispersivity.	0.1
Effective molecular diffusion coefficient m ² /day	0.0000864

3.2.1.16. [VDF] Variable density flow package

The variable density flow package is used by the SEAWAT code to improve the computational time (Langevin et al., 2003). The VDF solver solves the variable density flow equation. Concentrations resulting from the solute transport equation are used by an equation of state to calculate the fluid density (Langevin & Guo, 2006). The most important variables for the VDF package are the minimum/maximum densities and the $\partial\rho/\partial C$ variable. $\partial\rho/\partial C$ is the slope of the equation of state and is given by rewriting equation 6 into 9. The variables used for all models are given in table 4.

$$\frac{\partial\rho}{\partial C} = \frac{\rho_{i,j,k} - \rho_f}{C_{(i,j,k)}} \quad (9)$$

Table 4: Parameters for the slope of the equation of state.

$\rho_{i,j,k}$	1025 kg/m ³
ρ_f	1000 kg/m ³
$C_{(i,j,k)}$	35 TDS g/L
$\frac{\partial\rho}{\partial C}$	0.7143

3.2.2. Modelling different geologies

The setup of the models with different geologies will be discussed in the next section. To determine how sensitive the equilibrium time is to different geological scenarios, different scenarios were formulated. Alongside the geological scenarios, there are two different scenarios on the initial salinity condition of the system. All combinations between hydrogeological and geological scenarios have been tested for all six models.

3.2.2.1. 6 geology and 2 hydrogeological model scenarios.

To find the dynamic equilibrium time τ Tau, the initial concentration should be as far as possible from its dynamic equilibrium state. This can either be an entirely fresh initial model which will gradually become saline or an entirely saline model which can become fresh.

To start completely saline the BTN package is changed and the [SCONC] which gives the starting concentration is set to 35.0 g/L TDS. This way there is a freshwater input by the rivers and recharge.

To start completely fresh the BTN package was set to 0 for layers 2-10. However, to have a source of salt water, the offshore cells in the first model layer were given a fixed concentration of 35.0 g/L TDS. The cells inland from model layer 1 get a concentration of 0 g/L TDS. Because model layer 1 does not have one single value, IDF's for each model with the concentrations inland and offshore were created linked to the IBOUND definition of subsection 3.2.1.3. The salt to fresh scenario will be called B1, the fresh to salt scenario B2.

The distinction between an open and closed system is made. Most studies only model an open connection between aquifer and the sea, while this is uncertain (van Engelen et al., 2018). At the coastline clay layers either are continuous or cut off. With continuous clay layers inland and offshore the system is called closed (A1). There is less connectivity at the coastline compared to an open system (A2). For an open system, the offshore cells consist only of sand. In order to create these open and closed systems, the LPF package was changed. Different IDF's were made for the open scenario where clay cells have a conductivity of 0.005 m/d and cells that represent sand get a conductivity of 10 m/d.

Without local geological datasets, the next best thing is to test different geologies to determine the influence of these different geologies. In the absence of a global geological dataset different geological scenarios have to be designed to determine the influence of these scenarios on the simulated concentration distributions. It is difficult to estimate how many sequences of aquifers and aquitards have been preserved in the deltas. The age, geometry, amount of sediment, erosion rate, subsidence rate, of a delta influence the sedimentology of the system (Reijers, 2011; Curtis, 1970). Deltas which have been studied more thoroughly show that a delta which started to build-up around 5 million years ago (like the Nile (Van

Engelen et al, 2018), Rhine-Meuse (Oude Essink et al, 2010) and Niger delta (Amajor, 1991)) consist of roughly 5 aquifers and 5 aquitards (Kim Cohen, personal communication, 13 February, 2018) on top of the base of the system. This rough estimation was used as a rule of thumb for all 6 deltas. In many regions, the lack of subsurface data is one of the main limiting factors to determine the amount of fresh water in a system. Different geological scenarios regarding the number of aquifers/aquitards and the presence of gaps in the aquitards have been made. The connectivity of aquifers by non-continuous aquitards might influence the salt and fresh groundwater distribution. Scenario 1 has a confining clay layer on top and one large aquifer below (C1), scenario 2 has five continuous aquifers and aquitards (C2) and scenario 3 has five aquifers and aquitards but the aquitards consist for 30% of gaps. These gaps were created with a python script that randomly created gaps with a diameter of sixteen cells as shown in Appendix E. The effect of smoothing the borders of the gaps was tested but this did not change the model outcome significantly as shown in Appendix F. A schematic representation of the different geological scenario combinations is shown in Figure 18. The combination of the two initial scenarios with the six geological combinations is shown in table 5.

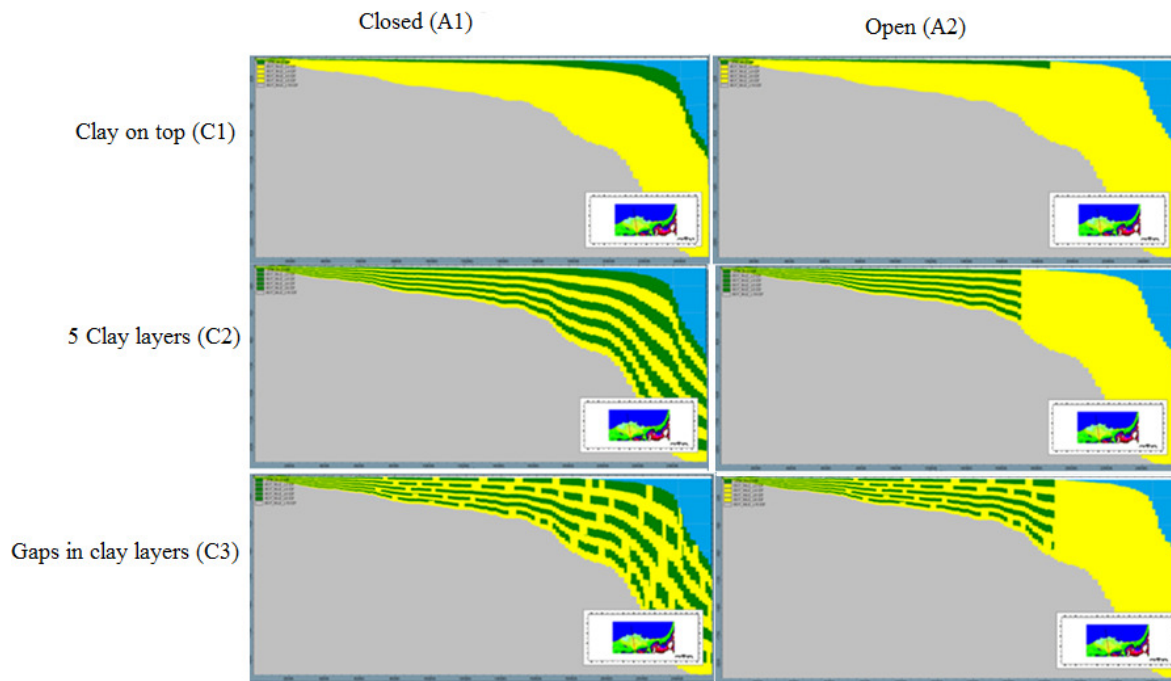


Figure 18: Schematic representation of the 6 different geological scenarios.

Table 5: Abbreviations for all 12 modelled scenarios.

A1B1C1	CLOSED_SALTTOFRESH_CLAYONTOP
A1B1C2	CLOSED_SALTTOFRESH_CLAYLAYERS
A1B1C3	CLOSED_SALTTOFRESH_GAPS_CLAY_LAYERS
A1B2C1	CLOSED_FRESHTOSALT_CLAYONTOP
A1B2C2	CLOSED_FRESHTOSALT_CLAYLAYERS
A1B2C3	CLOSED_FRESHTOSALT_GAPS_CLAY_LAYERS
A2B1C1	OPEN_SALTTOFRESH_CLAYONTOP
A2B1C2	OPEN_SALTTOFRESH_CLAYLAYERS
A2B1C3	OPEN_SALTTOFRESH_GAPS_CLAY_LAYERS
A2B2C1	OPEN_FRESHTOSALT_CLAYONTOP
A2B2C2	OPEN_FRESHTOSALT_CLAYLAYERS
A2B2C3	OPEN_FRESHTOSALT_GAPS_CLAY_LAYERS

4. Results

4.1 Initial model results

The initial model results show the model runs with a constant recharge of 1 mm/d for each cell. The initial salt distribution has salt cells offshore (35 g/L TDS) and fresh cells (0.0 g/L TDS) inland. The head and concentration of the steady-state model runs for each of the six deltas are shown in figure 19 and 20.

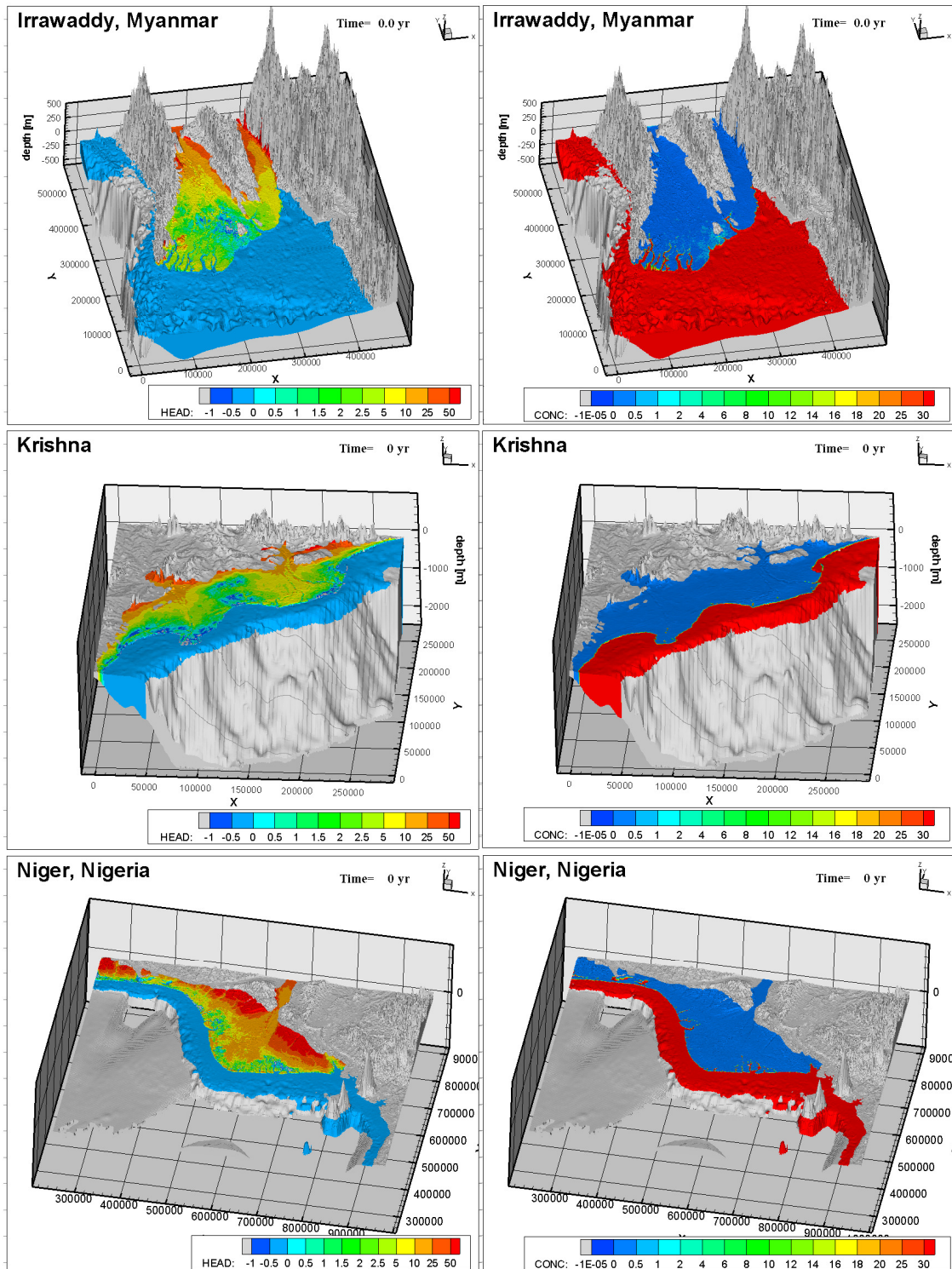


Figure 19: Initial model results for the Irrawaddy, Krishna and Niger delta. Hydraulic head (left) and concentration (right)

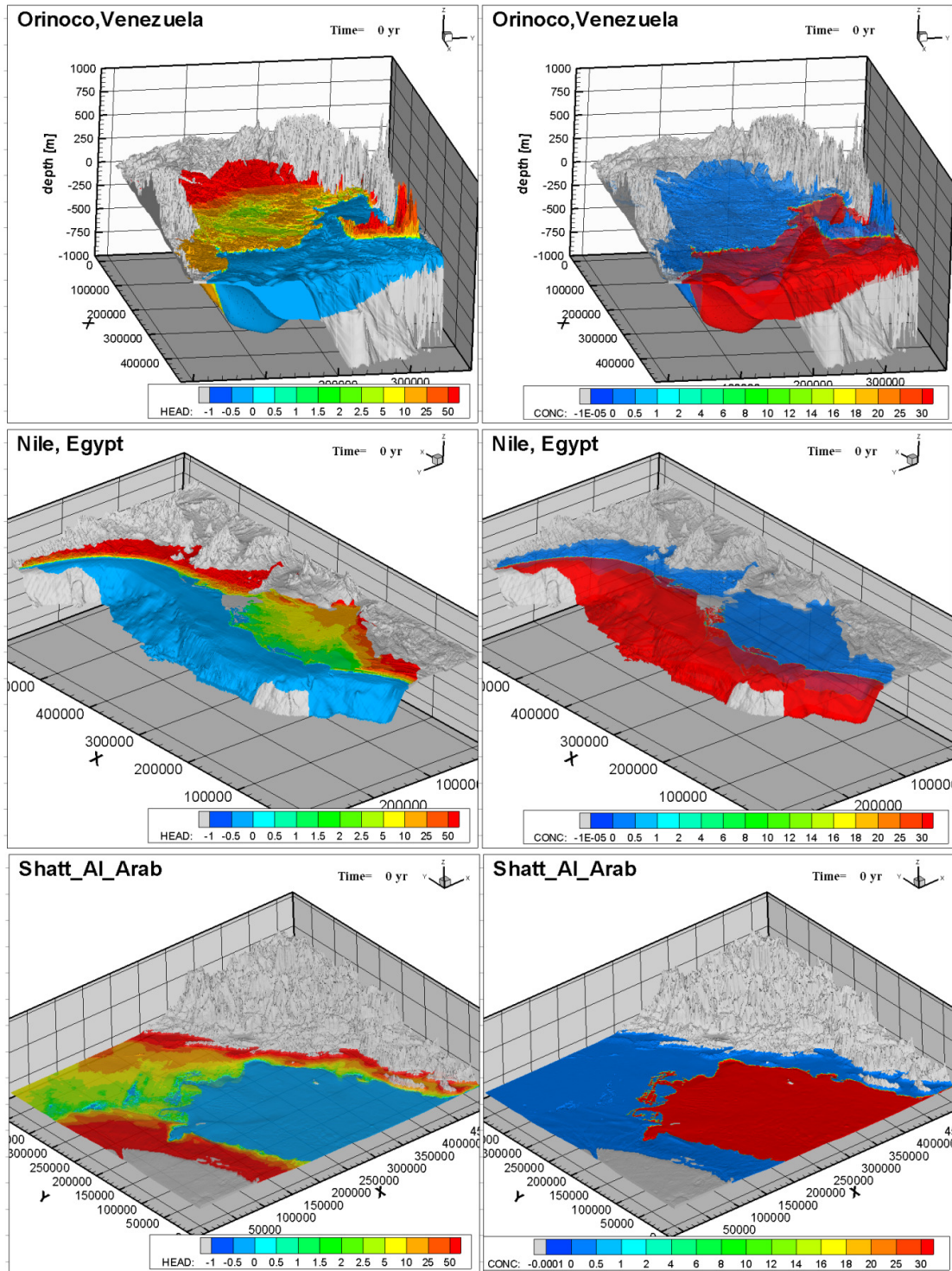


Figure 20: Initial model results for the Orinoco, Nile and Shatt al Arab delta. Hydraulic head (left) and concentration (right)

With a constant recharge for all six models, the hydraulic heads follow the topography of the models. To improve the models, the paleo-recharge was implemented. The initial model runs are the baseline scenario. The influence of the paleo recharge can later be compared to the baseline scenario. This results in a different head distribution shown in appendix G. The main goal of the initial model is to see if the model converges.

4.2 Dynamic equilibrium time Tau

4.2.1. Initial Tau results

The equilibrium time Tau is reached when the volumes of fresh and salt water are constant in time. This tau is assumed to be reached when +/- 5% of its estimated final equilibrium salt and freshwater volume is reached. Figure 21 shows the salt/fresh groundwater distribution at t=29000 years.

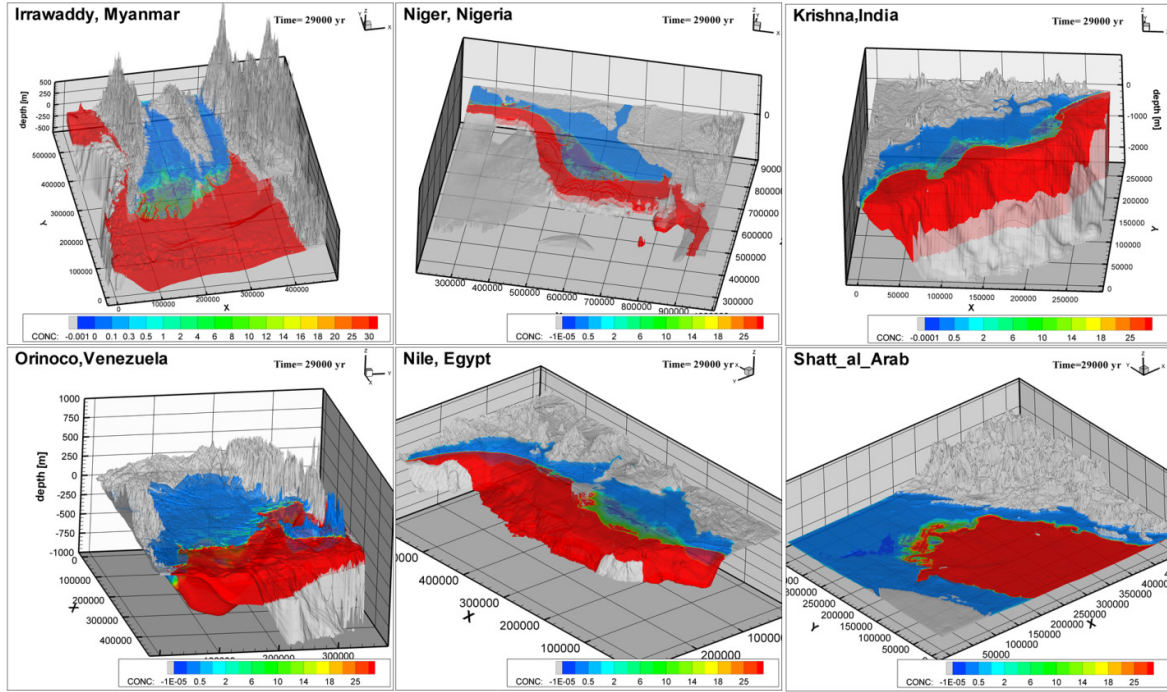


Figure 21: Computed concentration for scenario A1B1C1 after 29.000 years for all 6 deltas.

4.2.2. Tau results per delta for all 12 scenarios

Figure 22 shows a theoretical figure of the results for the six deltas to clarify the rest of the results for all 6 deltas. The models ran up until 61000 years (unless a model became stable before 61000 years). The lines from 61000 to 90000 years (black lines in the figure for the Irrawaddy delta) were mathematically computed in the following way. Some of the model runs do not reach a stable freshwater volume before 61000 years. To estimate how long it takes for the model to reach its dynamic equilibrium, a hyperbolic function was plotted through three points (volumes at t=50.000, t=55000 and t=61000). This estimation assumes that the rate of added freshwater volume goes to 0 and follows the general function: $y = a \cdot x^2 + b \cdot x + c$. This might not be the case, and this should be kept in mind when evaluating the model results.

Scenarios where the model was stable before 61000 years (no change for 5000 years or more) are not extrapolated and can be recognized as coloured lines which stop before the 61000 year mark.

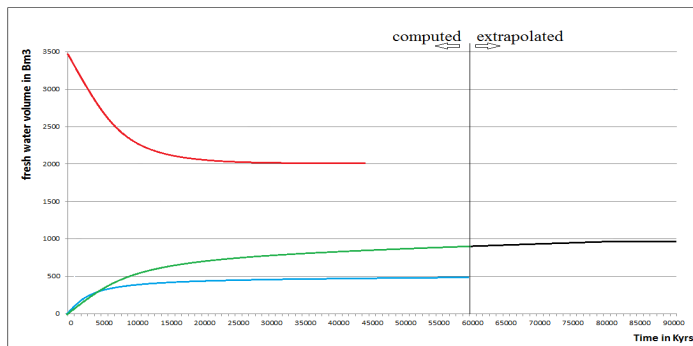


Figure 22: Theoretical evolution of Tau scenarios. For the Irrawaddy delta the lines are extrapolated (in black). If a scenario is stable before t=61000 years the simulation was stopped.

The following section gives observations that stand out when looking at the results for all 12 scenarios. First observations for the Irrawaddy delta will be made (23a). Second observations that stand out for the other 5 deltas will be made. The observations made in this section will be discussed in section 5.2 of the discussion.

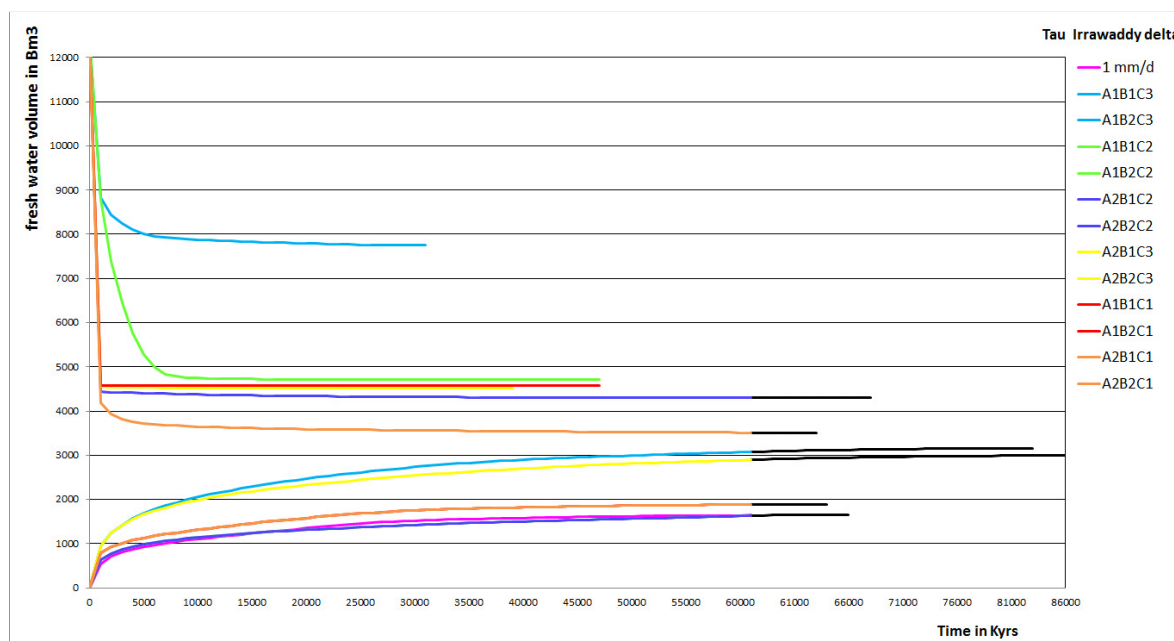


Figure 23a: Evolution of the 12 Tau scenarios for the Irrawaddy delta.

4.2.2.1. Observation 1

There is a significant difference in the A1B1C1 scenario with paleo recharge (A1B1C1(red) lies behind A2B1C1 (orange)) and the same scenario with 1 mm/d recharge.

4.2.2.2 Observation 2

Scenarios A1B1C1 (red) and A2B1C1 (orange) give the same model result. The difference in these two scenarios is the A1 (closed system) and A2 (open system), see figure 18. Also, A1B1C2 and A2B1C2 give the same model results; again the only difference is the open and closed geology.

4.2.2.3 Observation 3

Scenarios with confining layers (C2) end up with a smaller freshwater volume than the scenario with only one confining top layer (C1). The scenario with a confining top layer (C1) has a smaller volume of fresh water than the scenario with gaps in the clay layer (C3).

4.2.2.4 Observation 4

The figure shows that a dynamic equilibrium is reached, in freshwater volume, when modelling from salt to fresh for all scenarios somewhere between 60.000 years and 90.000 years.

4.2.2.5 Observation 5

The fresh-to-salt scenario reaches a constant freshwater volume much quicker than the salt-to-fresh scenario.

4.2.2.6 Observation 6

The stable freshwater volume estimations are a factor 2 to 3 times higher when modelling from fresh-to-salt.

Figure 23 b-f shows the evolution of Tau for the other 5 deltas.

4.2.2.7 Observation 7.

The largest difference between the deltas is that the “wet” delta areas (Niger, Orinoco and Irrawaddy) have a larger spread for different scenarios than the “dry” areas (Nile and Shatt al Arab).

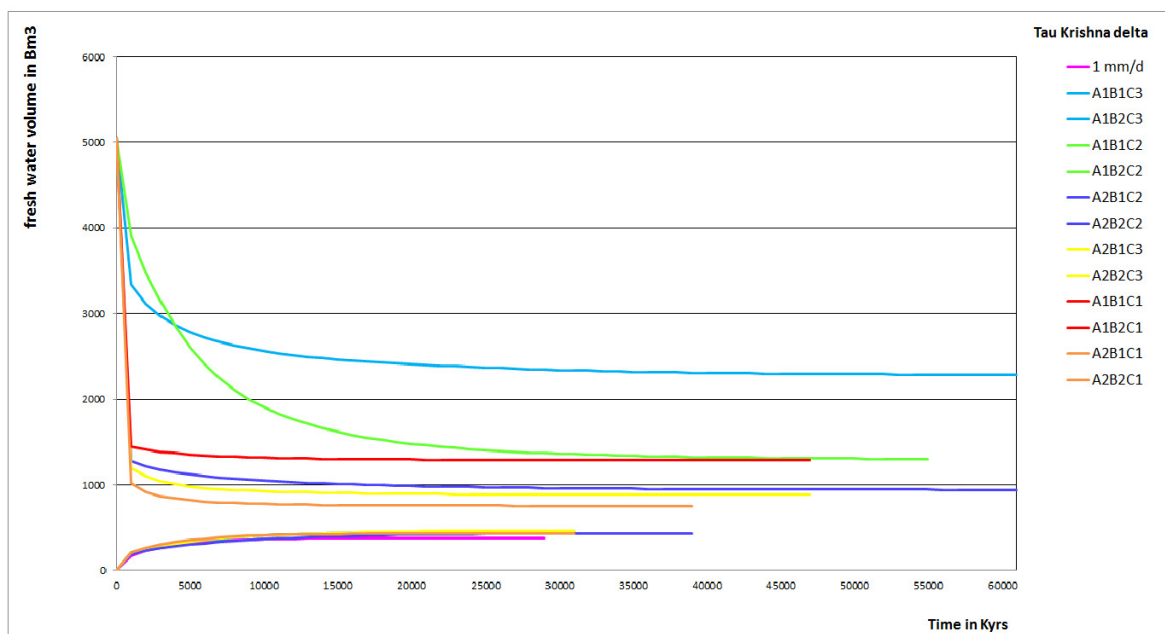


Figure 23b: Evolution of the 12 Tau scenarios for the Krishna delta.

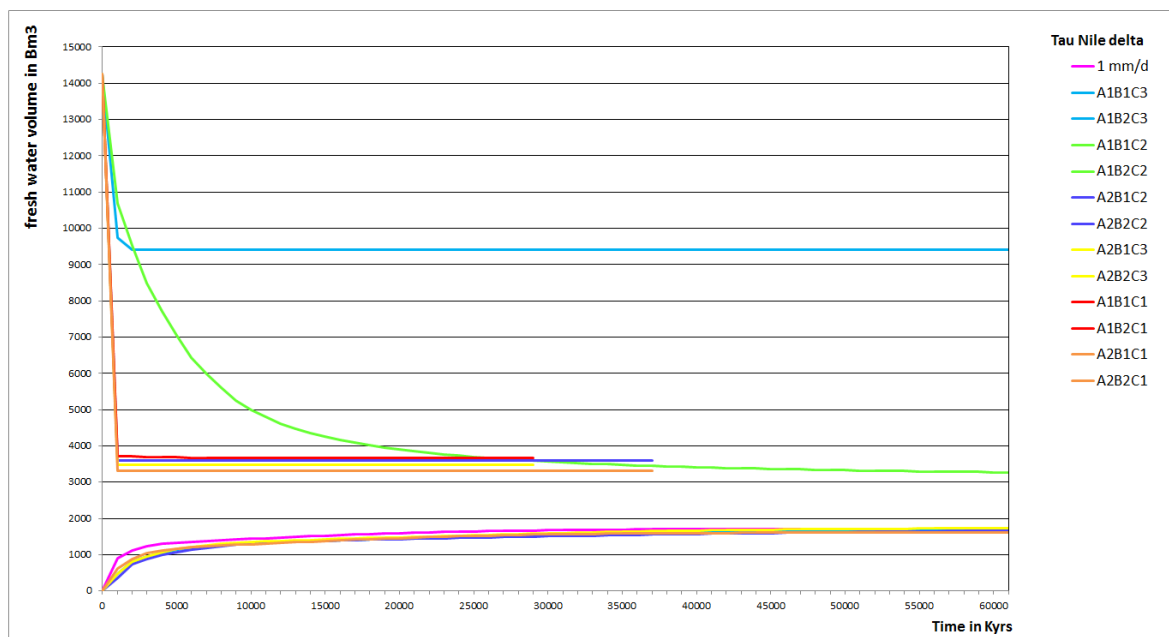


Figure 23c: Evolution of the 12 Tau scenarios for the Nile delta.

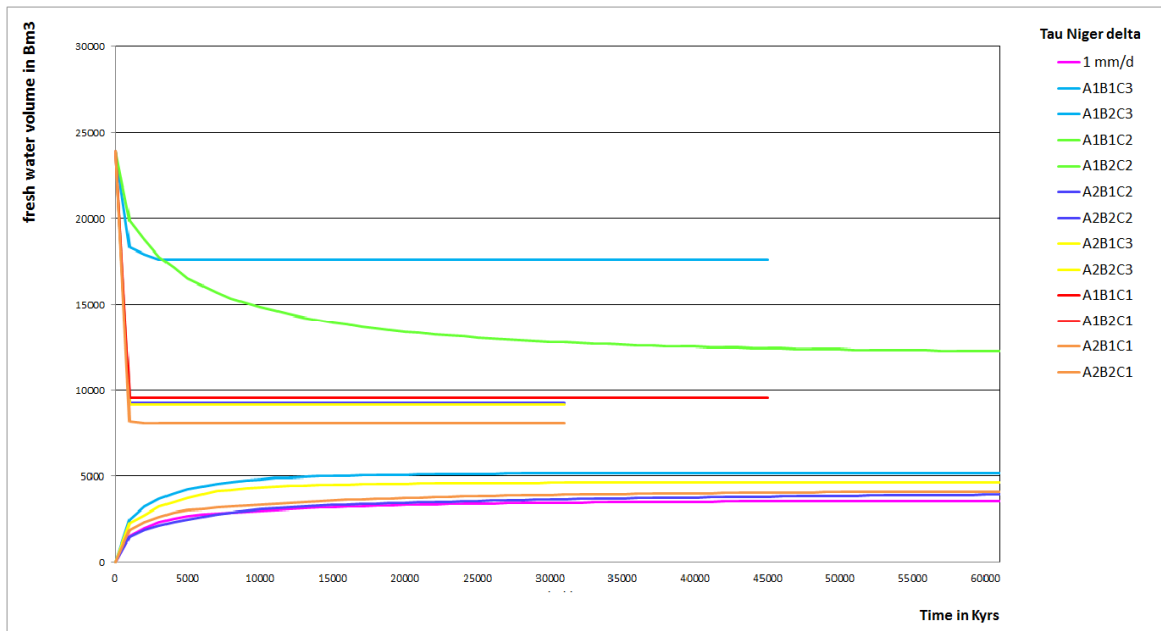


Figure 23d: Evolution of the 12 Tau scenarios for the Niger delta.

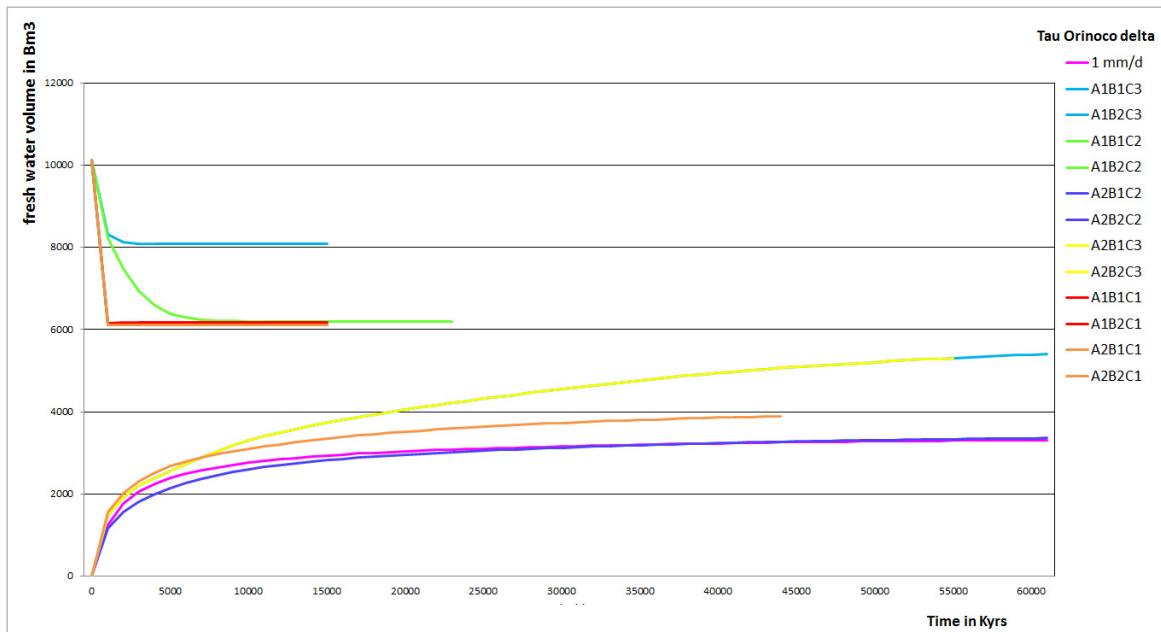


Figure 23e: Evolution of the 12 Tau scenarios for the Orinoco delta.

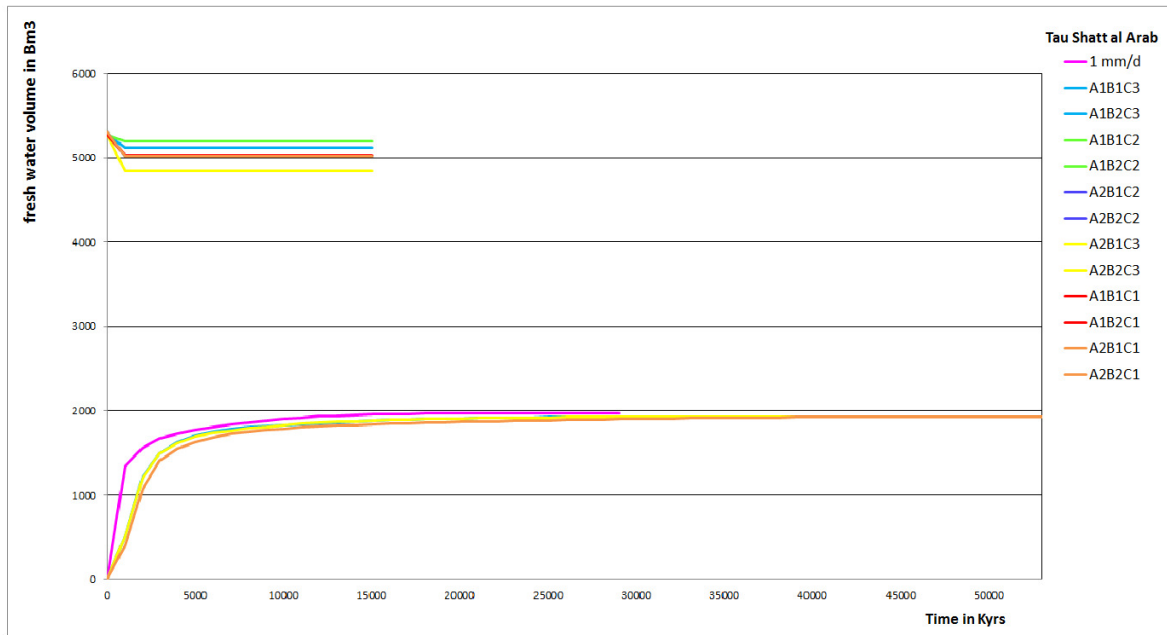


Figure 23f: Evolution of the 12 Tau scenarios for the Shatt al Arab delta.

4.2.2.8 Observation 8

One important observation is that the A1B2C3 scenario (light blue) has the most fresh water in the system. This is counter intuitive because you would expect that the gaps in the clay layers result in a better and faster spread of the salt and therefore a lower stable volume of fresh water. Figure 24 (left) shows the results of A1B2C3 after 31000 years. It seems that pockets of fresh water can remain next to pockets of salt groundwater. Figure 24 (right) shows the square gaps for scenario A1B2C3, visible as light red patches indicating a higher concentration.

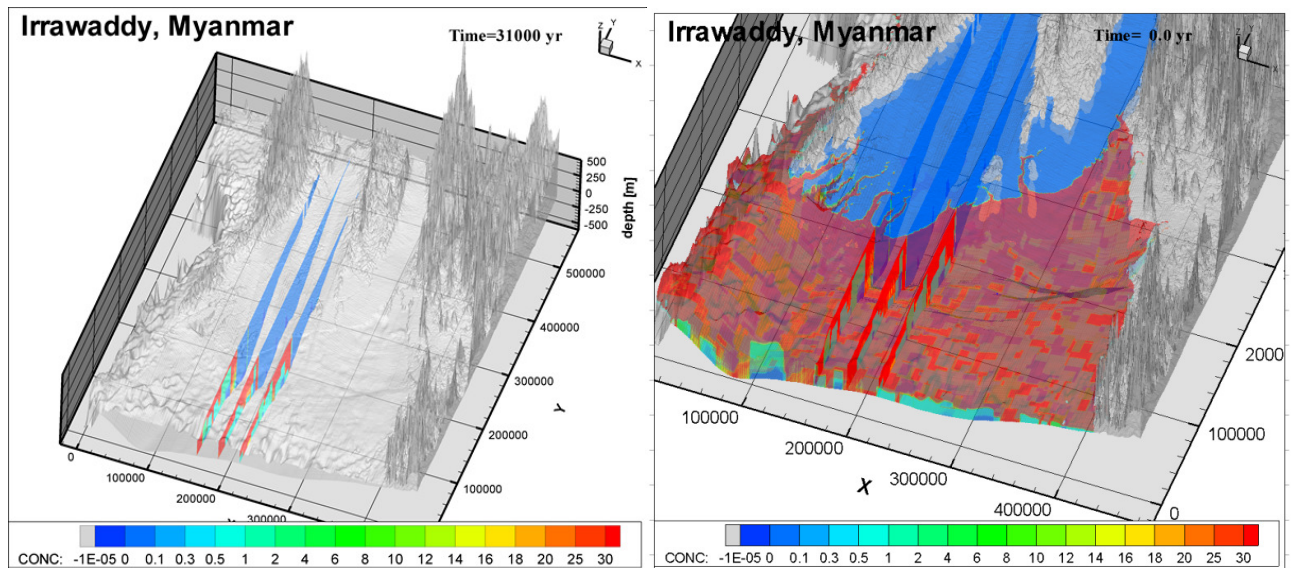


Figure 24: left: cross sections trough the Irrawaddy delta for scenario A1B2C3. Large pockets of fresh water surrounded by salt water are clearly visible. Right: close-up of a top-view of the Irrawaddy delta for scenario A1B2C3. The 'gaps' are visible as light red square patches indicating a higher concentration.

4.2.2.9. Range of available fresh water volumes per delta

Table 6 shows the range of fresh groundwater volumes per delta. Most deltas have a wide range. The difference between the minimum and maximum amount of fresh water could potentially be filled up by salt groundwater inland.

Table 6: The range in computed fresh groundwater volume.

Delta	Average volume fresh groundwater of Salt-to-Fresh vs Fresh-to-Salt
Irrawaddy	2000 – 4000 Bm ³
Krishna	500 – 1000 Bm ³
Niger	5000 – 9000 Bm ³
Nile	1500 – 3200 Bm ³
Orinoco	3800 – 6000 Bm ³
Shatt al Arab	2000 – 5000 Bm ³

4.2.3 Comparing different scenarios in detail

Section 4.2.3 will show a comparison of different scenarios where the difference between salt-to-fresh and fresh-to-salt is either large or small.

4.2.3.1. Scenario A1B1C1 VS A1B2C2

As shown in figure 25, the blue and red lines (representing A1B1C1 and A1B2C2) are not likely to meet (soon). A top view and cross sections of the evolution of the distribution of the freshwater volume for A1B1C1 and A1B2C2 in 3D is given in figure 26 to 29.

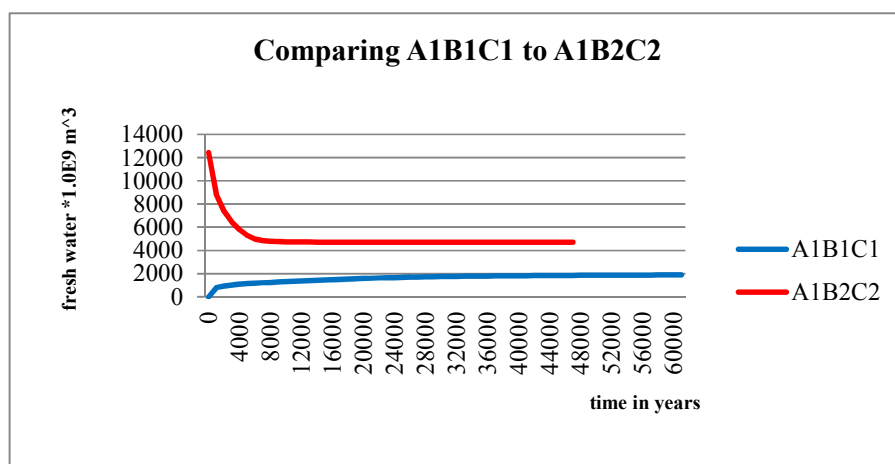


Figure 25: Evolution of the fresh water volume in the Irrawaddy delta for scenario A1B1C1 and A1B2C2. The lines for the fresh water volumes are parallel in the end and do not seem to meet.

Figure 26 shows the gradual freshening of the Irrawaddy delta. After 30.000 years the concentration still changes but the change is much slower than in the first 30.000 years. In the end, the freshwater volume does not seem to be able to push out the deep salt groundwater inland. The fresh and salt groundwater seem to be in equilibrium.

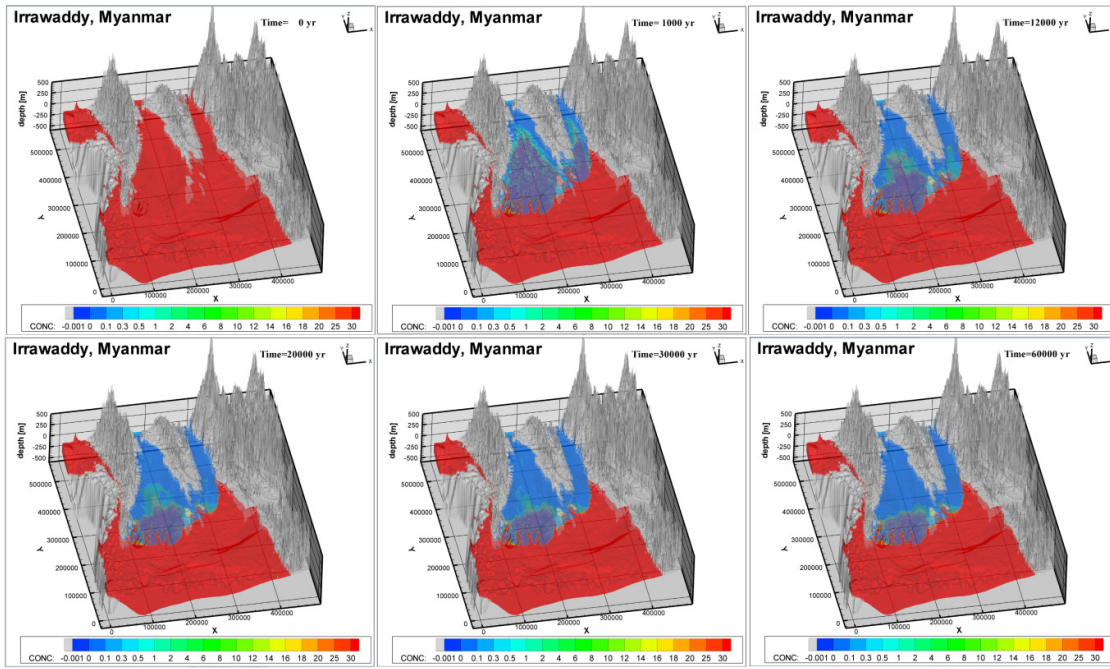


Figure 26: Translucent top view of the Irrawaddy delta for scenario A1B1C1 (Closed_Salt-to-Fresh_Clay-on-Top). In the first 12.000 years (top 3) the fresh water volume changes significantly. From 20.000 to 60.000 years (bottom 3) the volume only changes slightly.

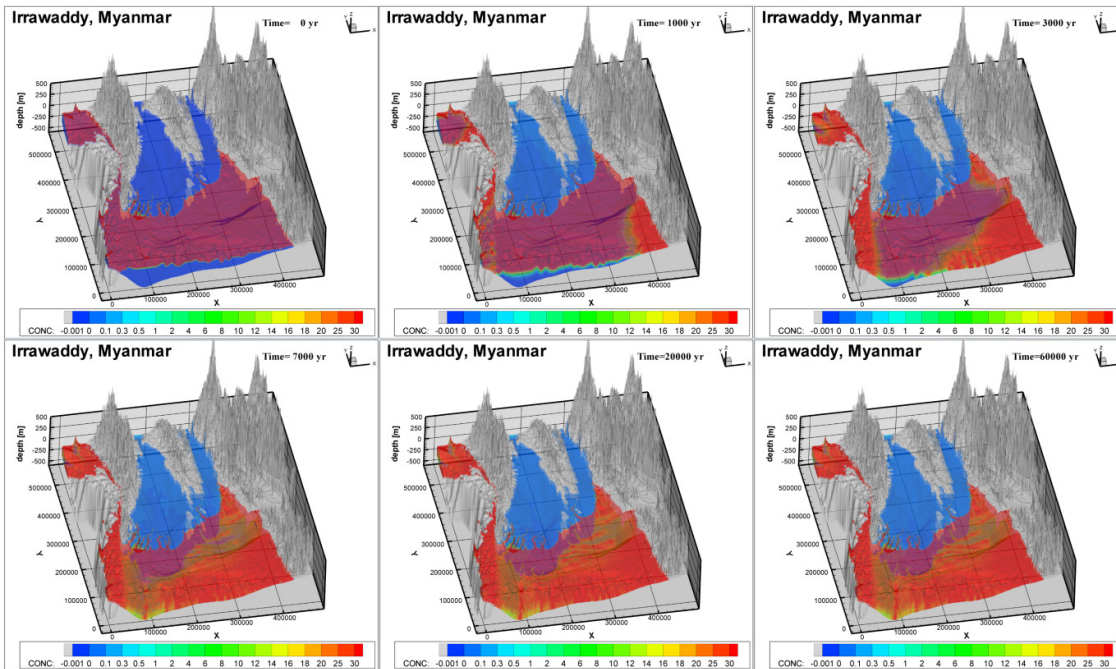


Figure 27: Translucent top view of the Irrawaddy delta for scenario A1B2C2 (Closed_Fresh-to-Salt_Claylayers). The timeframes are different from Figure 26. The reason why they are different is because a dynamic equilibrium is reached much faster. Within 7000 years (top 3 + bottom left) the volumes of salt and fresh groundwater seem at equilibrium.

The top view of scenario A1B1C1 and A1B2C2 show an established dynamic equilibrium, despite the different volumes in fresh and salt water. When looking at the cross sections in figure 28 and 29 the different fresh-saline boundaries becomes visible. The same timeframes as for figure 26 and 27 have been used. The fresh water is not able to replace the salt water at a measurable rate (figure 28). At the same time, figure 29 shows a steep salt/fresh distribution boundary. Salt water does not seem to migrate inland.

Aquitard layers follow the shape of the bottom of the model and are therefore tilted in the offshore direction. This could cause the diminishing of horizontal flow. With zero to no horizontal flow or vertical flow, the salinization comes to a hold.

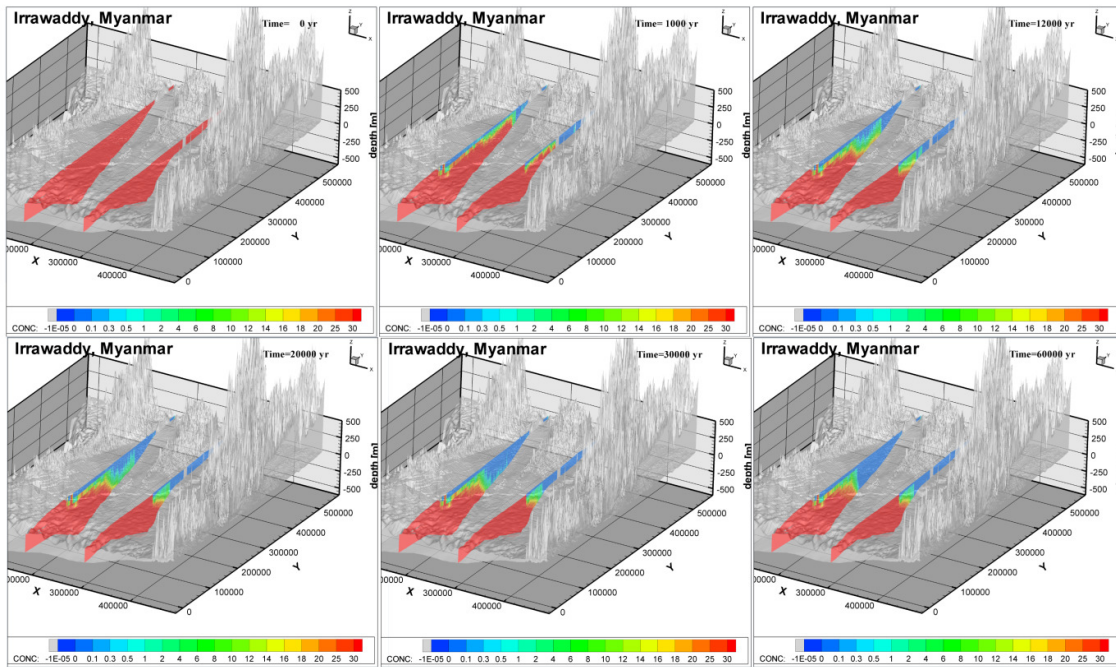


Figure 28: Cross section through the Irrawaddy delta for scenario A1B1C. At 60,000 years (bottom right) there is still a large brackish and salt groundwater volume inland.

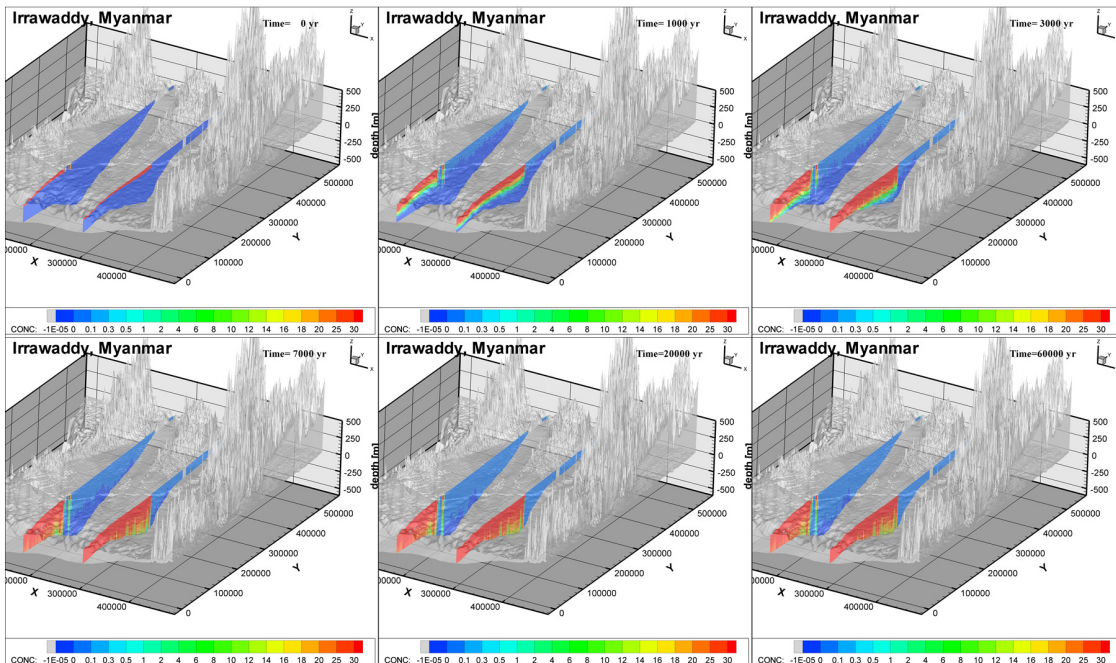


Figure 29: Cross section through the Irrawaddy delta for scenario A1B2C2. At 60,000 years (bottom right) all offshore cells are salt (TDS >5 g/L). When comparing the results to figure 28 it becomes clear that deep salt groundwater is stagnant in Figure 28.

4.2.3.2. Scenario A1B1C3 VS A2B2C1

There are also scenarios where the volumes of freshwater look like they can potentially meet when modelling from fresh-to-salt and salt-to-fresh. Figure 30 shows the evolution of the freshwater volume for scenario A1B1C3 (Closed_Salt-To-Fresh_Gaps-in-Clay-layers) and A2B2C1 (Open_Fresh-To-Salt_Clay-On-Top).

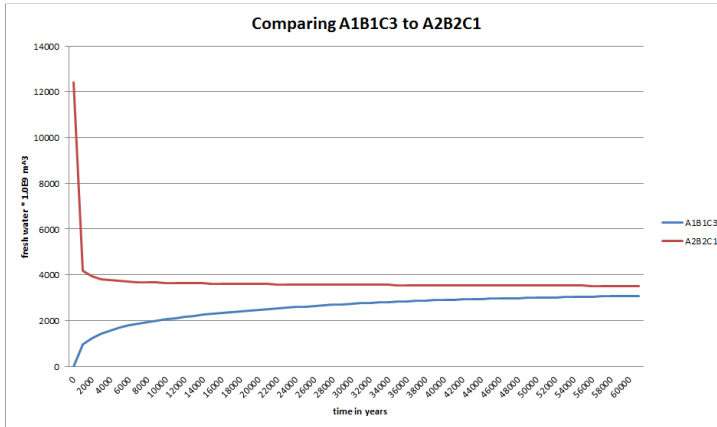


Figure 30: Evolution of fresh water volumes in the Irrawaddy delta for scenarios A1B1C3 and A2B2C1. The lines almost meet which means that almost the same fresh water volume is present at the dynamic equilibrium.

The volumes of fresh water at $t=60.000$ are $A1B1C3 = 3075.8 \cdot 1.0E9 \text{ m}^3$ and $A2B2C1 = 3512.2 \cdot 1.0E9 \text{ m}^3$, and they both still have a slope. When fitting a quadratic function with the standard form of $y=ax^2+bx+c$ from the slope from the last 11.000 years (from 50.000 years - 60.000 years) A1B1C3 will reach its peak of $3154.6 \cdot 1.0E9 \text{ m}^3$ at 83.000 years. The same technique for A2B2C1 results in a freshwater volume of $3510.2 \cdot 1.0E9 \text{ m}^3$ at 66.000 years. To find out why these scenarios almost meet, translucent top views and cross sections of the computed concentrations were made.

Figure 31 shows a top view of the evolution of scenario A1B1C3. It is clearly visible from the top view that more freshwater is able to penetrate into the inland cells than for scenario A1B1C1. The amount of cells with a hydraulic conductivity of 0.005 m/d is much higher in scenario C3 compared to C1. However, the connectivity of the top system is much better because of the gaps in the top clay layer which are not present in scenario C1. The connectivity of the top system to the aquifers below results in a higher overall freshwater volume when the dynamic equilibrium is reached.

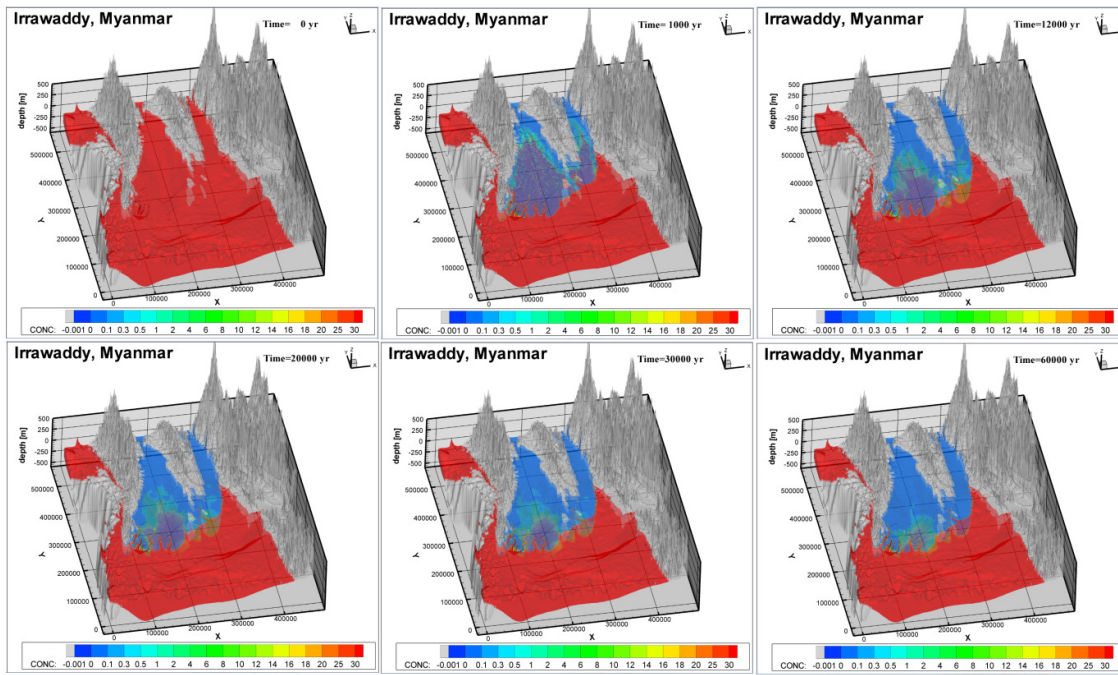


Figure 31: Translucent top view of the Irrawaddy delta for scenario A1B1C3. In the first 12,000 years (top 3) the fresh water volume changes significantly. From 20,000 - 60,000 years (bottom) the fresh water volume still changes slowly.

Figure 32 shows the salinization of the Irrawaddy delta under scenario A2B2C1 (closed_fresh-to-salt_clay-on-top). Velocities are high because layers 2-10 consist completely of cells with a hydraulic conductivity of 10 m/d. Only the top layer consists of cells with a k-value of 0.005 m/d but this has little to no effect because the initial salt distribution states that the offshore cells in layer 1 are salt.

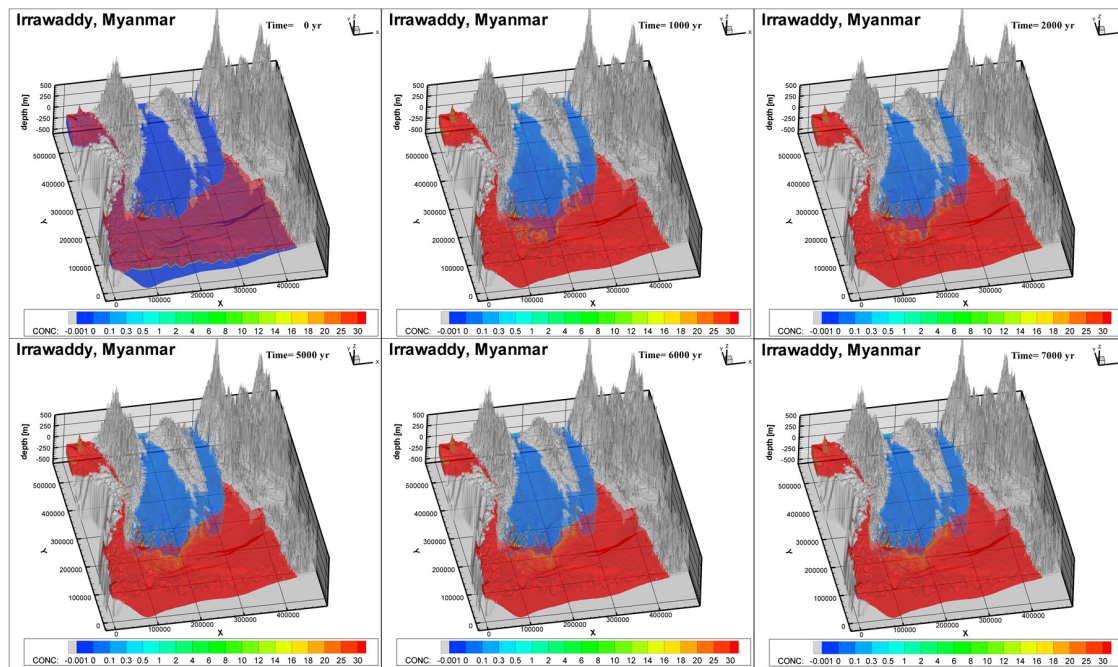


Figure 32: Translucent top view of the Irrawaddy delta for scenario A2B2C1. 6 frames from 0 - 7000 years are shown. In 7000 years all offshore cells get a concentration of 35 g/L TDS.

By comparing the top view, and cross-sections at 60.000 years for scenario A1B1C3 and A2B2C1, it becomes clearer that they can potentially meet (Figure 33 and 34). The top views and cross-sections look much similar than the cross-section and top view of scenario A1B1C1 and A1B2C2.

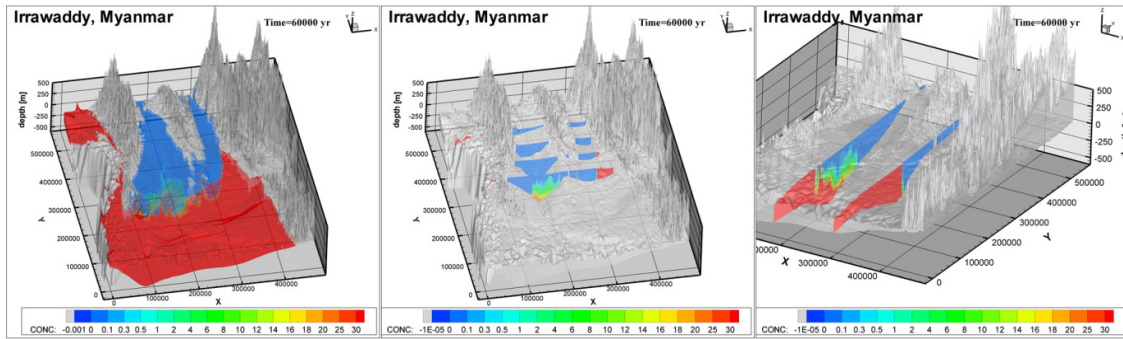


Figure 33: Top view and cross sections in X and Y-direction at $t=60.000$ years for Scenario A1B1C3. A small amount of salt groundwater is present in the deep inland parts of the Irrawaddy delta.

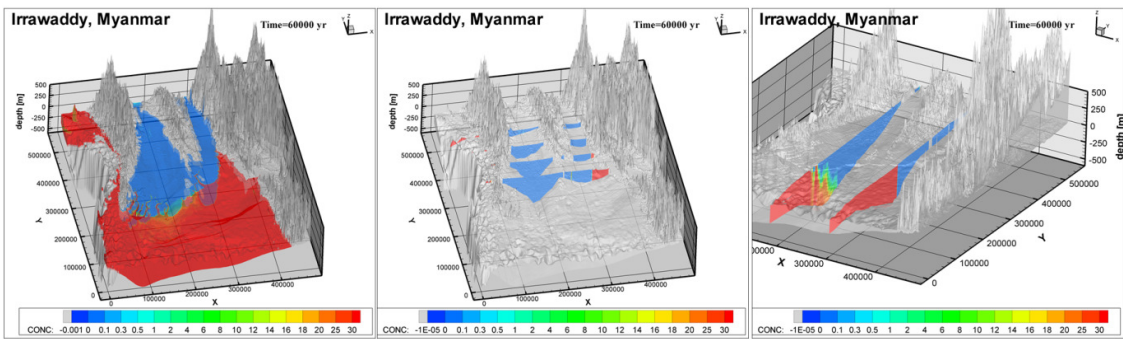


Figure 34: Top view and cross sections in X and Y direction at $t=60.000$ years for scenario A2B2C1. All offshore cells are salt and a brackish fresh/salt interface has formed inland. The cross sections look similar to figure 33.

4.3 Computational time different models, scenarios and solvers.

4.3.1 Average computational time over the 12 scenarios per model

Different models have different computational times. The initial models ran for 100 years in steady state. To see how the computational time can vary, the time per model per scenario was documented. Unfortunately, the computational time of the first scenario was lost in the process, the computational time for the other 11 scenarios have been documented. Figure 35 shows the average computational time per model for 1 runfile of 8000 years. Figure 36 shows the average computational time per for 1 runfile of 8000 years per scenario.

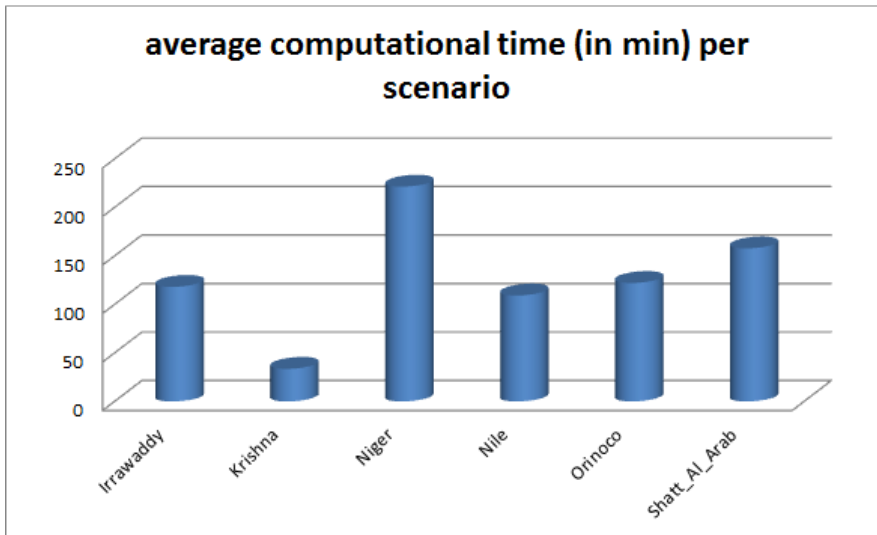


Figure 35: The average computational time it takes to model 1 scenario to compute the head and concentration for the 6 deltas

4.3.2. Average computational time over the 6 models per scenario

Figure 36 shows that there is no significant difference in computational time between scenarios that start with A1 (closed) or A2 (open). If there would have been a difference the right-hand side would be larger or smaller than the left-hand side. This is not the case. There is also no significant change in the B1 (salt to fresh) or B2 (fresh to salt) scenarios. The figure alternates per 3 scenarios between B1 and B2 and these alternations have roughly the same shape and size. The biggest difference comes from the change in C's. The C2 scenario has a smaller computational time than the C1 and C3 scenarios.

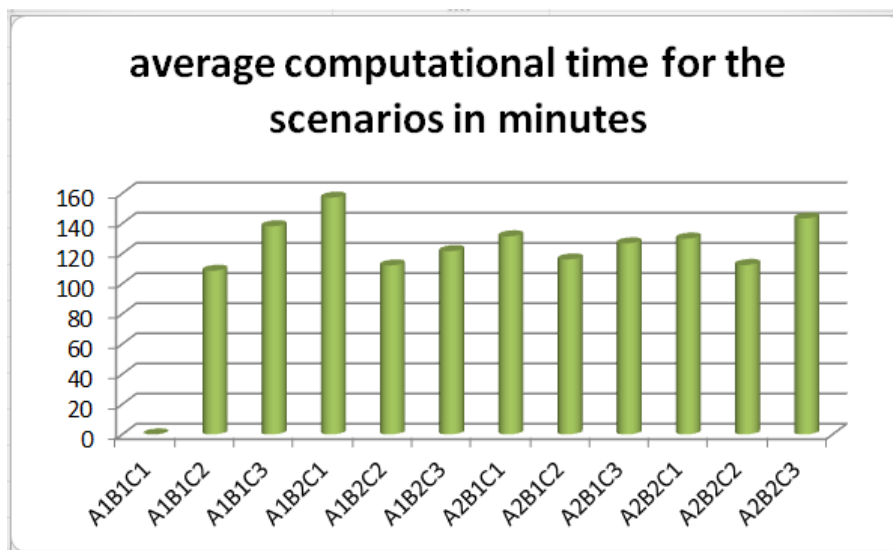


Figure 36: The average computational time it takes to model 1 delta to compute the head and concentration for 11/12 scenarios.

4.3.3. Comparing different solvers

All models and scenarios used the Finite Difference solver. Table 7 shows the difference in computational time per solver for the Krishna delta scenario A1B1C1. For that case the TVD and MOC solvers were also tested.

Table 7: Difference in computational time per solver.

FD solver	35 minutes
TVD solver	10 hours 21 minutes
MOC solver	2 days 3 hours

There is a huge difference in computational time. Figure 37 shows the evolution of the freshwater volume for the Krishna model. Scenario A1B1C1 was computed with the FD, TVD and the MOC solver.. The volumes do not significantly differ and that is why the choice for the FD solver is valid in this thesis.

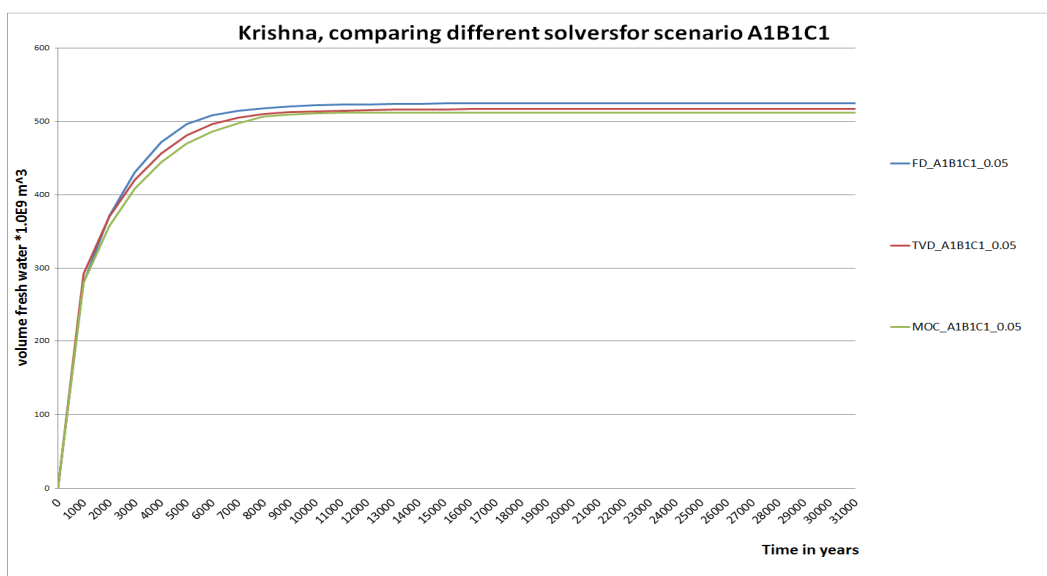


Figure 37: Comparison of the computed fresh water volume over time for the MOC, FD and TVD solver.

The volume of fresh water in a delta can be the same but the difference in the brackish zone can still be extensive. Figure 38 shows the absolute difference in concentration between the FD and MOC/ the FD and TVD/ and the TVD and MOC solver.

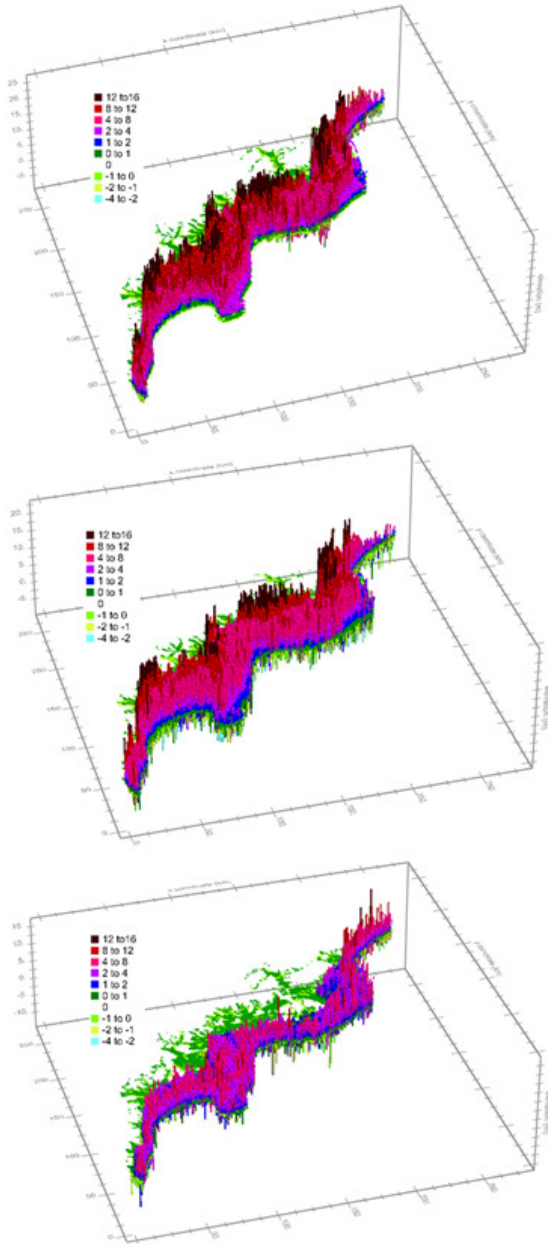


Figure 38: Top view of concentration difference for scenario A1B1C1. From top to bottom = TVD minus FD, MOC minus FD and TVD minus MOC.

4.4. Comparing different conductivities for the top system

The connectivity of the top system plays an important role in the overall volume of fresh groundwater. To see how important the conductivity of the top layer can be a sensitivity analysis for the Krishna delta was executed. Scenario's A1B1C1 and A1B2C1 were tested with different hydraulic conductivities for the homogeneous top-system. The hydraulic conductivities of 0.005 m/d, 0.05 m/d 0.1 m/d and 1.0 m/d were tested (figure 39).

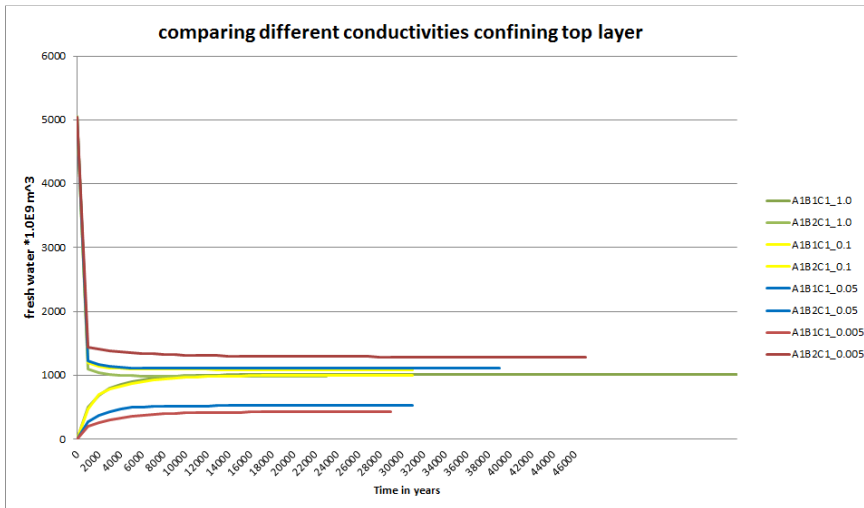


Figure 39: Comparing different conductivities of the top layer for scenario A1B1C1 and A2B2C1. The Krishna model was used to construct the sensitivity analysis for hydraulic conductivity of the confining top system.

Figure 40 shows the cross sections for scenario A1B1C1 with conductivities 0.005 m/d, 0.05 m/d, 0.1 m/d and 1.0 m/d. The higher the conductivity of the top-layer the more deep salt groundwater will be flushed out. The conductivity and connectivity of the top system is very important for deep fresh/salt groundwater distribution.

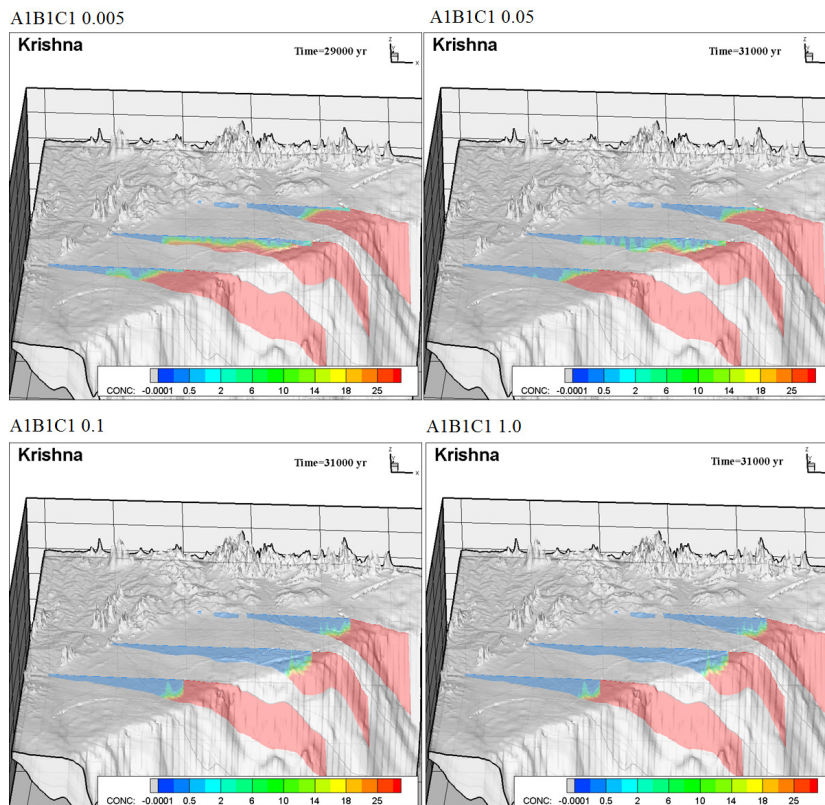


Figure 40: Cross sections through the Krishna delta for scenario A1B1C1. Different conductivities of the top layer have a strong effect on the dynamic equilibrium of fresh and salt groundwater. The higher the conductivity of the top system the more salt groundwater remains stable inland.

5. Discussion

The results in sections 4.1 to 4.4 will be discussed in the same order from sections 5.1 to 5.4. Hypotheses will be given and tested on the model results.

5.1 Parameters in initial model results

The initial model results are a first test to see if the setup of the models is correct. The most important inputs are the:

- Boundary conditions
- Top and bottom of the system
- The location and conductance of the rivers
- The conductance of the drains

The initial precipitation is set at 1 mm/day. The paleo recharge used in the rest of the models has ranging values and is spatial variable. To improve the models (Paleo) recharge estimates are necessary because they influence the hydraulic heads of the system. The same holds if we look at geology. The initial model can be used to test if a plausible distribution of the heads can be produced. Adding the geology (from regional data) can greatly improve the validity of the models.

5.2 hypotheses how dynamic equilibrium forms under different scenarios

Initially, all six models ran for 29.000 years under the A1B1C1 scenario. From these results, it became clear that the Tau would not be reached for many scenarios and models and that the runtime had to be increased. The runtime was doubled resulting in more data and better understanding of the evolution of a dynamic equilibrium. 6 observations were made in the results section 5.2.2. which will be explained in section 5.2.1. of the discussion.

5.2.1. Explanation to observations in results section 4.2.2.

Observation 1: paleo recharge results in higher final freshwater volume for the Irrawaddy delta.

The paleo precipitation has higher values and results in more fresh water in the system. The Nile and Shatt al Arab show a smaller final volume of fresh water because the paleo precipitation is lower than the initial 1mm/d precipitation.

Observation 2: the A1 (closed system) and A2 (open system) give (almost) the same model result.

The main reason why these scenarios do not differ could be explained by the fact that velocities are low due to the confining clay layers inland. Fresh groundwater does not reach the coastline. Inland, the open and closed scenario are the same so this results in the same evolution of the fresh water volume when fresh water does not reach the shore.

Observation 3: difference in geological scenarios C1 (closed top system), C2 (5 aquifers and 5 aquitards) and C3 (gaps in the 5 aquitards).

It appears that the connectivity of the top system with aquifers below is important for the final volume of fresh water. This makes sense because although C3 has more cells with a low hydraulic conductivity of 0.005 m/d than C1, the connectivity between model layer 1 and 2 is much better in C3 than for scenario C1. Therefore more fresh water can flow to deeper parts of the delta which results in higher

fresh groundwater volume. C2 has the lowest amount of fresh water because the connectivity between the aquifers is small due to the homogeneous confining layers in-between.

Observation 4: from salt to fresh a dynamic equilibrium is reached somewhere between 60.000 and 90.000 years.

This is the results of the tests so far, but a lot of assumptions are made which need to be addressed. The most important one is that it is assumed that the slope for some scenarios at 60.000 years will go to 0 when fitting a quadratic function through 3 points (volume at $t = 50.000$, $t = 55.000$ and $t = 60.000$ years) this might not be the case. When the slope between 60.000 and 61.000 years for Irrawaddy scenario A1B1C3 remains constant the model would flush all inland salt water out in 1.7 million years. The actual shape of the dynamic equilibrium lines in the long run (million years) remains unknown. However, all data so far suggest that the change of fresh-water-volume over time goes to zero.

Observation 5: dynamic equilibrium from fresh to salt is reached much faster than from salt to fresh.

The open (A2) scenario does not have confining layers offshore. This results in large velocities in the z-direction. Therefore the salt drops to the bottom of the delta almost immediately after the simulation starts. A1B2C1 has a confining top layer but this layer has been made salt in the initial salt distribution. This source of salt in layer 1 has no confining layer beneath so therefor velocities are also high and salt enters the deeper parts of the delta very easily.

Observation 6: The final volumes of fresh water when modelling from fresh to salt are much higher.

Salt will not reach so far inland as in the salt-to-fresh scenarios, because the salt to fresh scenario has salt cells trapped in deep inland parts of the delta where the velocities for concentration difference over time go to 0. This results in trapped paleo salt groundwater which results in a smaller overall volume of fresh groundwater when the dynamic equilibrium is reached. From measurements in the Nile delta it is known that hyper saline paleo groundwater exists in deep parts of the delta (van Engelen et al., 2018). Several major delta systems originate from the Miocene/ beginning of the Pliocene more than 5 million years ago (Gamero,1996; Amajor,1991 Rizzini et al., 1978). In the last 5 million years numerous sea level transgression periods could resulted in salinization of the groundwater.

The model results indicate the possibility of two dynamic equilibria. It is also possible that there is one dynamic equilibrium. A finer discretization of the model layers and a longer computational time could test which of the hypotheses is valid.

Observation 7: difference between the “wet” delta areas (Niger, Orinoco and Irrawaddy) and the dry deltas (Nile and Shatt al Arab)

The salt-to-fresh volumes for different scenarios are closer to each other for dry deltas than for wet deltas. The reason for this is that there is not enough water to push out salt groundwater. This also results in a larger difference between the fresh-to-salt scenarios for dry areas. The low precipitation values result in a smaller difference from the initial state where all cells are salt.

Observation 8: A1B2C3 scenario has the most fresh water in the system, despite the gaps in the clay layers which could connect the pockets of salt water which each other.

The discretization of the model domain in 10 layers might help to explain why this is the case: In the deeper parts of the delta, there are still only 10 layers. This means that 1 cell can be as much as 120 meters thick when the delta is 1200 meters thick. When looking at the velocities there are only velocities in the z-direction and not in the x and y-direction. The dense salt water in the top system and the gaps in the clay layers cause a flux of salt mainly from the top to the bottom. It seems that the gaps created huge vertical preferential flow paths with no flow to the sides. In figure 24 the square gaps are visible as light

red patches indicating a higher concentration. It can be assumed that that with a finer discretization the spread of the salt will also occur in horizontal directions.

5.3 Computational time under different scenarios and solvers

The difference in computational time per delta is mainly caused by the number of cells the model consists of. Logically, a larger number of cells in the model domain leads to larger calculation time. Also, the input data is larger and reading/loading the input files takes more time.

The difference in computational time per scenario is mostly caused by the difference in build up with aquifers/aquitards and whether or not they are linked with gaps in the confining layers. What stands out the most is that the C2 scenario's (5 aquifers and 5 aquitards without gaps) has the lowest computational time. The main reason for this is that the confining layers decrease the velocities in the x, y and z-direction which results in less computational time. The stability criteria are reached sooner with smaller velocities (Zheng and Wang, 1999)

The difference in computational time for different solvers is large. The main reason for this is that the FD solver was set to take time steps of 1000 days. The TVD solver determines these steps itself to keep the Courant number at 1. This results in time steps of around 50 days. For the MOC solver, the number of particles that are allowed to move for each time step has to be set. This increases the accuracy of a model but increases the computational time drastically.

The results for the total amount of fresh water (concentration between 0-1 g/L TDS) is not significantly different for the 3 models. The largest difference is noticeable in the brackish zone. The results with the TVD and MOC solver both show a higher concentration of TDS for inland cells. The difference is not noticeable when comparing fresh cells (0 – 1 g/L TDS) and salt cells (>5 g/L TDS), but is noticeable in the range of concentrations between 5 and 35. The objective of this thesis is to understand and quantify how long it can take for a disturbed system to reach a dynamic equilibrium. When the objective is to determine the amount of fresh water and the brackish water in a system, as precise as possible the MOC or TVD solver are the better options. With advances in parallel computing computational times are decreasing which makes the MOC and TD solver much faster. However, the FD solver fits the purpose of this research given the number of deltaic areas modelled and the number of model scenarios for each of these areas.

5.4 Influence of top system on deep paleo groundwater

The connectivity and conductivity of the top system is an important factor for the overall freshwater volume in the delta. When the hydraulic conductivity of a confining layer goes up the fresh water volumes estimates of the fresh-to-salt and salt-to-fresh scenarios might become closer. However, the model scenario where a delta consists completely of layers with a high conductivity is unlikely (GliM dataset (Hartmann and Moosdorf, 2012) shows continuous clay deposits at the surface for all 6 deltas). In reality a delta can consist of large confining systems where salt groundwater can be trapped for millions of years (Engelen et al., 2018). The theoretical scenarios with confining layers show that salt groundwater can be at equilibrium in the deep parts of the inland delta. When modelling the total amount of fresh water in a system, the possibility of deep inland salt groundwater should not be overlooked. When a stakeholder assumes that deep groundwater is always of high quality at 100 km from the coast extraction of this groundwater could result in the extraction of paleo salt water. Also upconing of the salt paleo water can be a threat to the current fresh groundwater supply (Oude Essink et al., 2010). To model if this is the case future scenarios with extraction estimates and sea level rise should be tested to see which delta systems have a higher chance of depleting their natural fresh groundwater reserves.

6. Conclusions

The conclusion section will answer the sub-research questions in order of appearance. After the sub-research questions the main research question shall be answered.

6.1 What are the most relevant hydrogeological processes that have to be taken into account to end up with a plausible model?

The plausibility of the model relies heavily on the quality of the input data. With the development of better global data sets the models constructed with global data will further improve. Some of the global data is already of high quality and can replace large scale regional data sets where necessary. Examples are; the digital elevation data from GEBCO and precipitation estimates from global hydrological models. A second group of global data-sets can be of help when regional data is completely absent. The second group consists of the aquifer thickness estimates (Zamrsky et al., 2017) and river network data set from GAIA. The estimated thickness estimates do not always cover the whole delta. When regional data on aquifer thickness is available this data can be used to validate the dataset from Zamrsky et al. (2017). However, most regions do not have regional data on aquifer thickness, and especially their hydraulic conductivity. The GAIA data set could be improved when estimates on the conductance of the river bed are implemented. The data set which is missed most is a global hydrogeological data with aquifer and aquitard thickness estimates. When geology is largely unknown it is difficult to make solid assumptions on the discretization of the deltaic area in aquifers and aquitards. However, when geology is unknown the second best option is to make a hydrogeological model with variable-density flow and coupled salt transport from global data sets from group 1 and 2

6.2 What is the equilibrium time (time to the dynamic equilibrium of the fresh-saline distribution) of the different delta models? How far back in time do you need to go to determine the initial fresh-saline distribution with paleo-reconstruction?

The dynamic equilibrium time can vary significantly between different deltas and different geological scenarios. The assumption that the computed fresh water volumes encounter when modelling from fresh-to-salt and salt-to-fresh does not seem to hold. The change in fresh water volume over time will eventually slow down and for most scenarios a gap in fresh water volumes between the salt-to-fresh and fresh-to-salt scenarios remains stable. This “gap” is filled by salt water that is at equilibrium. The computed dynamic equilibrium time for all six models and 12 scenarios seem to lie between 30.000 and 90.000 years. The discretization in 10 model layers might not be enough to find a gentle slope in the now horizontal change in fresh water volume over time. It is also possible that the salt groundwater inland is at equilibrium and therefore stagnant. This would mean that paleo-reconstruction of a deltaic area would have to go back in time 30 to 90 thousand years, and that the stagnant salt paleo groundwater around the coastal areas and further inland has to be computed. If paleo salt groundwater is not taken into account the fresh water volumes in a delta can be overestimated.

6.3 What factor (theme/process/parameter/solver) causes the biggest increase in computational time?

The biggest increase in computational time comes from the difference in solver. The TVD and the MOD solver do model the brackish zone more accurately. The distinction between fresh (0-1 TDS) and salt (>5 TDS) does not differ significantly between the FD, TVD and MOC solver.

As might be expected the number of cells will also increase the computational time. The Niger delta, on average, has a computational time of 6 times the Krishna delta. This is not only caused by size but also by the calculated velocities. High velocities cause more computational time. For that reason a scenario with 5 homogenous clay layers (C2 scenarios) will have a smaller computational time.

6.4 Can salt water from before the Holocene be present in deep parts of a delta?

During the build-up most the delta systems were covered by the sea for most of the time. During the Pleistocene on average the sea level dropped but fluctuated a lot between glacial and interglacial periods. During the interglacial the sea level reached a peak. The last peak in sea level was 120.000 years ago when the sea level was a few meters above the current sea level. When computing the equilibrium time τ it became clear that trapped salt water can remain stable at deep parts of the inland delta. For some geological scenarios the salt paleo groundwater was trapped as much as 150km inland. It is therefore very plausible that salt paleo water is present in deep parts and far inland of deltaic areas.

6.5 The main research question

To what extent are 3D models of variable density-groundwater flow and coupled salt transport constructed with global data sets able to properly represent hydrogeological processes?

The use of models constructed with global data sets was proven valid to increase the understanding of dynamic equilibria in fresh and salt groundwater volumes. The range of computed fresh groundwater volumes is large when testing twelve different scenarios. This large range gives a high uncertainty when determining the amount of fresh water in a delta. The global data models do help to give a first order estimate of the available fresh water resources in areas where no data is available. Second, the applicability for the models is that they can serve as a base model which can be improved with regional data sets. Each time a data set improves (more and better data on geology, data sets for the top system or finer scale data sets) the model as such will improve.

7. Recommendations

- The model results and the method to determine the dynamic equilibrium time of a model should be further evaluated. One way to evaluate the models and the method is to compare the results with an existing validated model made with regional data sets (For example the Nile delta).
- Increase the vertical and horizontal resolution to see if this gives a different outcome than models which consist of only 10 layers. The model discretization might have an effect on the results.
- Do a paleo reconstruction (for a regional data with data on chloride concentrations) with and without determining a volume of stagnant inland salt groundwater. The difference can show if the volume of fresh groundwater is over or under estimated without using the Tau method.
- Run the models with the estimated extraction data and multiply need of fresh water with population growth. In this way the models can be used to predict the stress on the available fresh groundwater resources.
- When quantifying the fresh groundwater volumes with hydrogeological models built with global data sets these models should be enhanced with regional geological data to improve the quality of the results.

8. References

- Amajor, L. C. (1991). Aquifers in the Benin Formation (Miocene—recent), eastern Niger Delta, Nigeria: lithostratigraphy, hydraulics, and water quality. *Environmental Geology and Water Sciences*, 17(2), 85-101.
- Andreadis, K. A., G. J.-P. Schumann, and T. Pavelsky (2013), a simple global river bankfull width and depth database, *Water Resour. Res.*, 49, 7164–7168, doi:10.1002/wrcr.20440.
- Anthony, E. J. (2015). Wave influence in the construction, shaping and destruction of river deltas: a review. *Marine Geology*, 361, 53-78.
- Aonashi, K., Awaka, J., Hirose, M., Kozu, T., Kubota, T., Liu, G., Shige, S., Kida, S., Seto, S., Takahashi, N. and Takayabu, Y. N. (2009): GSMaP passive, microwave precipitation retrieval algorithm: Algorithm description and validation. *J. Meteor. Soc. Japan*, 87A, 119-136.
- Asano, T. (Ed.). (2016). *Artificial recharge of groundwater*. P.464 Elsevier.
- Aung T T 2003 Myanmar: the study of processes and patterns National Centre for Human Resources Publishing S/R No. 21 Yangon
- Badon Ghijben W, Drabbe J. Nota in verband met de voorgenomen putboring nabij Amsterdam. *Tijdschrift van het Koninklijk Instituut voor Ingenieurs* 1888–1889; 1889:8–22.
- De Boer, B., Van de Wal, R. S. W., Bintanja, R., Lourens, L. J., & Tuenter, E. (2010). Cenozoic global ice-volume and temperature simulations with 1-D ice-sheet models forced by benthic δ 18 O records. *Annals of Glaciology*, 51(55), 23-33.
- Becker, J. J., Sandwell, D. T., Smith, W. H. F., Braud, J., Binder, B., Depner, J., ... & Ladner, R. (2009). Global bathymetry and elevation data at 30 arc seconds resolution: SRTM30_PLUS. *Marine Geodesy*, 32(4), 355-371.
- Berendsen, H. J. A. (2004). *De vorming van het land* (Vol. 1). Uitgeverij Van Gorcum.
- Bartoli, G., Sarnthein, M., Weinelt, M., Erlenkeuser, H., Garbe-Schönberg, D., & Lea, D. W. (2005). Final closure of Panama and the onset of northern hemisphere glaciation. *Earth and Planetary Science Letters*, 237(1), 33-44.
- van Beek, L. P. H., and M. F. P. Bierkens (2009), The global hydrological model PCR-GLOBWB: Conceptualization, parameterization and verification, report, Dep. of Phys. Geogr., Utrecht Univ., Utrecht, Netherlands.
- Bender F K 1983 *Geology of Burma* Gebruder Borntraeger Verlagsbuchhandlung, Berlin and Stuttgart
- Curtis, D.M., 1970. Miocene deltaic sedimentation, Louisiana Gulf Coast. [In:] J.P. Morgan (Ed.): Deltaic sedimentation – modern and ancient. SEPM Special Publication 15, 293–308.
- Danielson, J. J., and D. B. Gesch (2011), Global Multi-resolution Terrain Elevation Data 2010 (GMTED2010), U.S. Geol. Surv., Reston, Va.
- Delsman, J. R., Hu-a-ng, K. R. M., Vos, P. C. C., De Louw, P. G. B., Oude Essink, G. H. P., Stuyfzand, P. J., & Bierkens, M. F. P. (2014). Paleo-modeling of coastal saltwater intrusion during the Holocene: An application to the Netherlands. *Hydrology and Earth System Sciences*, 18(10), 3891–3905. <https://doi.org/10.5194/hess-18-3891-2014>
- Durogbitan AA (2016) Morphology of the Niger Delta: Local Facies Belts Orientation versus Depobelts and Growth Fault Orientations. *J Marine Sci Res Dev* 6:190.
- van Engelen, J., Oude Essink, G. H., Kooi, H., & Bierkens, M. F. (2018). On the origins of hypersaline groundwater in the Nile Delta Aquifer. <https://doi.org/10.1016/j.jhydrol.2018.03.029>
- Faneca Sánchez, M., Bashar, K., Janssen, G., Vogels, M., Snel, J., Zhou, Y., ... & Oude Essink, G. (2015). SWIBANGLA: Managing salt water intrusion impacts in coastal groundwater systems of Bangladesh.
- Galloway, W.E. (1975) Process framework for describing the morphologic and stratigraphic evolution of deltaic depositional systems. In: Broussard ML (ed) *Deltas: models for exploration*. Houston Geological Society, Houston, pp 87–98
- de Gamero, M. L. D. (1996). The changing course of the Orinoco River during the Neogene: a review. *Palaeogeography, Palaeoclimatology, Palaeoecology*, 123(1-4), 385-402.
- Gunnink, J.L., Maljers, D., van Gessel, S.F., Menkovic, A. & Hummelman, H.J., 2013. Digital Geological Model (DGM): a 3D raster model of the subsurface of the Netherlands. *Netherlands Journal of Geosciences* 92: 33–46
- Hall, J. K. (2006), GEBCO Centennial Special Issue—Charting the secret world of the ocean floor: The GEBCO Project 1903–2003, *Mar. Geophys. Res.*, 27(1), 1–5, doi:10.1007/s11001-006-8181-4.
- Hansen, J., Sato, M., Russell, G., & Kharecha, P. (2013). Climate sensitivity, sea level and atmospheric carbon dioxide. *Phil. Trans. R. Soc. A*, 371(2001), 20120294.
- Hartmann, J., and N. Moosdorf (2012), The new global lithological map database GLiM: A representation of rock properties at the Earth surface, *Geochem. Geophys. Geosyst.*, 13, Q12004, doi:10.1029/2012GC004370.
- Hayes M O 1979 Barrier island morphology as a function of tidal and wave regime in Leatherman S P ed Barrier islands – from the Gulf of St Lawrence to the Gulf of Mexico Academic Press, New York 1–27
- Hedley, P. J., Bird, M. I., & Robinson, R. A. (2010). Evolution of the Irrawaddy delta region since 1850. *The Geographical Journal*, 176(2), 138-149.

- Herzberg A. Die Wasserversorgung einiger Nordseebaden. *Zeitung für Gasbeleuchtung und Wasserversorgung* 44;1901:815–9;842–4.
- Hijmans, R.J., Cameron, S.E., Parra, J.L., Jones, P.G., Jarvis, A., 2005. Very high resolution interpolated climate surfaces for global land areas. *International Journal of Climatology* 25, 1965–1978.
- Isaev, V. A., & Mikhailova, M. V. (2009). The hydrography, evolution, and hydrological regime of the mouth area of the Shatt al-Arab River. *Water resources*, 36(4), 380.
- Jarvis, A., Reuter, H. I., Nelson, A., & Guevara, E. (2008). Hole-filled SRTM for the globe Version 4. available from the CGIAR-CSI SRTM 90m Database (<http://srtm.csi.cgiar.org>)
- Kallepalli, Akhil & Kakani, Nageswara Rao & B. James, David & Richardson, Mark. (2017). Digital shoreline analysis system-based change detection along the highly eroding Krishna–Godavari delta front. *Journal of Applied Remote Sensing*. 11. 036018-1. 10.1117/1.JRS.11.036018.
- Kopp RE, Hay CC, Little CM, Mitrovica JX (2015) Geographic variability of sea-level change. *Curr Clim Chang Reports* 1:192–204 69. Review of the processes that cause sea level to be spatially variable, with detailed discussion of GIA.
- Kloppmann W, Bourhane A, Schomburgk S. Salinisation des masses d’eaux en France métropolitaine et dans l’Outre-mer. Rapport BRGM/RP-59496-FR 2010.
- T. Kubota, S. Shige, H. Hashizume, K. Aonashi, N. Takahashi, S. Seto, M. Hirose, Y. N. Takayabu, K. Nakagawa, K. Iwanami, T. Ushio, M. Kachi, and K. Okamoto, 2007: Global Precipitation Map using Satelliteborne Microwave Radiometers by the GSMaP Project : Production and Validation, *IEEE Trans. Geosci. Remote Sens.*, Vol. 45, No. 7, pp.2259-2275.
- Kumar, R., Singh, R. D., & Sharma, K. D. (2005). Water resources of India. *Current science*, 794-811.
- Lambeck, K., Yokoyama, Y., & Purcell, T. (2002). Into and out of the Last Glacial Maximum: sea-level change during Oxygen Isotope Stages 3 and 2. *Quaternary Science Reviews*, 21(1-3), 343-360.
- De Lange, W. J. (1996). Groundwater modeling of large domains using analytical elements.
- Langevin, C. D., & Guo, W. (2006). MODFLOW/MT3DMS–Based Simulation of Variable-Density Ground Water Flow and Transport. *Groundwater*, 44(3), 339-351. 53
- Langevin, C. D., Shoemaker, W. B., & Guo, W. (2003). MODFLOW-2000, the US Geological Survey Modular Ground-Water Model--Documentation of the SEAWAT-2000 Version with the Variable-Density Flow Process (VDF) and the Integrated MT3DMS Transport Process (IMT) (No. 2003-426)
- Lehner, B., Verdin, K., & Jarvis, A. (2006). HydroSHEDS technical documentation, version 1.0. World Wildlife Fund US, Washington, DC, 1-27.
- De Louw, P. G. B. (2013). Saline seepage in deltaic areas: Preferential groundwater discharge through boils and interactions between thin rainwater lenses and upward saline seepage.
- MacKee, E.D., Nordin, C.F. and D. Perez-Hernandez (1998). The Waters and Sediments of the Rio Orinoco and its major Tributaries, Venezuela and Colombia. United States Geological Survey water-supply paper, ISSN 0083; 2326/A-B. Washington: United States Government Printing Office.
- Momta, P. S., Etu-Efeotor, J. O., & Ugwueze, C. U. (2015). Petrophysical Characterization and Flow Models for Agbada Reservoirs, Onshore Niger Delta, Nigeria. *American Journal of Geoscience*, 5, 40-52.
- Mostafa H. Sharqawy, John H. Lienhard V, and Syed M. Zubair, "Thermophysical properties of seawater: A review of existing correlations and data," *Desalination and Water Treatment*, Vol. 16, pp.354-380, April 2010.
- Milliman, J. D., & Farnsworth, K. L. (2013). *River discharge to the coastal ocean: a global synthesis*. Cambridge University Press.
- Mulder, T (2017). Implementing detailed subsurface data for the province of Zuid- Holland in a supra-regional iMOD-SEAWAT model: internship report.
- K.G. Nayar, M.H. Sharqawy, L.D. Banchik, and J.H. Lienhard V, "Thermophysical properties of seawater: A review and new correlations that include pressure dependence," *Desalination*, Vol. 390, pp.1-24, 2016. doi:10.1016/j.desal.2016.02.024
- Nicholls R. J. and J. A. Lowe 2004. Benefits of mitigation of climate change for coastal areas, *Global Environmental Change*, vol.14: 229-244.
- Nicholls, R. J., Wong, P. P., Burkett, V., Codignotto, J., Hay, J., McLean, R. & Brown, B. (2007). Coastal systems and low-lying areas.
- Nyi Nyi 1967 The physiography of Burma The Geological Society, Rangoon Arts and Science University (RASU), Rangoon
- Okamoto, K., Iguchi, T., Takahashi, N., Iwanami, K., and Ushio, T., (2005). The Global Satellite Mapping of Precipitation (GSMaP) project, 25th IGARSS Proceedings, pp. 3414-3416.
- Orton G J and Reading H G 1993 Variability of deltaic processes in terms of sediment supply, with particular emphasis on grain size *Sedimentology* 40 475–512

- Oude Essink, G. H. P. & Waterman, R. E. (2018). Impacts of offshore land reclamation on fresh groundwater volumes under coastal dunes and surface water in the hinterland, submitted to Hydrological Processes
- Oude Essink, G. H. P. (2001). Improving fresh groundwater supply—problems and solutions. *Ocean & Coastal Management*, 44(5), 429-449.
- Oude Essink, G.H.P., E.S. van Baaren, and P.G.B. De Louw 2010, Effects of climate change on coastal groundwater systems: A modeling study in the Netherlands, *Water Resour. Res.*, 46, W00F04
- Oude Essink, G.H.P., Louw, P., Stevens, S., Veen, B., Prevo, C., Marconi, V., Pauw, P., van Baaren, E.S., Visser, M., 2014. Controlled level drainage, a feasible measure to increase a fresh water lens in creek deposits. *Proceedings SWIM 2014*, Husum, Germany.
- Post, V. E. A., Plicht, H., and Meijer, H.: The origin of brackish and saline groundwater in the coastal area of the Netherlands, *Netherlands J. Geosci./Geol. en Mijnb.*, 82, 133–147, 2003.
- Reijers, T. (2011). Stratigraphy and sedimentology of the Niger Delta. *Geologos*, 17(3), 133-162.
- Rizzini, A., Vezzani, F., Cococetta, V., & Milad, G. (1978). Stratigraphy and sedimentation of a Neogene—Quaternary section in the Nile Delta area (ARE). *Marine Geology*, 27(3-4), 327-348.
- Robinson R A J, Bird M I, Oo N W, Hoey T B, Aye M M, Higgitt D L, Lu X X, Swe Aung, Tun Tin and Lhaing Win Swe 2007 The Irrawaddy river sediment flux to the Indian Ocean: the original nineteenth-century data revisited *Journal of Geology* 115 629–40
- Rohling, E. J., Grant, K., Bolshaw, M., Roberts, A. P., Siddall, M., Hemleben, C., & Kucera, M. (2009). Antarctic temperature and global sea level closely coupled over the past five glacial cycles. *Nature Geoscience*, 2(7), 500.
- Rovere, A., Stocchi, P. & Vacchi, M. *Curr Clim Change Rep* (2016) 2: 221. <https://doi.org/10.1007/s40641-016-0045-7>
- Seeliger, U., & Kjerfve, B. (Eds.). (2013). *Coastal marine ecosystems of Latin America* (Vol. 144, p.61). Springer Science & Business Media.
- Schot, P. P., Poot, A., Vonk, G., & Peeters, W. H. M. (2001). A Surface Water Model for the Orinoco river basin.
- Small, C., & Nicholls, R. J. (2003). A global analysis of human settlement in coastal zones. *Journal of Coastal Research*, 584-599.
- Tanabe S, Saito Y, Sato Y, Suzuki Y, Sinsakul S, Tiyaipairach N and Chaimanee N 2003a Stratigraphy and Holocene evolution of the mud-dominated Chao Phraya delta, Thailand *Quaternary Science Reviews* 22 789–807
- Ushio, T., Kubota, T., Shige, S., Okamoto, K., Aonashi, K., Inoue, T., Takahashi, N., Iguchi, T., Kachi, M., Oki, R., Morimoto, T. and Kawasaki, Z. (2009). A Kalman filter approach to the Global Satellite Mapping of Precipitation (GSMaP) from combined passive microwave and infrared radiometric data. *J. Meteor. Soc. Japan*, 87A, 137-151.
- Vallejos, A., Sola, F., & Yechieli, Y. (2017). Influence of the paleogeographic evolution on the groundwater salinity in a coastal aquifer. *cabo de gata aquifer, se spain. Journal of Hydrology*. <https://doi.org/10.1016/j.jhydrol.2017.12.027>
- van de Ven, G. P. (1993), *Man-Made Lowlands: History of Water Management and Land Reclamation in the Netherlands*, 294 pp., UitgeverijMatrijs, Utrecht, Netherlands.
- Verkaik J, Janssen GMCM. 2015. User Manual iMOD-SEAWAT DOI: 10.1007/SpringerReference_28001
- Vermeulen, P. T. M., Hendriksen, G., Snepvangers, J. J. C., Berendrecht, W. L., Lourens, A., Tambach, T., ... & Minnema, B. (2006). iMOD Interactive Modelling Environment. *TNO Software*.
- Watson, D. F., and G. M. Philip. "A Refinement of Inverse Distance Weighted Interpolation." *Geoprocessing* 2:315–327. 1985.
- Wada, Y., Van Beek, L. P. H., & Bierkens, M. F. P. (2011). Modelling global water stress of the recent past: on the relative importance of trends in water demand and climate variability. *Hydrology and Earth System Sciences*, 15(12), 3785–3808. <https://doi.org/10.5194/hess-15-3785-2011>
- Wada, Y., Van Beek, L. P. H., Van Kempen, C. M., Reckman, J. W. T. M., Vasak, S., & Bierkens, M. F. P. (2010). Global depletion of groundwater resources. *Geophysical Research Letters*, 37(20), L20402. <https://doi.org/10.1029/2010GL044571>
- Waelbroeck, C., Labeyrie, L., Michel, E., Duplessy, J. C., McManus, J. F., Lambeck, K., ... & Labracherie, M. (2002). Sea-level and deep water temperature changes derived from benthic foraminifera isotopic records. *Quaternary Science Reviews*, 21(1-3), 295-305.
- Watanabe, S., Hajima, T., Sudo, K., Nagashima, T., Takemura, T., Okajima, H., ... & Ise, T. (2011). MIROC-ESM 2010: Model description and basic results of CMIP5-20c3m experiments. *Geoscientific Model Development*, 4(4), 845.
- Weerasekera, W. L. (2017). Groundwater Modelling of the Red River Delta, Vietnam.
- Werner, A. D., Bakker, M., Post, V. E., Vandenbohede, A., Lu, C., Ataie-Ashtiani, B., ... & Barry, D. A. (2013). Seawater intrusion processes, investigation and management: recent advances and future challenges. *Advances in Water Resources*, 51, 3-26.
- Werner, A. D., & Simmons, C. T. (2009). Impact of sea-level rise on sea water intrusion in coastal aquifers. *Groundwater*, 47(2), 197-204.

- Wessel, P., & Smith, W. (2013). Gshhg—a global self-consistent, hierarchical, high-resolution geography database. Honolulu, Hawaii, Silver Spring, Maryland.
- Zachos, J. C., Dickens, G. R., & Zeebe, R. E. (2008). An early Cenozoic perspective on greenhouse warming and carbon-cycle dynamics. *Nature*, 451(7176), 279.
- Zamrsky, D., Oude Essink, G. H. P., & Bierkens, M. F.(2017). Estimating the thickness of unconsolidated coastal aquifers along the global coastline.
- Zheng, C., & Wang, P. P. (1999). MT3DMS: a modular three-dimensional multispecies transport model for simulation of advection, dispersion, and chemical reactions of contaminants in groundwater systems; documentation and user's guide. Alabama University.

WRI, Watersheds of the world, 2005 ;

<http://netedu.xauat.edu.cn/jpkc/netedu/jpkc2009/szylyybh/content/wlzy/4/Watersheds%20of%20the%20World%202005.pdf>

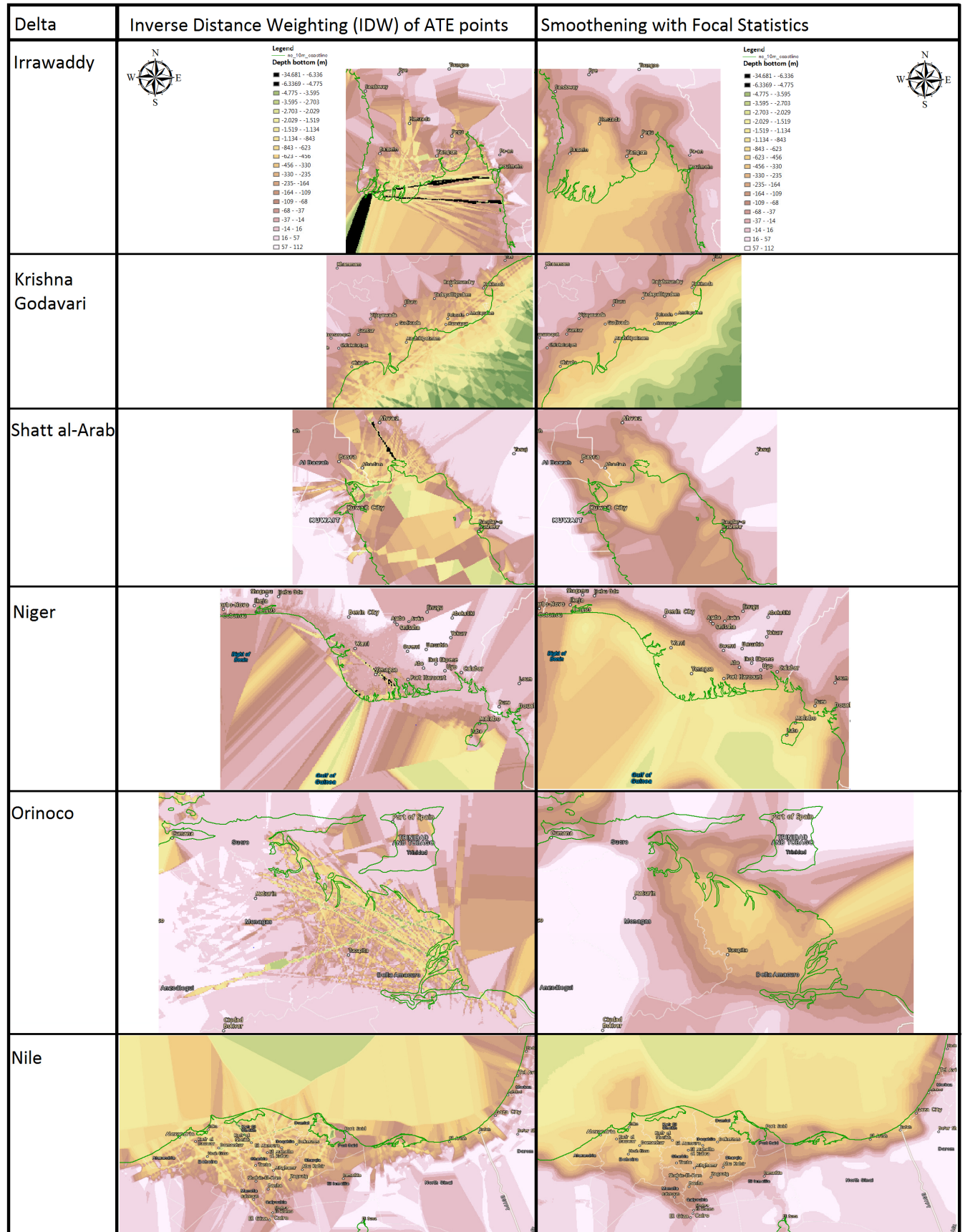
visited 13-15 march 2018.

9. Appendices

Appendix A

Temp, °C	Salinity, g/kg													
	0	10	20	30	35	40	50	60	70	80	90	100	110	120
0	999.9	1007.9	1016.0	1024.0	1028.0	1032.0	1040.0	1048.0	1056.1	1064.1	1072.1	1080.1	1088.1	1096.2
10	999.5	1007.4	1015.2	1023.0	1027.0	1030.9	1038.7	1046.6	1054.4	1062.2	1070.1	1077.9	1085.7	1093.6
20	998.0	1005.7	1013.4	1021.1	1024.9	1028.8	1036.5	1044.1	1051.8	1059.5	1067.2	1074.9	1082.6	1090.3
25	996.9	1004.5	1012.2	1019.8	1023.6	1027.4	1035.0	1042.6	1050.3	1057.9	1065.5	1073.1	1080.7	1088.4
30	995.6	1003.1	1010.7	1018.2	1022.0	1025.8	1033.4	1040.9	1048.5	1056.1	1063.6	1071.2	1078.7	1086.3
40	992.2	999.7	1007.1	1014.6	1018.3	1022.1	1029.5	1037.0	1044.5	1052.0	1059.4	1066.9	1074.4	1081.8
50	988.1	995.5	1002.9	1010.3	1014.0	1017.7	1025.1	1032.5	1039.9	1047.3	1054.7	1062.1	1069.5	1076.9
60	983.2	990.6	998.0	1005.3	1009.0	1012.7	1020.0	1027.4	1034.7	1042.1	1049.5	1056.8	1064.2	1071.5
70	977.8	985.1	992.5	999.8	1003.5	1007.1	1014.5	1021.8	1029.1	1036.5	1043.8	1051.2	1058.5	1065.8
80	971.8	979.1	986.5	993.8	997.5	1001.1	1008.5	1015.8	1023.1	1030.5	1037.8	1045.1	1052.5	1059.8
90	965.3	972.6	980.0	987.3	991.0	994.7	1002.0	1009.4	1016.8	1024.1	1031.5	1038.8	1046.2	1053.5
100	958.3	965.7	973.1	980.5	984.2	987.9	995.2	1002.6	1010.0	1017.4	1024.8	1032.2	1039.6	1047.0
110	950.9	958.3	965.8	973.2	976.9	980.6	988.1	995.5	1003.0	1010.4	1017.8	1025.3	1032.7	1040.2
120	943.0	950.6	958.1	965.6	969.3	973.1	980.6	988.1	995.6	1003.1	1010.6	1018.1	1025.6	1033.1

Appendix B



Appendix C

Example 1:

The function for river conductance is given as:

$$C = K * l * w / b \quad (8)$$

- C= conductance (m²/d)
- K = the hydraulic conductivity (m/d)
- l = length (m)
- w = width (m)
- b = thickness of stream bed sediments (m)

River width = 800 meters

Hydraulic conductivity of bedsoil = 0.05 m/d

Thickness of bedsoil = 3 meters

Length of cell = 1000 meters

Number of big rivers in 1 model cell: ~1

Surface contact river type 1 (big river) = $800 * 1000 * 1 = 800000 \text{ m}^2$

The river conductance would be: $13.333 \text{ m}^2/\text{d}$.

In this estimation the width * 10 would give a conductance of 8000 for this cell.

Example 2.

River width = 30 m

Hydraulic conductivity of bedsoil = 0.01 m/d

Thickness of bedsoil = 0.5 meters

Length of cell = 1000 meters

Number of rivers in 1 model cell: ~2

Surface contact river type 1 (small river) = $30 * 1000 * 2 = 60000 \text{ m}^2$

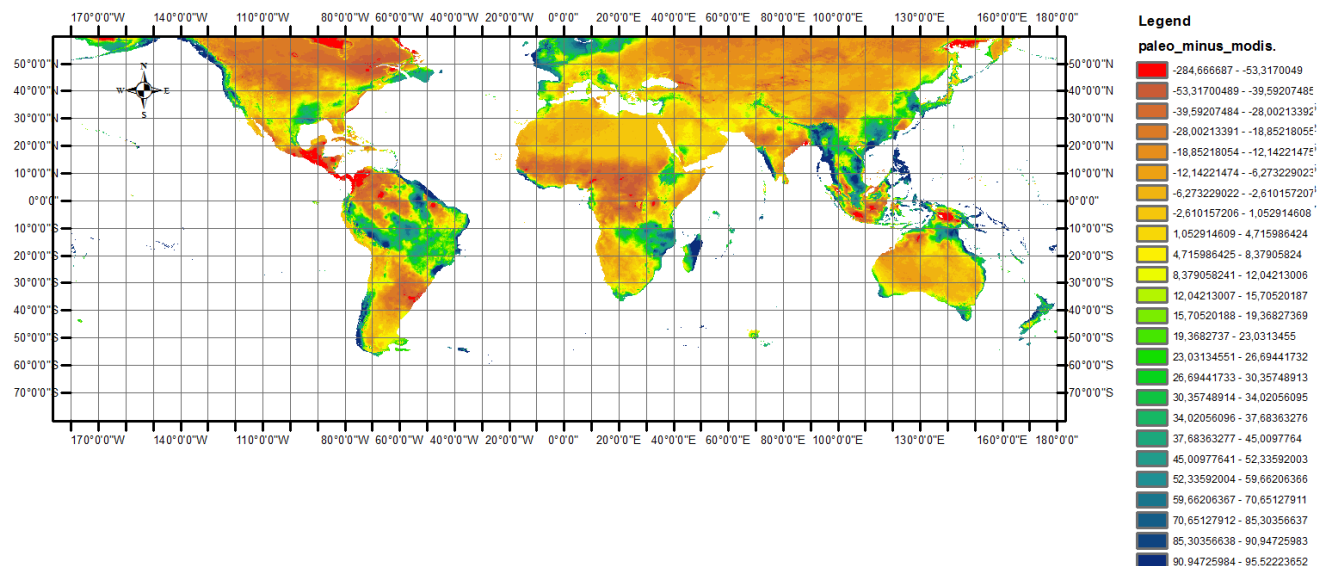
The river conductance would be $1200 \text{ m}^2/\text{d}$.

In this estimation the width * 10 would give a conductance of 600 for this cell.

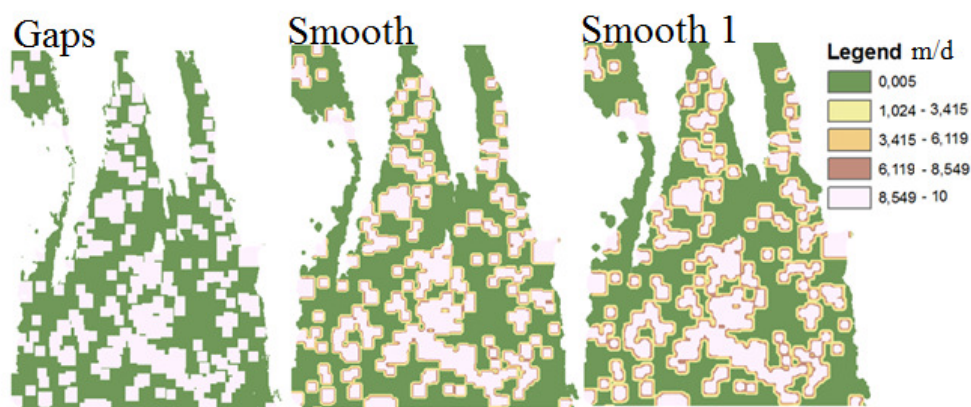
The examples show that for a reasonable estimation of K and b the rough estimation of the conductance by multiplying the width of a factor 10 holds

Appendix D

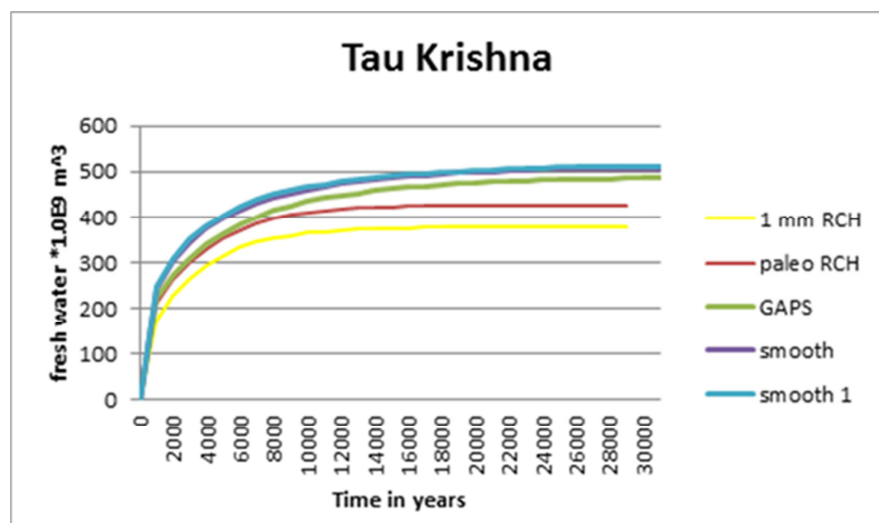
Paleo precipitation minus GSMaP current precipitation: mm/month. GSMaP data set does not give proper estimations in the polar regions of the northern hemisphere ($> 60.0^\circ\text{N}$)



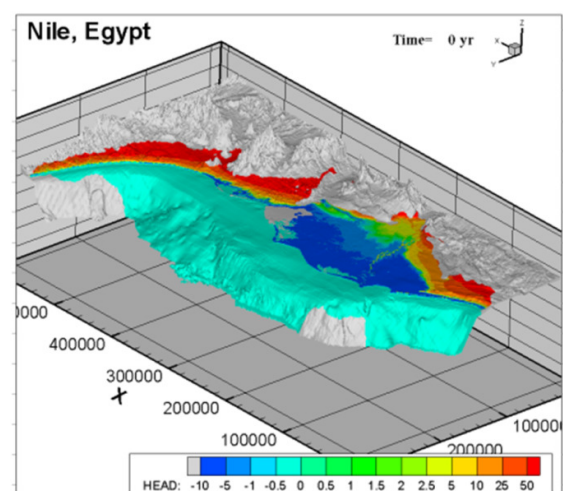
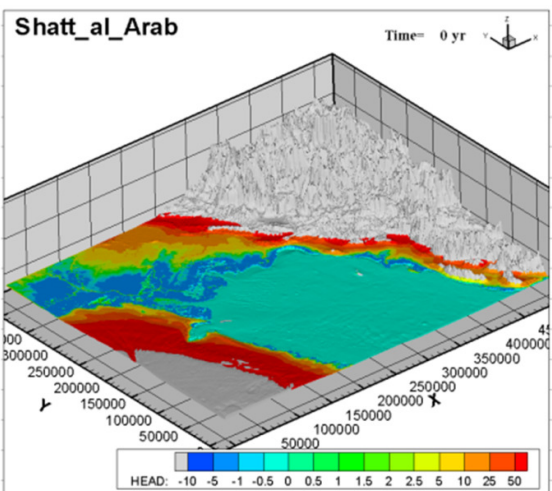
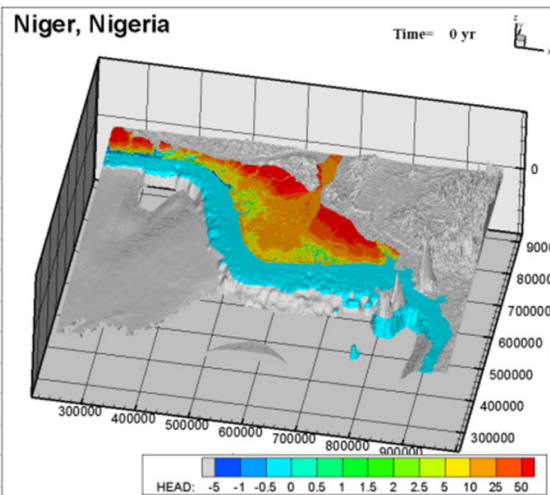
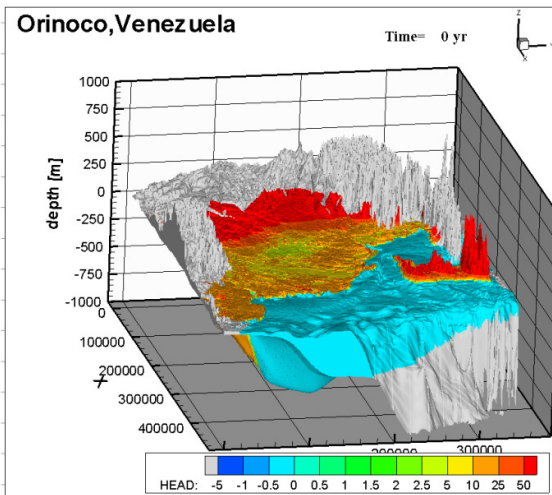
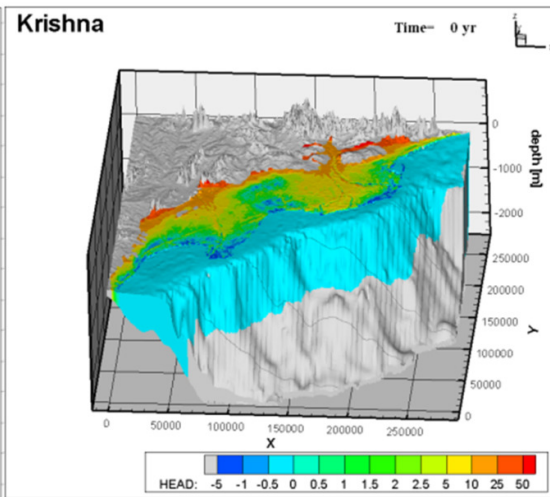
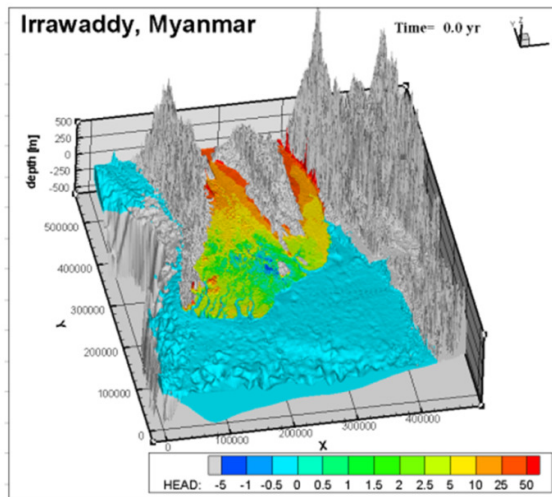
Appendix E



Appendix F



Appendix G



Appendix H

Use FONT is

```
#####
# Irrawaddy delta iMOD run-file for SEAWAT v4
#
#
# Valid tokens to use with _T (species), _P (stress period),
# _S (sub-system), _L (model layer), _R (row), _C (column) are: $, ? and &
#####

[GEN] # GENeral settings
MODELNAME = Irrawaddy_01      # name of the model
WRITEHELP = TRUE              # if true, write run-file help to a csv-file
RESULT_DIR = .\results\      # results folder
PACKAGES = DIS, BAS6, OC, LPF, GHB, RIV, DRN, RCH, PCG, BTN, ADV, DSP, GCG, SSM, VDF #set active packages
COORD_XLL = 9025736.00 #9024736.00 # lower left x-coordinate
COORD_YLL = 1833442.00 #1832442.00 # lower left y-coordinate
RUNTYPE = SEAWAT

#####

[DIS] # MODFLOW DIScretization Package
NLAY = 10 # number of layers
NROW = 543 # number of rows
NCOL = 469 # number of columns
NPER = 2 # number of stress periods
DELC_R? = 1000. # cell width along columns (or y-axis)
DELR_C? = 1000. # cell width along rows (or x-axis)
TOP = \DBASE\DEM\DEMFINAL_IRRA.IDF # top elevation of the first model layer
BOTM_L1 = \DBASE\BOT\BOT_IRRA_L1.IDF
BOTM_L2 = \DBASE\BOT\BOT_IRRA_L2.IDF
BOTM_L3 = \DBASE\BOT\BOT_IRRA_L3.IDF
BOTM_L4 = \DBASE\BOT\BOT_IRRA_L4.IDF
BOTM_L5 = \DBASE\BOT\BOT_IRRA_L5.IDF
BOTM_L6 = \DBASE\BOT\BOT_IRRA_L6.IDF
BOTM_L7 = \DBASE\BOT\BOT_IRRA_L7.IDF
BOTM_L8 = \DBASE\BOT\BOT_IRRA_L8.IDF
BOTM_L9 = \DBASE\BOT\BOT_IRRA_L9.IDF
BOTM_L10 = \DBASE\BOT\BOTTOMFINAL2.IDF
LAYCBD_L? = 0 # flag for unconfined computation ( if 0 no confining bed below if not 0 there is a confining bed below.)
PERLEN_P1 = 0.001 # stress period length
PERLEN_P2 = 36525.0 #365.25
NSTP_P? = 1.
SSTR_P1 = SS # transient / steady-state flag
SSTR_P2 = TR

[BAS6] # MODFLOW BASic Package
IBOUND_P?_L? = \DBASE\BND\IBtest1_Irra_L1.IDF # boundary indicator array
HNOFLO = -9999. # value of head to be assigned to all no-flow cells
STRT_P1_L? = 0.0 # \data\BAS\INITH\NHI_GVG_NAP_L1_SCALED.IDF #NHI_GVG_NAP_L1_SCALED.IDF # initial (starting) head

[OC] # MODFLOW Output Control option
SAVEHEAD_P?_L? = TRUE # save head at the end of the stress period
SAVECONCLAYER_L? = TRUE # save concentrations for specified layers
SAVEBUDGET_P?_L? = TRUE # save budget at the end of the stress period
SAVEHEADTEC_P?_L? = TRUE # logical,F,Save head at the end of the stress period (Tecplot)
SAVECONCTEC_P?_L? = TRUE # logical,F,Save concentration at the end of the stress period (Tecplot)
SAVEVXTEC_P?_L? = TRUE # logical,F,Save vx at the end of the stress period (Tecplot)
SAVEVYTEC_P?_L? = TRUE # logical,F,Save vy at the end of the stress period (Tecplot)
SAVEVZTEC_P?_L? = TRUE # logical,F,Save vz at the end of the stress period (Tecplot)
#OC,TECFILE,character,concvelo.tec,Tecplot output file
#OC,SAVEHEADOUT_P?_L?,logical,F,Save head difference at the end of the stress period
#OC,SAVECONCOUT_P?_L?,logical,F,Save concentration difference at the end of the stress period
#OC,OUTFILE,character,concvelo.out,Output file with differences
#OC,HEADCOLID,integer,-,Head class identifiers
#OC,CONCCOLID,integer,-,Concentration class identifiers
#OC,HEADCOLVAL,real,-,Head class values
#OC,CONCCOLVAL,real,-,Concentration class values

[LPF] # MODFLOW Layer-Property Package
Hdry = 1E+30 # head that is assigned to cells that are converted to dry during a simulation
NPLPF = 0 # number of lpf parameter,(not used!)
```

```

LAYTYP_L? = 0
LAYAVG_L? = 0
CHAN1_L? = 1.0
HK_L1 = 0.005    # hydraulic conductivity along rows
HK_L2:10 = 10.
VKA_L1 * 0.4 = 0.005    # vertical hydraulic conductivity
VKA_L2:10 * 0.4 = 10.
SS_L1:10 = 0.0021    # specific storage
                    # Flag / unit number for writing cell-by-cell flow terms (> 0: write to unit number; = 0: no write; < 0: write for constant-head cells)

[GHB] # MODFLOW General Head Boundary Package
MXACTB = 2500000
IGHBCB = 0
MGHBSYS = 1
# BHEAD_P?_S?_L1 = \DATABASE\GHB\GHBHEAD_IRRA_L1.IDF #for slr lvl+1.idf
BHEAD_P?_S?_L1:10 = \DATABASE\GHB\GHBHEAD_IRRA_L2.IDF
# COND_P?_S?_L1 = \DATABASE\GHB\GHB_IRRA_L1.IDF # for dlr conductance+1.idf
COND_P?_S?_L1:10 = \DATABASE\GHB\GHB_IRRA_L2_L10.IDF
GHBSSMDENS_P?_S?_L1:10 = 1000.0 #.\data\GHB\DENSITY_L1.IDF

[RIV] # MODFLOW RIVER package. Rivers are all located in the first active IBOUND layer.
MXACTR = 2500000    # maximum number of river reaches
IRIVCB = 0    # flag and unit number for saving
MRIVSYS = 1    # maximum number of river systems
STAGE_P?_S?_L1 = \DATABASE\RIV\level_IRRAWADDY.IDF    # head in the river
COND_P?_S?_L1 = \DATABASE\RIV\COND_IRRAWADDY.IDF    # riverbed hydraulic conductance
RBOT_P?_S?_L1 = \DATABASE\RIV\DEPTH_NAP_IRRAWADDY.IDF    # elevation bottom of the riverbed
RIVSSMDENS_P?_S?_L? = 1000.

[DRN]
MXACTD = 2500000
IDRNCB = 0
MDRNSYS = 1
ELEVATION_P?_S?_L1 -0.5 = \DATABASE\DEM\DEMFINAL_IRRA.IDF
COND_P?_S?_L1 = 1000.0 #.\data\drm\COND_B_250_SCALED_L1.IDF

[RCH]
NRCHOP = 1    # recharge option code (1 = recharge is only to the top grid layer, 3 = recharge is applied to the highest
active cell in each vertical column)
IRCHCB = 0
RECH_P? = \DATABASE\RCH\PALEO_RCH_IRRA3.IDF

[WEL] # MODFLOW WELI Package
MWELSYS = 1    # number of well sub-systems
WEL_P1_S1_L1:48 = \data\wel\layer_?.ipf

[PCG] # MODFLOW Preconditioned Conjugate-Gradient Package
MXITER = 1000    # 50 maximum number of outer iterations. Esther: 5000
ITER1 = 50    # 30 number of inner iterations. Esther: 30
HCLOSE = 0.001    # 0.0001 head change criterion for convergence; in units of length. Esther: 0.001
RCLOSE = 1000.    # 0.001 residual criterion for convergence; in units of cubic length per time
RELAX = 0.98    # relaxation parameter used with NPCOND = 1
NBPOL = 0    # flag for eigenvalue estimation if NPCOND = 2
IPRPCG = 1    # printout interval for PCG
MUTPCG = 1    # flag that controls printing of convergence information for the solver (3: only if convergence fails)

#####

[BTN] # MT3DMS Basic Transport Package
DZ_L1:10 = \BTN\DZ_L1.IDF
PRSITY_L1:10 = .3    # porosity (or "mobile" porosity if the dual-domain model is used)
ICBUND_L1:10 = \DATABASE\BND\IBTest1_IRRA_L1.IDF # boundary indicator array    # model boundary
SCONC_L1:10 = \DATABASE\BTN\CONC_L1.IDF # starting concentration
CINACT = -9999    # value indication inactive cells
NPRS = 0    # interval for printing or saving simulation results
IFMTCN = -1    # output control option
CHKMAS = true    # flag for saving mass budget summary file
NPRMAS = 10    # output frequency
NPROBS = 1    # observation point output frequency
DT0_P? = 1000.    # transport time size
MXSTRN_P? = 10000    # maximum transport time step
TTSMULT_P? = 1.    # transport step multiplier (only for fully implicit finite-difference method)

[ADV] # MT3DMS ADvection package
MIXELM = -1    # advection solution option (= 0: Finite-Difference; = 1: MOC; = 2: MMOC; = 3: HMOC; = -1: TVD)

```

```

PERCEL = .75                # number of cells that advection is allowed to move in one transport step (Courant number) 2
MXPART = 1000000           # maximum number of moving particles allowed 0
ITRACK = 1                 # Particle tracking option (= 1: first-orderEuler; = 2: fourth-order Runge-Kutta; = 3: hybrid)
WD = 0.5                   # Concentration weighting factor

[DSP] # MT3DMS DiSPersion package
AL_L? = 10.                # longitudinal dispersivity 0.01
TRPT_L? = 0.1              # ratio of horizontal transverse dispersivity to longitudinal dispersivity
TRPV_L? = 0.1              # ratio of vertical transverse dispersivity to longitudinal dispersivity.
DMCOEF_L? = 0.0000864      # 10-9 * 24 * 3600 effective molecular diffusion coefficient

[GCG] # MT3DMS Generalized Conjugate Gradient Solver Package
MXITER = 10                # maximum number of outer iterations
ITER1 = 500                # maximum number of inner iterations
ISOLVE = 3                 # type of preconditioner used with Lanczos/ORTHOMIN acceleration (= 1: Jacobi; = 2: SSOR; = 3:
MIC)

[SSM] # MT3DMS Sink Source Mixing Package
MXSS = 20000000
CRCH_T1_P? = 1.1
CRIV_T1_P? = 1.1
CDRN_T1_P? = 1.1
CGHB_T1_P?_L1 = \DBASE\GHB\GHB_CONC_L1.IDF
CGHB_T1_P?_L2:10 = \DBASE\GHB\GHB_CONC_L2_L10.IDF

[VDF]
MTDNCONC = 1
MFNADVFD = 2
NSWTCPL = 1
IWTABLE = 0
DENSEMIN = 1000.
DENSEMAX = 1025.
DENSEREF = 1000.
DENSESLP = 0.7143 #=DRHODC?

```